Faculty of Graduate Studies

“Kinetic and Thermodynamic adsorption of Levofloxacin in aqueous solution using Fe^0 pencil graphite composite”

"امتزاز الليفوفلوكساسين من محلول مائي باستخدام توليف من جسيمات الحديد صفر التكافؤ المدعم الجرافيت قلم الرصاص دراسة: الثيرموديناميكية وحركية"

This thesis is submitted to partially satisfy the requirements for a master’s degree in applied chemistry at the Graduate School of Birzeit University, Palestine

Abdallah Idrees

1185083

Supervisors:

Dr. Saleh Sulaiman & Dr. Mohammed Al-Jabari

2021

"Kinetic and Thermodynamic adsorption of Levofloxacin in aqueous solution using Fe^0 pencil graphite composite"

By

Abdallah Idrees

This thesis was defended successfully on 5/9/2021 and approved by:

Committee Members	**Signature**
Dr. Saleh Sulaiman Supervisor Department of Chemistry, Birzeit University	_____
Dr. Mohammad Al-Jabarei Supervisor Department of Chemistry, Birzeit University	_____
Dr. Diab Qadah Member of a thesis committee Department of Chemistry, Birzeit University	_____
Prof. Shehdeh Jodeh Member of the thesis committee Department of Chemistry, An-Najah National University	_____

Acknowledgments

First of all, I want to thank Allah Almighty for giving me the power to accomplish this achievement. I would like to sincerely thank my supervisor Dr. Mohammed Al-Jabarei and Dr. Saleh Sulaiman for providing me with valuable advice and for always using their knowledge and experience to guide and to enlighten me. Thank you for your continued efforts and for providing me with the motivation to complete this work.

I also would like to thank the thesis committee; Prof. Shehdeh Jodeh and Dr. Diab Qadah for their valuable time and efforts in reading and discussing the thesis.

I would like to thank the members of the Department of Chemistry of Birzeit University and the laboratory technicians: Mr. Asem Mubarak, Mr. Azmi Dudin, and Dr. Ibrahim Shalash for facilitating my work in the laboratory. I also like to thank Dr. Adel hidmi, forI have benefited greatly from his instructions and advice. Also, my utmost appreciation goes to Mr. Munther Matani and Mr. Rateb Mohammad for their patience, support, and help in completing the biological activity part of my thesis.

I would like to deeply thank my father, mother, brothers, sisters, and friends for their encouragement and support.

Finally, I want to dedicate this thesis to my beloved family

Abdallah Idrees

2021

Table of contents

List of Figures

List of Table

List of Abbreviation

Symbol	Abbreviations
LEV	levofloxacin
EOCs	Emerging Organic Contaminants
PCPs	Personal Care Products
FT-IR	Fourier Transform - Infrared Spectroscopy
STP	Sewage Treatment Plants
NP’s	Nanoparticles
PP	Pharmaceutical Pollutants
RO	Reverse Osmosis
AOP	Advanced oxidation process
NF	Nanofiltration
PG	Pencil graphite
CNTs	Carbon nanotubes
AC	Activated carbon
SEM	Scanning Electron Microscopy
PhACs	Pharmaceutical Compounds
TEM	Transmission Electron Microscopy
UV-Vis	Ultraviolet-Visible Spectrophotometer
WWTPs	Wastewater Treatment Plants
XRD	X-Ray Diffraction
SWCNT	Single-walled carbon nanotubes
MWCNT	Multi-walled carbon nanotube
nZVI	Nano zero valent iron

"Kinetic and Thermodynamic adsorption of Levofloxacin in aqueous solution using Fe^0 pencil graphite composite"

By

Abdallah Idrees

Supervisors:

Dr. Saleh Sulaiman & Dr. Mohammed Al-Jabari

Abstract

Various pollutants from industry permeate the soil to groundwater without treatment daily, this will bring different health problems to humans and animals, The main problem here is to detect the concentration of a pollutant such as levofloxacin (LEV) and try to remove it by adsorption.

Recently, nanomaterials as effective substances for removing drug residues from wastewater have attracted widespread attention. In this study, a simple and effective method to prepare magnetic nanoparticles PG-Fe^0 composite nanostructure hybrids supported by pencil-shaped graphite is described. In this method, the synthesis of multi-component nanostructure systems involves the covalent bonding of PG and Fe^0 is described as well.

The adsorption properties, possible removal, and mechanism of (LEV) adsorption on the surface of the PG-Fe^0 composite is investigated in this study.

To demonstrate the effective attachment of Fe^0 to PG, well-established material characterization techniques like ultraviolet spectroscopy (UV), Fourier transform infrared (FTIR) spectroscopy, energy-dispersive X-ray spectroscopy (EDX), transmission electron microscope (TEM), and scanning electron microscopy (SEM) were used on the synthesized magnetic nanoparticles.

The effect of pH, adsorbate concentration, contact time, and temperature on the removal efficiency of (LEV) from the surface of superparamagnetic pencil graphite-assisted magnetic nanoparticle PG-Fe^0 composite was investigated. The adsorption efficacy decreased as the pH decreased from ~85% to~75%. The adsorption efficiency, on the other hand, decreased as the temperature was reduced from ~75% to~32%, the adsorption efficiency increased as the contact time increased from ~58% to~80%.

The best equilibrium isotherm model for each adsorption process is Investigate based on the value of the correlation coefficient of Langmuir and Freundlich isotherm adsorption models. Adsorption dynamics was also studied using pseudo-first-order, pseudo-second-order, and intra-particle diffusion kinetic models. In addition, the Van't Hoff diagram of each adsorption type was also studied to determine the values of enthalpy change and entropy change, and to determine whether the adsorption processes were

spontaneous or not, and processes were exothermic or endothermic. The results revealed that all these adsorptions' processes followed the pseudo-second-order kinetics description, and the adsorption kinetic data fitting were better than the pseudo-first-order kinetics. Moreover, compared with the Freundlich isotherm, Langmuir adsorption isotherm was effectively obeyed. All the thermodynamic parameters of adsorption suggested that these processes were endothermic ΔH^0(1.812452 J/mol) and spontaneous ΔG^0(from -5.553 to -6.152 KJ/mol).

The synthesized PG-Fe^0-LEV nanoparticles were also studied as antibacterial agents against different types of gram-positive bacteria; (E. faecalis, S. epidermidis, and S. aureus) and gram-negative bacteria; (E. coli, K. pneumonia, and P. Mirabilia) by agar well diffusion method.

The method developed might be useful for removing LEV drug residue from natural water supplies at specific pH values using 0.5g amounts of adsorbent and a 180min agitation period.

الملخص بالعربية

تتغلغل الملوثات المختلفة من الصناعات المختلفة إلى التربة والمياه الجوفية يوميا دون معالجة, مما يجلب مشاكل صحية مختلفة للبشر والحيوانات. المشكلة الرئيسية هنا هي كيفية التخلص من أحد أكثر الملوثات انتشارا في البيئة الليفوفلكساسين(levofloxacin) والعمل على إزالتها بواسطة طريق الامتزاز.

وقد اجتذبت المواد النانوية، في الآونة الأخيرة، بوصفها مواد فعالة لإزالة مخلفات الأدوية من المياه المستعملة، اهتماماً واسع النطاق. في هذه الدراسة، سوف يوصف طريقة بسيطة وفعالة لإعداد الجسيمات النانوية المغناطيسية $PG\text{-}Fe^0$ الهجينة المدعومة بالجرافيت المستخلص من اقلام الرصاص. وفي هذه الطريقة، ينطوي تصنيع نظم البنية النانوية المتعددة المكونات على الترابط التساهمي بين PG و Fe^0.

في هذا العمل، سيتم التحقق من خاصية الامتزاز، وآلية الإزالة المحتملة، من الليفوفلكساسين على سطح الجسيمات النانوية $PG\text{-}Fe^0$. سيتم وصف الجسيمات النانوية المغناطيسية المركبة بتقنيات توصيف مثل التحليل الطيفي للأشعة فوق البنفسجية (UV) ، ومطياف تحويل الأشعة تحت الحمراء (FTIR) ، والمطياف الشعاعي للطاقة (EDX) ، والمجهر الإلكتروني (TEM) ، وجهاز المسح المجهري الإلكتروني (SEM) حيث سيتم استخدامها لإثبات نجاح عملية تركيب جسيمات الحديد النانوية على الجرافيت المأخوذ من أقلام الرصاص .

تم التحقق من درجة تأثير درجه الحموضه، تركيز الامتزاز، الوقت ، ودرجة الحرارة على كفاءة إزالة الليفوفلوكساسين (LEV) باستخدام مادة الحديد النانوية المغناطيسية المركبة على الجرافيت المستخلص من أقلام الرصاص $PG\text{-}Fe^0$. وفقاً للنتائج، تم ملاحظة انخفاض فعالية الامتزاز مع

انخفاض درجة الحموضة من ~ 85٪ إلى ~ 75٪. من ناحية أخرى، فقد تبين أن كفاءة الامتزاز تنخفض مع انخفاض درجة الحرارة من 75٪ إلى ~ 32٪. كذلك فإن كفاءة الامتزاز تزداد بزيادة وقت الاتصال بين الملوث والمادة النانوية من 58٪ إلى ~ 80٪.

أفضل نموذج للتوازن الحراري لعملية الامتزاز هو استناداً إلى قيمة معامل الارتباط Langmuir ونموذج Freundlich للامتزاز. كما تمت دراسة الامتزاز الديناميكي باستخدام نماذج حركية انتشارية من الدرجة الأولى ومن الدرجة الثانية بين الجسيمات. وبالإضافة إلى ذلك، تم درس الرسم التخطيطي Van't Hoff لكل نوع من أنواع الامتزاز لتحديد قيمة تغيير الطاقة الداخلية الكامنة والعشوائية، وذلك لتحديد ما إذا كانت عملية الامتزاز تلقائية أو غير تلقائية ، طاردة للطاقة أو ماصة الطاقة . تظهر النتائج أن كل هذه الامتزازات تتبع وصف الحركة من الدرجة الثانية و تتبع تركيب البيانات الحركية للامتزاز. وعلاوة على ذلك ، فإن عملية الامتزاز تتطابق مع Freundlich isotherm و Langmuir isotherm على نحو فعال. جميع نتائج الديناميكا الحرارية لعملية الامتزاز تثبت أن هذه العمليات هي ماصة للحرارة (ΔH1.812452 J/mol) endothermic وتلقائية ((-5.553 to -6.152 KJ/mol) ΔG^0.

تمت دراسة الأنشط الحيوية للجسيمات النانوية (LEV, PG-Fe^0 and PG-Fe^0-LEV) باستخدام طريقة الانتشار في الآجار ضد ثلاثة أنواع من البكتيريا سلبية النتائج للطريقة الصبغية (E. coli, K. pneumonia, and P. Mirabilia) وثلاثة أنواع من البكتيريا إيجابية للطريقة الصبغية (E. faecalis, S. epidermidis, and S. aureus), وأظهرت الجسيمات النانوية فعالية كبيرة ضد أنواع متعددة من البكتيريا.

ويمكن أن تكون الطريقة التي تم تطويرها مفيدة لإزالة بقايا عقار ليفوفلوكساسين من إمدادات المياه الطبيعية ضمن قيم درجة حموضة محددة باستخدام كميات قليلة من الممتز وفترة قصيرة من ال

Chapter One

Introduction

1.1-Water pollution and pharmaceuticals.

Nowadays, environmental pollution is one of the most critical issues in the world. The key components of our atmosphere (water, air, and soil) are growing and threatened by pollution.[1]

Water is one of life's most important requirements. It constitutes 55 to 70% of the body of a man and occupies nearly 70% of the surface of the earth, while only 0.002% of water can be used safely by humans.[2] In addition, output and economic growth are inextricably related to global health and energy. Safe water supply [3], and access to safe water is the main global challenge of the 21st century, mainly due to human activities, especially, those causing water pollution. [4-5]

Shortage of freshwater is considered a major problem work life. Around 1-2 billion people don't have clean water, millions of people die every year due to unsafe drinking water diseases.[6] Water is affected in various ways in addition to biological pollutants, it may also include chemical pollutants, such as heavy metals (e.g., arsenic, lead, mercury, etc.), organic compounds such as (pesticides, gasoline, dry-cleaning solvents, degreasing agents.

Trichloroethane, carbon tetrachloride, polyaromatic hydrocarbons (PAHs), polychlorinated biphenyls (PCBs), etc.), inorganic anions such as (nitrate, phosphate, perchlorate, fluoride, chloride, and sulfate, …etc.)[7].

Different examples of trace organic pollutants such as surfactants, pesticides, fertilizers, plastics, polyethylene bags, medicines, and many other chemical substances can enter environmental water resources and cause water pollution, posing a threat to human health.[8] The impacts of new products on the environment, continuous production of new products, and development of chemicals may lead to the proliferation of environmental pollution. As a result, more emerging organic pollutants will be detected in wastewater, which may affect surface water and groundwater.[9]

Emerging organic pollutants (EOC) such as pharmaceuticals, pesticides, personal care products (PCP), and veterinary products which have been detected in the aquatic environment have adverse effects on human health and the environment. Many studies focused on EOCs.[10]

Drugs and endocrine disrupting compounds (EDC) are structurally different emerging pollutants that have been found worldwide, especially in surface water, groundwater, estuarine water, and in drinking water. These compounds including but “not are limited” to prescription drugs, over-the-counter drugs,

natural compounds with physiological effects, and consumable compounds (that are beneficial to human health safety). The most common way for these compounds to enter the environment is wastewater (treated and untreated).[11-12]

In the environment, drugs have become potentially biologically active chemical substances, so they are receiving more and more attention.[13] Although directives and legal frameworks have not yet been established, they are still not regulated or undergoing formalization procedures and are therefore regarded as emerging pollutants in water bodies. Drugs are continuously introduced into the environment and prevail in low concentrations.[14] These affect quality of drinking water supplies, ecosystems and human health.[15]

The Pharmaceuticals present in water can be attributed to personal hygiene products, pharmaceutical industry waste, hospital waste and therapeutic drugs[16]. The survival of trace drugs and other heterologous compounds in finished drinking water is another public health issue, because little is known about the potential chronic health effects associated with the long-term intake of mixtures of these compounds through drinking water.[16]Therefore, it has become an emerging issue in the field of environmental science and engineering to effectively remove drugs and other priority pollutants from

wastewater before it is discharged. Therefore, the main objective of this study is to investigate this issue and to mitigate its impact in water pollution.[17]

More pharmaceutical compounds have been found in surface water contaminated by sewage treatment plants (STP) effluents, but less in groundwater and drinking water.[18-19] Pharmaceutical compounds in the aquatic environment are divided into β-blockers, hormones, antibiotics, anti-inflammatory drugs and analgesics.[20]

The combination of microbial metabolites and parent compounds produced by the complete or partial degradation of drugs and their metabolites enters the surface and groundwater through wastewater discharge, and drug pollutants can be transferred to sewage sludge through the adsorption process that occurs during the treatment process. The continuous injection of pharmaceutical wastewater from sewage treatment plants made it to be one of the persistent pollutants in the water environment.[21]

Recently, water treatment has become one of the core subjects, and people are paying great attention to issues related to environmental pollution that affect their health. Remedial process refers to removing, minimizing or neutralizing pollutants in water which can harm human health or ecosystems, Remedial

techniques can be divided into three categories: (1) thermal, (2) physical chemistry and (3) biological methods.

Heat is primarily use to sterilize and/or separate components through thermal water treatment.[22] Treatment normally takes place using physiochemical methods, including physical processes such as adsorption, chemical filtration, oxidation methods, photochemical methods, or electrochemical methods deterioration methods.[22-23] Biological approaches apply using bacteria, such as, Fungal discoloration, aerobic and anaerobic degradation.[24-25]

Most conventional wastewater treatment methods, including extraction, adsorption and oxidation, are unsuccessful in removing chemical compounds and recalcitrant pollutants. Such conventional methods have little effect on the removal of most contaminants and thus the residual quantities of pollutants are accumulated. Wastewater management should therefore develop strategies to solve the problem of growing water pollution, strategies that should result in improving sanitation and ensuring safe drinking of water.[26]

Anti-inflammatory drugs are the most resistant compounds in wastewater, and treated wastewater, so it is necessary to research and develop a new method that has the ability to eliminate such pollutants from an aquatic environment.[27]

1.2- Methods of pharmaceutical removal.

Wastewater treatment is considered an essential area of environmental science. Water treatment and purification methods have been extensively developed and continuously optimized through various standards based on the water source, the use of treated water, the type of pollutants, and the feasibility of implementing the treatment method on the wastewater source.

Pharmaceutical products have been widely used in many fields, such as medicine, industry, animal husbandry, aquaculture and people's daily life. The pharmaceutical compounds present in the water come from two different Sources: Production process in the pharmaceutical industry and the use of pharmaceutical compounds that are ubiquitous in urban and agricultural can introduce drugs into the environment through direct and indirect methods.[28] The establishment of toxic substances of drugs in the environment and the necessity of judging their environmental risks have greatly increased. [29-33] Due to their wide application and poor removal in conventional wastewater treatment plants, they are becoming common in the environment. Both industrial and domestic wastewater contain a variety of organic pollutants, such as pharmaceuticals, personal care products and pharmaceutical pollutants (PP). [34]

Chlorine is now the most common traditional form of drinking water disinfection. Various studies about chlorination of aromatic compounds indicates that the chlorine reaction rate is strongly affected by the presence of different functional groups in the benzene ring. The response is usually Amine-containing drug products which are quickly absorbing chloride.[35]

Micro-pollutants that resist to conventional processes can be removed by membrane filtration (nanofiltration and reverse osmosis) or adsorption on activated carbon. However, the retention capacity of both methods can be reduced by being blocked by natural organic matter presence in water.[36-37]

Recently, advanced treatment technologies such as advanced oxidation and activated carbon adsorption have received extensive attention. The results showed that the removal is incomplete and expensive.[38-40]

Removed pharmaceuticals from wastewater done by using various treatment methods, such as physical, chemical and biological processes. Physical treatment methods involve adsorption process, electrodialysis, reverse osmosis (RO), evaporation, filtration, precipitation and flocculation.[41] In-addition using a variety of technologies to remove drugs from wastewater, such as advanced oxidation process (AOP), where the basic principle of the

process is "The most diffused oxidant can actually oxidize any compound present in the water matrix".[42]

In AOP, ozonation is the most important and preferred method for wastewater treatment.[43] Ozonation is a non-selective oxidation process.[44–45] Fenton oxidation is another important type of AOP methods, which involves iron salt and hydrogen peroxide to eliminate the required contaminants. The operating mechanism of Fenton oxidation is to use several metal-based metals to decompose hydrogen peroxide to generate hydroxyl radical's catalyst.[46] UV treatment is also another AOP method, usually used after biological treatment and sanding filtration in wastewater treatment. UV treatment is effective mechanism of breaking chemical bonds in which Ultraviolet rays directly irradiate pollutants.

Aerobic and anaerobic approaches for the removal of pollutants from wastewater require biological treatment processes. Often, the elimination of micro-pollutants from wastewater by biological treatment alone is not adequate. It is combined in order to increase its effectiveness with other traditional treatment methods. The best approach investigated is the combination of AOP with biological treatment.[47-48]

The use of a membrane is another method for purifying polluted .[49-51] The use of a membrane has been demonstrated to be the most successful technique of treatment, although the cost of this treatment unit has been found to be considerable. Another membrane-based nanofiltration device was used to handle pharmaceutical effluent (NF).[52-53]

Many adsorbents, [54] have been studied for the high-binding elimination of toxins from wastewater such as activated carbon (AC),[55] CNTs (Carbone nanotubes) [56], and zeolites.[57]

Activated carbon has good adsorption properties, such as, developed microspores, large surface area, strong adsorption capacity, etc. So, it is widely used as a good adsorbent in water treatment. However, the widespread use of this technology has many limitations such as re-cycling problems and its high cost.[58-61]

The main advantage of using activated carbon to remove drugs is that it does not produce toxic or pharmacologically active products. [62] Extensive research was conducted to study the adsorption of antibiotics (nitroimidazole) on different types of activated carbon, and it was found that the adsorption rate increased with decreasing oxygen percentage and with increasing carbon

hydrophobicity. Therefore, in general, the hydrophobic interaction seemed to determine the adsorption kinetics.

Carbon nanotubes have attracted a lot of attention because of its unique characteristics and potential applications. Carbon nanotube is a hollow graphite material composed of one or more Graphene sheets (single-walled carbon nanotubes) SWCNT and multi-walled carbon nanotube MWCNT respectively). The length of carbon nanotubes is small ranging from hundred nanometers to a few microns. Its diameter varies if the nanotube consists of one or more layers. The SWCNT range is 1 to 10 nm, the MWCNT range is between 5 and 100-200 nm wider.[63] Therefore, effective removal of drugs using carbon nanotubes (i.e., by extracting drugs from contaminated water) was achieved and yielded higher removal efficiency compared to that obtained for removing heavy metals, dyes, phenols and other organic chemicals.[64-67].

In recent years, many scientific research work was published on the potential applications of zeolite adsorbent for the removal of various pharmaceutical contaminants.[68] For example, sulfonamide antibiotics and emerging pollutants were removed effectively from contaminated water by zeolite adsorbents.[69-71]

With the continuous release of drug residues to the aquatic environment, there is an urgent need to develop a cost-effective and high-capacity method to remove drug contaminants from the aquatic environment.[72]

Nanotechnology can effectively contribute to the treatment of wastewater in various physiochemical and biological wastewater treatment processes.

Overall, nanotechnology has a great ability to boost the efficiency of the treatment processes. The most common applications of nanotechnology in contamination treatments are categorized as follows:

(i) Restoration (or repair) and cleaning of polluted material.

(ii) Sensing and detecting emissions

(iii) Reduction of contamination by the implementation of material technologies.

1.3-Levofloxacin

Quinolones (also called fluoroquinolones) have broad spectrum activities; for Instance, ofloxacin, norfloxacin, ciprofloxacin and moxifloxacin are a few examples of fluoroquinolone compounds.[73-74]

The chemical name of LEV (Figure 1.1) (levorotatory) is (-) -(S)-9-fluoro-2,3-dihydro-3-methyl-10-(4-methylpiperazin-1-yl)-7-oxysubstitute -7H-pyridyl[1,2,3-de] -1,4-benzoxazine-6-carboxylic acid, common name is Levaquin, light yellow crystalline powder. The solubility of levofloxacin is constant at a pH range of 0.6 to 5.8. It's soluble in acetic acid, chloroform and methanol with moderate solubility in water.[75-76]

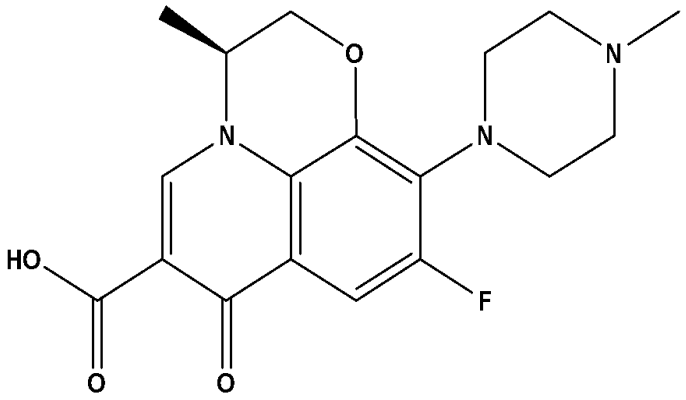

(3S)-9-Fluoro-3-methyl-10-(4-methylpiperazin-1-yl)-7-oxo-2,3-dihydro-7H-[1,4]oxazino[2,3,4-ij] quinoline-6-carboxylic acid

Figure 1.1: Chemical structure of Levofloxacin.

Levofloxacin (LEV) is one among the antibiotics in fluoroquinolone, which has a large variety of activities against gram-positive and gram-negative bacteria. LEV ($C_{18}H_{20}FN_3O_4$, 361.368 g/mol) is a commonly used ofloxacin optical S- (-) isomer. The PH-dependent cationic, anionic, neutral, and zwitterionic activity of LEV chemical structures was demonstrated at various pH levels (Figure 1.2).[77-78] At pH 5, LEV is usually present in its cationic form, while at pH 8.5, it's mostly present in its anionic form.[79] At pH values between pK_{a1} (6.02) and pK_{a2} (8.15), the zwitterionic and neutral forms are present.[80]

It is essential to spot this antibiotic due to its side effects and hence the potential to develop resistance. However, because of its low biodegradability, it is difficult to remove LEV from waste water using traditional process technologies. [82] The presence of LEV in waste water can also can cause environmental toxicity and bioaccumulation.[83] To determine pharmaceuticals in environment compartments, new methods having superior properties over current ones are therefore, crucial.[84]

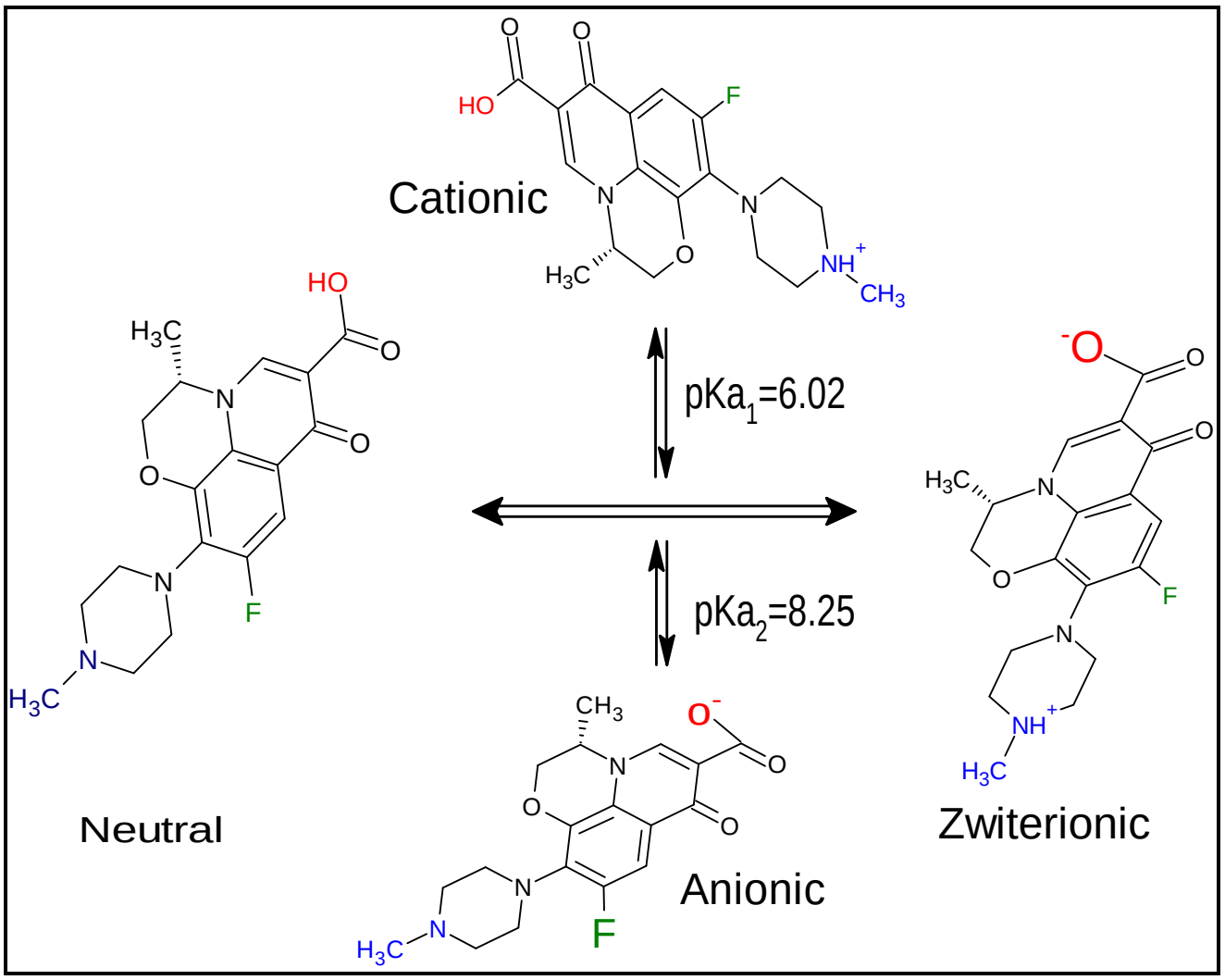

Figure 1.2: Levofloxacin drug's pH-dependent chemical structures.[81]

It is well known that adsorption removal of LEV is a quick, cost-effective, and green wastewater process.[85]As adsorption is the most important mechanism in this process,[86] several studies were aimed at identifying these economical and non-toxic substances.[87] However, filtration and centrifugation are typical ways to remove the adsorbents from the reaction mixture. Adsorbent isolation

from the reaction mixture, and loss of nanoparticles during the isolation process are some drawbacks of these processes.

The magnets are an emerging type of adsorbents which display a strong magnetism, a phenomenon that makes recovering the nanoparticles using an external magnetic field possible, and therefore no additional separation technique is needed. Magnets are therefore, important adsorbents having great potential in industrial applications. [88-89]

The widespread use of LEV in hospitals and farms inevitably contributes to water pollution through waste disposal processes, municipal wastewater influents, and manure application to farmlands, such human activities are adversely affecting aquatic microorganisms. [89]

1.4-Graphite

Graphite is a mineral that contains a hexagonal crystal structure created by carbon stacking atoms. It is the most stable pure carbon under standard conditions. Graphite is very light, has a low specific gravity, not reactive and highly conductive (electrically and thermally). [90]

It is found naturally in igneous and metamorphic rocks.[91] Compressible at high temperatures and high pressure. Graphite can also be synthesized using high carbon content heating materials, such as petroleum coke or carbon tar pitch. The rich-carbon material is heated to 2500 – 3000°C, at such high temperatures, impurities are purified, and a hexagonal plate structure is formed. [91]

There are several other carbon allotropes or types, each of which has its own crystal structure (Figure 1.3). Among them is graphene, a single layer of carbon atoms in a hexagonal form.[92] Another renowned carbon allotrope is diamond. While diamonds are also pure carbon, they have almost entirely different physical properties.[93]

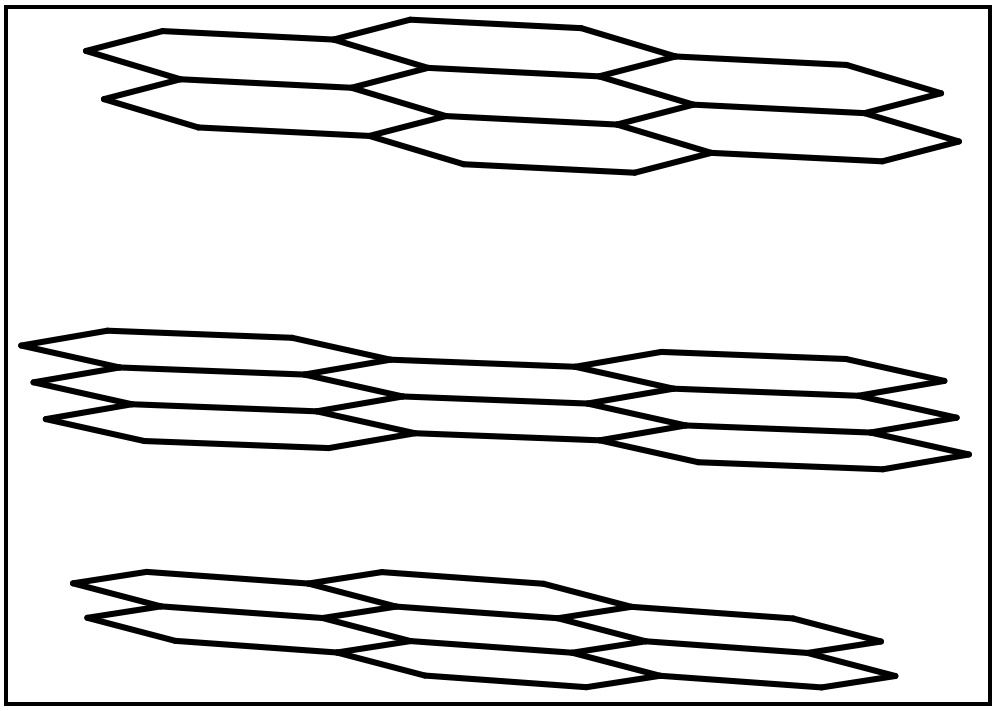

Figure 1.3: structure of graphite .[94]

Graphite is employed for several applications requiring high temperatures and materials which are not melting or decaying. In the steel industry, graphite is used for the production of sinks.[90] In certain nuclear reactors (for example, Soviet Union RBMK), graphite was used as a neutron moderator, as it can slow down fast neutrons. A total of other popular graphite uses include: Pencil leads, Lubricants, Heavy Vehicle Brake Pads, and Battery Electrodes.[95]

Pencil leads

Pencil-graphite leads are graphite (~65%), clay (~30%), and binder substance (wax, resin, or high polymer)[96-97]. The graphite incorporates composite components. The letter Scale is designated by the European letters H (hard) and B (black) with numbers denoting hardness or blackness between 9H (hardest) and 8B.[98] The additional clay was shown by Kariuki to have significant chemical (e.g., ion exchange) and structural qualities (e.g., distortion and surface structure) influence.[99]

Pencil graphite leads are currently recognized as pencil graphite electrodes, as working electrodes (PGEs). Besides being cheap, PGEs are easier to use and more convenient, moreover, and cleaning/polishing the electrode surface is not cleaning/polishing time-consuming. The PGEs utilized provide repeatable signals, producing well-defined voltametric summaries, using several types of voltametric procedures to quantify a number of analytes of a wide range of samples. These electrodes were having been shown to be practical, renewable, and economically effective components of electrochemical instruments with high sensitivity and reproducibility.[100]

1.5-Nanoparticles

Nanotechnology can effectively contribute to the treatment of wastewater in various physicochemical and biological wastewater treatment processes, because of special features such as large surface to volume ratio, strong affinity, reuse, high capacity, and selectivity for heavy metals and other pollutants.[101-102]

As the particle size decreases, the proportion of surface atoms increases, while causing surface atoms to be more inclined to interact, adsorb and react with foreign atoms or molecules, and thereby achieving surface stability.[103-104]

Nanotechnology is applied to produce effective nanomaterials. As an environmentally friendly and effective substance, these nanomaterials can remove drug residues from wastewater; being so, they have received widespread attention. Due to its extraordinary properties (such as high surface area), antibacterial activity, magnetism, and photosensitivity, it was used effectively in many applications.[105-107]

Iron (Fe) is a transition metal with atomic number 26, located in the 8^{th} group and 4^{th} period of the Periodic Table. The element appears in different isotopes, among them is ^{56}Fe, the richest and most stable isotope and is considered to be the fourth most abundant element in the earth's crust.[108]

Iron may possess a wide variety oxidation state, as with other group 8 elements, it could have several oxidation numbers, ranging from -2 to +6. H In the presence of water and or oxygen, it could acquire oxidation states of +2 and +3 (according to its redox potential, refer to Table 1.1). Iron in its elemental form (i.e., Fe^0), is reactive and can be oxidized immediately to form magnetite (Fe_3O_4), or hematite (Fe_2O_3) through corrosion.

Table1.1: Standard iron species abatement potential [109].

Redox Reaction	E^0/V
$Fe^{2+}+2e^- \rightarrow Fe^0$	-0.447
$Fe^{3+}+3e^- \rightarrow Fe^0$	-0.037
$Fe^{3+}+1e^- \rightarrow Fe^{2+}$	0.771

Nano zero valent iron (nZVI) is one of the environmentally friendly materials in the past two decades, the material was proven to be very effective in removing a variety of pollutants, such as pharmaceuticals, chlorinated organic compounds, and heavy metals.[110] The efficiency of nZVI is mainly due to its low redox potential, very high surface area and small particle size.[111-113]

It was shown that nZVI particle has a spherical shape with a core-shell structure (Figure 1.4). The shell usually consists of a layer of iron oxide with

a thickness of a few nanometers. On the other hand, the core was found to be composed of metallic iron Fe^0. With its unique structure, nZVI could act as a reducing agent through the Fe^0 core, or as an adsorbent through iron oxide shell. nZVI could also be used as a coagulant for various anions in groundwater by dissolving Fe (II) from the surface of nZVI. In the purification process, the interface reactions (dissolution, adsorption, redox reaction and precipitation) of nZVI could occur simultaneously or sequentially on the surface of nZVI.[114]

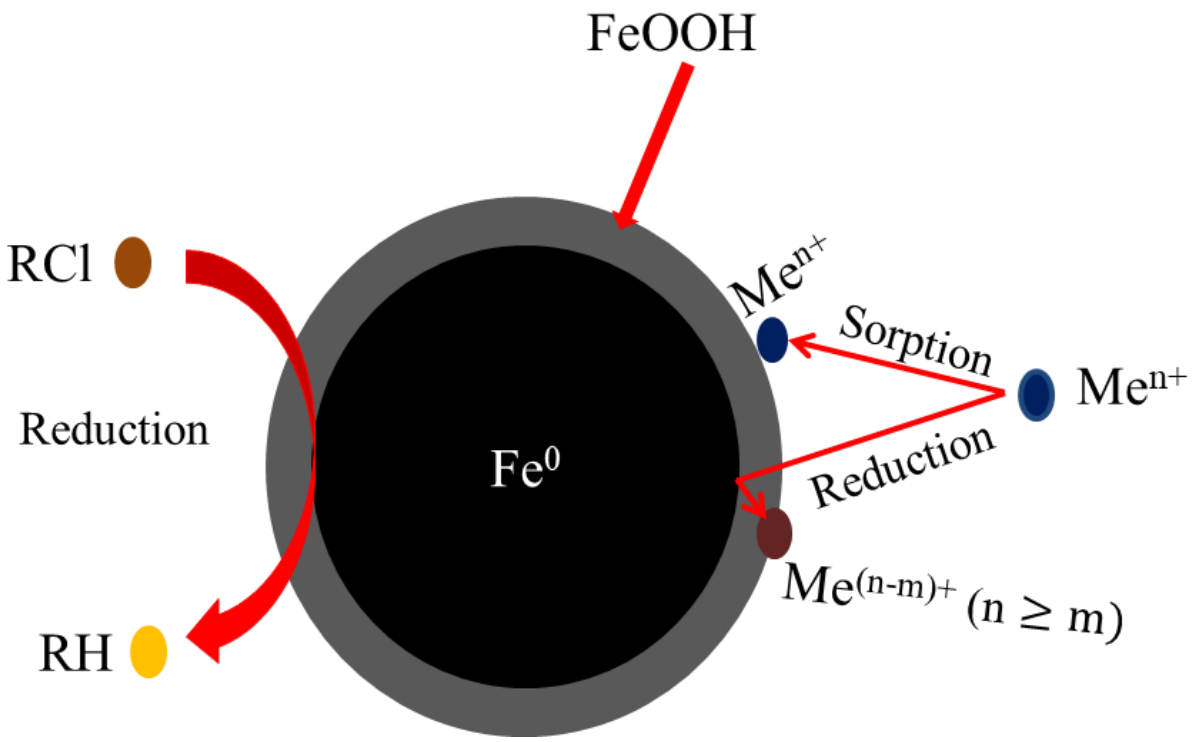

Figure 1.4: The core-shell model of zero-valent iron nanoparticles.[115]

Therefore, the details of the nZVI removal mechanism might be complex and dynamic. The removal process is also affected by the transformation of nZVI structure. In the process of removing contaminants, the transformation of nZVI particles could be divided into two categories, namely, accumulation on the surface of nZVI due to the formation of hydroxide, or co-precipitation and corrosion of nZVI nuclei due to reaction with nZVI, pollutants, water, oxygen and other oxidants.[116]

There are many applications for nZVI in wastewater treatment. A well-known field application started in 1990, involved the use of a permeable reactive barrier (PRB) method to treat contaminated water in the aquifer without having to pump the water to the surface and re-inject it into the aquifer. In the PRB method, groundwater flows through Iron wall that reduces, absorbs or transforms when pollutants in contact with nZVI surface.[117]

In addition, magnetic nanoparticles were used in biomedical areas, including distribution of guided medications, and biological magnet separation and treatment of hyperthermia.[118]

1.6-Adsorption

Adsorption is the fixation of the surface molecules. The translation and accumulation process involves the transition of molecules from the liquid phase to the solid phase. The molecule transmitted is called the adsorbate and the solid stage is the adsorbent.[119-120]

Two kinds of adsorption are available: physical adsorption and chemical adsorption. In chemical adsorption, adsorbate interacts with the adsorbent chemically and forms chemical bonds between active parts. The energy associated with chemical adsorption is greater than 30kcal/mol .[121] In addition, chemical adsorption would cease when the adsorbate covers all the adsorbent's surface.[122]

In physical adsorption, molecular and atomic forces such as Van der Waals and hydrogen bonds are involved, resulting in a weak physical bonding between adsorbates and the rigid surface. The energy associated with physical adsorption is lower than that encountered with chemical adsorption (i.e., <30kcal/mol).[123]

1.6.1-Adsorption isotherm

The ratio of the absorbed amount by the adsorbent to the operation (pressure or concentration) of the adsorbent in the fluid phase at a constant temperature is known as the adsorption isotherm. A number of Models describing a variety of absorption isotherms are available in literature, among them are, Langmuir, Friendlich, Brunauer Emmett and Teller (BET) isotherms.[124]

The adsorption isotherm is a mathematical model which interprets the experimental data obtained by batch adsorption tests under a specified temperature. Various isothermal equations were analyzed to represent the adsorption mechanism of the equilibrium. These define the relation between the adsorbed amount adsorbate in mg per gram of adsorbent (q_e) and the concentration of the solution at equilibrium after adsorption (C_e).[125-126]

$$q_e = (C_0 - C_e)\frac{V}{m} \qquad (1)$$

$$q_t = (C_0 - C_t)\frac{V}{m} \qquad (2)$$

Where C_0, C_e, C_t are the initial, equilibrium and at any time adsorbate concentrations, while V(L) and M(g) are the solution volume and the adsorbent dose, respectively.

1.6.2-Langmuir isotherm

The Langmuir isotherm supposes that one layer of adsorbent is adsorbed onto a surface of adsorbed, and the adsorbent's distribution is uniform, thereby ensuring that each location on the adsorbent is the same and has the same affinity for adsorbate molecules. The nonlinear Langmuir adsorption isotherm model is represented by the following equation:[127-128]

$$Q_e = \frac{k_L Q_m C_e}{1 + k_L C_e} \qquad (3)$$

The linear Langmuir form:

$$\frac{C_e}{Q_e} = \frac{1}{Q_m} k_L + \frac{C_e}{Q_m} \qquad (4)$$

$$\frac{1}{Q_e} = \frac{1}{Q_m} + \frac{1}{Q_m k_L C_e} \qquad (5)$$

$$Q_e = Q_m - \frac{Q_e}{k_L C_e} \qquad (6)$$

$$\frac{Q_e}{C_e} = k_L Q_m - k_L Q_e \qquad (7)$$

Where:

Q_e = the amount of adsorbate per gram of the adsorbent at equilibrium (mg/g).

Q_m = maximum monolayer coverage capacity (mg/g)

K_L = Langmuir isotherm constant (L/mg).

C_e = the equilibrium concentration of adsorbate (mg/L)

1.6.3-Freundlich isotherm

The Freundlich isotherm assumes that the surface of the adsorbent is heterogeneous, which means that the active sites on the surface have different affinities. The Freundlich equation is given by:[129-131.]

$$Q_e = k_f \, C_e^{\frac{1}{n}} \qquad (8)$$

The linear Freundlich form:

$$lnQ_e = ln\ ln\ k_f + \frac{1}{n} lnC_e \qquad (9)$$

Where k_f and 1/n are the Freundlich constants, Q_e is the amount of adsorbate per gram of the adsorbent at equilibrium (mg/g), C_e is the equilibrium concentration of adsorbate (mg/L).

1.6.4-Adsorption kinetics

The adsorption rate could be investigated, and the knowledge of the adsorbent/adsorbate interaction could be applied to experimental data using various kinetic models (physisorption or chemisorption). Pseudo-first-order, pseudo-second-order, and intra-particle diffusion, are three common models that could be used. [132]

1.6.5-Pseudo-First-Order Equation

The pseudo-first-order equation is given by Lagergren and Svenska (1898) The rate constant to determine the adsorption process is given as below:

$$ln(q_e - q) = lnq_e - k_1 t \qquad (10)$$

Where q_e is the equilibrium adsorption potential (m g/g), q_t is the amount of adsorbate at time t (mg/g), and k_1 is the pseudo-first-order rate constant (Min^{-1}). The values of k_1 and q_e are calculate for various concentrations using the slope and intercept (i.e., ln $K_1$and lnQ_e), respectively upon plotting log(qe-qt) vs. t.[132-133]

1.6.6-Pseudo-Second-Order Equation

Equation of pseudo-second-order linear form based on equilibrium adsorption could be expressed as:

$$\frac{t}{Q} = \frac{1}{k_2 Q_e^2} + \frac{1}{Q_e} t \qquad (11)$$

The quasi-second order adsorption rate constant k_2 (g / mg•min). The slope and the intercept of the plot of t/q_t versus t could be used to calculate the values of q_e and k_2. [132-133]

1.6.7- Intra-Particle Diffusion

The intra-particle diffusion kinetic model is based on the principle suggested by Weber and Morris. The adsorption kinetic equation is written as follows:[134]

$$q_t = K_{id}\, t_{1/2} + Z \quad \ldots\ldots\ldots\ldots \quad (12)$$

Where;

K_{id}: is the Intra-Particle diffusion rate constant ($mg/g.min^{1/2}$).

Z: is a constant that gives information about the thickness of the boundary layer (mg/g) .[134]

Plotting qt versus $t_{1/2}$ would yield a linear relationship for intra-particle diffusion kinetic model with constant Z as the y-intercept and K_{id} as the slope.

1.7-Types of adsorbents.

The most common types of adsorbents that were used in previous studies are activated alumina, silica gel, activated carbon, and polymer. It should be noted that the adsorbents could be also classified as natural and synthetic. Natural adsorbents include zeolite, clay, clay minerals, coal, and ores. These materials are cheap in most cases and have great potential to change and ultimately improve. Synthetic adsorbents are adsorbents made from agricultural products and waste, household waste, industrial waste, sludge, and polymer capacitors. Some examples of adsorbents prepared from waste materials include fruit waste, coconut shells, waste tires, bark, and other rich tannins, sawdust, rice husks, petroleum waste, fertilizer waste, fly ash, sugar industry, slag waste, stone kilns, chitosan, the material of seaweed, algae, peat moss, red mud, and many others. Each adsorbent has its own properties, such as porosity, pore structure, and properties of the adsorption surface. [135]

1.8-Research Objectives

1-The research's major goal was to create new innovative materials for water/wastewater treatment. These PG-Fe^0 composite will prevent levofloxacin from entering drinking water or surface water from contaminated aqueous sources.

2-as previously illustrated, LEV has a charge which is dependent on the pH of the solution, in this study the removal efficiency will be investigated at pH 6.5and 8.0. Study removal efficiency as a function of several parameters such as adsorbent concentration, contact time, and temperature on the removal efficiency.

3-Evaluate kinetic and thermodynamic parameters at pH 6.5 and 8.0.

4-Examine the PG-Fe^0-LEV antibacterial activity.

5-Characterizingthe synthesized nanoparticles using Scanning Electron Microscopy (SEM), Transmission Electron Microscopy (TEM), X-Ray powder diffraction (XRD), and Fourier-transform infrared spectroscopy (FT-IR).

Chapter Two

Experimental

2.1-Chemicals and Reagents.

All chemicals were analytically pure and used directly without further purification. The chemicals ferric chloride hexahydrate ($FeCl_3.6H_2O$, ≥ 99%), absolute ethanol ($CHCH_2OH$≥ 99%), Sodium borohydride ($NaBH_4$, ≥ 97%), Pencil graphite (0.5), and levofloxacin ($C_{18}H_20FN_3O_4$, ≥99%), were purchased from Sigma-Aldrich Chemical Company (Milwaukee, U.S.A.). Aqueous solutions were prepared using Milli-Q water having a resistivity of 18.2 MΩ.cm. All bacteria strains (Escherichia coli, Staphylococcus aureus, Proteus mirabilis, Klebsiella pneumonia, Staphylococcus epidermidis, and Enterococcus faecalis) were donated by the Department of Biology and Biochemistry at Birzeit University.

2.2.1-Synthesis of pencil graphite-supported Fe_3O_4 nanoparticles.

Iron oxide magnetite nanoparticles were synthesized via Fe^{+2} and Fe^{+3} at the ratio of (1.2). According to the following chemical equation: [136]

$$Fe^{+2} + 2Fe^{+3} + 8OH^{-} \longrightarrow Fe_3O_4 + 4H_2O \ldots\ldots\ldots \text{ eq (1)}$$

For each batch, 12.5 mL of ammonium hydroxide was added to 150 mL of Milli-Q water and kept solution under continuous stirring in three neck flasks. The solution was heated to 333K using silicon oil under nitrogen gas bubbling to keep inert condition. Then, 0.596 g and 0.973 g of $FeCl_2.4H_2O$ and $FeCl_3$ respectively, were dissolved into two separate beakers, each of which contained 10 ml of de-aerated MQ water. 3.138g of pencil graphite was grinded by hands then added to the ammonium solution and the reaction was heated to 343K for 2h. After that, the color of the solution changed to black, indicating the formation of Fe_3O_4 magnetic nanoparticles. After that, the composite was collected by an external magnet, washed with distilled water to maintain the pH ~7. Finally, the synthesized Fe_3O_4 nanoparticles were dried in the oven at 343K for 24 h and transferred to a tightly closed bottle to prevent further oxidation.

2.2.2-Synthesis of pencil graphite-supported iron nZVI nanoparticles

Zero-valent iron nanoparticles (nZVI) and pencil graphite-supported nZVI (PG-nZVI) were synthesized using the liquid-phase reduction method [137]

$$4Fe^{3+} + 3BH_4^- + 9H_2O \longrightarrow 4Fe^0 + 3H_2BO^{3-} + 12H^+ + H_2\uparrow$$

The preparation consisted of PG-nZVI with an iron/pencil graphite mass ratio of 1:1, ferric chloride hexahydrate ($FeCl_3.6H_2O$) (4.84 g) was dissolved in 100 mL of miscible liquids (Milli-Q water and absolute ethanol at a volume ratio of 1:4 v/v), then 4.84g of grinned pencil graphite was added to the solution. The mixture was stirred vigorously with an electric rod under a nitrogen atmosphere for 15 minutes, then 100 of 0.47M $NaBH_4$ solution was added dropwise to the mixture at a rate of 1-2 drops per second under the same conditions (i.e., vigorous stirring under nitrogen gas).

The color of the mixture changed from reddish brown to light yellow, and finally to black. At the same time, the mixture gradually produced more black particles in the three-necked flask.

After addition of all of the $NaBH_4$ solution, the mixture was stirred under the nitrogen atmosphere continuously for another 20 min to completely deplete $NaBH_4$ and $FeCl_3.6H_2O$. Vacuum filtration was employed to collect the nZVI composite, which was quickly rinsed three times with absolute ethanol (This

rinsing could prevent nZVI from oxidizing), and then dried overnight under vacuum at 298 K, after drying, the composite was stored in a tight- closed bottle for future use.[138]

2.3-Standard solution and calibration curve

40.0 mg/L of LEV stock solution was prepared by dissolving 10.0 mg of LEV in 250 ml Milli-Q water, then five working standard solutions were prepared using this stock solution to obtain the following concentrations: 40.0, 20.0, 10.0, 5.0, and 2.5 mg/L.

LEV calibration curve was constructed in the range of 2.5- 40.0 mg/L (Figure 2.1). The absorbance was recorded at λ_{max} of 289 nm using a UV-Visible spectrophotometer (Brand name, company, country: Cary 50 UV-Visible. Varian, Australia). An aliquot of the stock solution was scanned over a wide range of wavelengths (190 to 500 nm) to determine the maximum wavelength of absorption (i.e., λ_{max}).

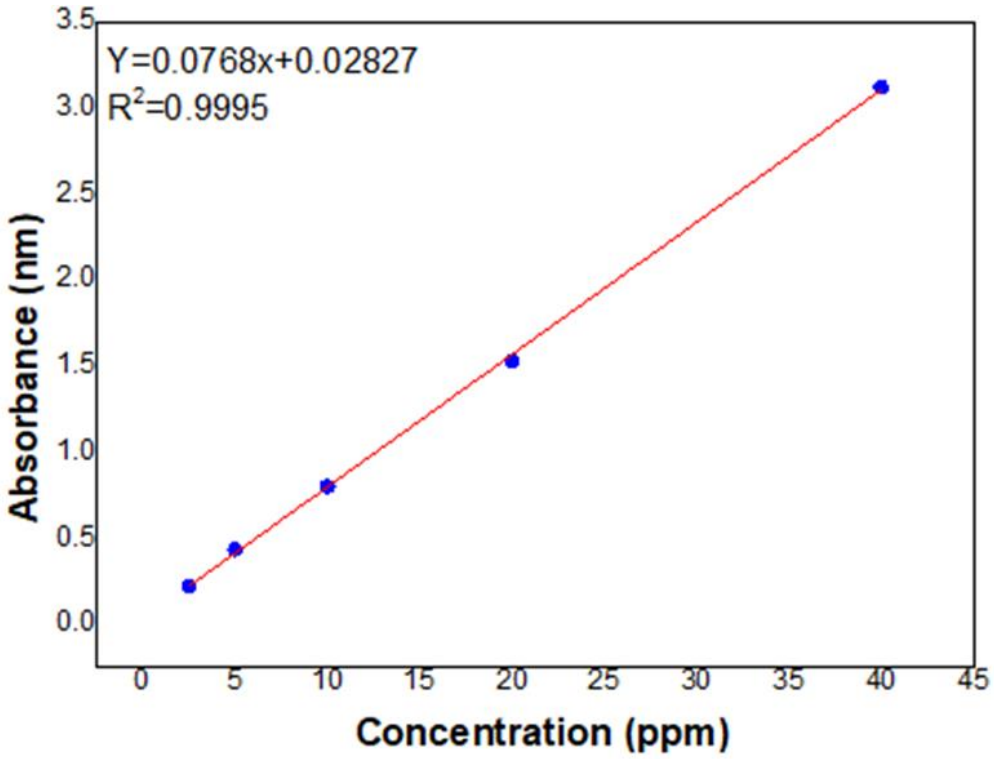

Figure 2.1: Calibration curve of levofloxacin obtained using UV-Vis spectrophotometer.

2.4-Characterization Techniques

The techniques used to characterize PG-Fe^0composite and PG-Fe^0-LEV NPs are described below.

2.4.1-Ultraviolet-Visible (UV-Vis) Spectrophotometry.

The spectrophotometer is equipped with a dual-beam "Czerny-Turner" monochromator that operates at a wavelength range between 190-1100 nm. The light source was composed of a full-spectrum xenon pulse lamp and had a double silicon diode detector

The absorption spectra of samples were recorded using a single beam UV–visible spectrophotometer (Hp 8453, Agilent, U.S.A.) equipped with a deuterium lamp and a photodiode array (PDA) detector.

The spectrophotometer was used to obtain the data required to construct the calibration curves (by plotting Abs. vs. concentration of LEV) in the range. Absorbencies (at λ max of 289 nm) of the previously prepared working standard solutions (2.5-40.0 mg/L LEV) were measured. The constructed calibration curve is shown in Figure 2.1.

2.4.2-Transmission Electron Microscopy (TEM).

Transmission Electron Microscopy (TEM) records images with JOEL-2100F field emission transmittance electron microscope (FE-TEM) instrument. The samples were prepared by immersing the nanoparticles in ethanol, soliciting for 30 minutes, and then dried on carbon-coated copper plates under vacuum. Analysis was performed at King Fahd University of Petroleum and Minerals (Dhahran, Saudi Arabia).

2.4.3-Powder X-Ray Diffraction (XRD).

The diffraction patterns of PG-Fe^0 composite were obtained by Mini-XRD, (Rigaku ultima, company name, country) with a CuK α source and 2θ angle in the range 0 – 80° at a slow scan rate of 2θ min^{-1}. Analysis were performed

at the Nanotechnology Center of Excellence, King Fahd University of Petroleum and Minerals (Dhahran, Saudi Arabia).

2.4.4-Scanning Electron Microscopy (SEM)

Scanning Electron Microscopy (SEM) was used to characterize the surface morphology, shape and size of nanoparticles using a Lyra3, Tuscan field emission scanning electron microscope. Scanning electron microscope coupled with energy dispersive X-ray (SEM-EDX) (Jeol 6700LV). Analysis was conducted at King Fahd University of Petroleum and Minerals (Dhahran, Saudi Arabia).

2.4.5-Fourier Transform Infrared Spectroscopy (FTIR).

The Fourier Transform Infrared Spectroscopy (FT-IR) spectrum of the nanoparticles was obtained using a Bruker TENSOR II spectrometer (City, Country). The KBr precipitate was used for analysis. The spectrum was recorded in the range of 4000-400cm^{-1}. Analysis was performed at the Chemistry department, Birzeit University, (Birzeit, Palestine).

2.5-LEV Removal Experiments

To study the removal efficiency of LEV, various parameters were investigated, such as contact time between adsorbents and drug (kinetic experiments), initial pollutant's concentration, temperature, and pH of solution. All adsorption experiments were performed under atmospheric pressure. UV-Vis's spectrophotometer was used for monitoring LEV concentration during each step. To measure the analyte concentration at the corresponding wavelength λ, the adsorbent was separated from solution by double filtration using 0.45 μm.

The amount of PG-Fe^0 composite that was used in all batches was 0.5g (i.e., equivalent to 80mg Fe^0 effective mass).

Note, all results were represented by both masses.

2.5.1-Effect of Initial drug concentration

To determine the optimum removal concentration of LEV. Batch experiments were performed by adding 0.5 g of PG-Fe^0 composite to 100 ml of LEV solution at variable concentration:10.0, 20.0, 25.0, 30.0 and 35.0 mg/L. The solutions were shaken at 120 rpm at 298 K. Samples from each batch were collected at different time intervals (i.e., at5,10,15,20,30,40, 80, and 320 min).

2.5.2-Effect of pH

The effect of pH on LEV adsorption was investigated at several pH values (3.0, 5.0, 6.5, 8.0, and 10.0). 0.1M NaOH and 0.1M HCl solutions were used to adjust the pH value of 100 ml of 20 mg/L LEV solution. 0.5g of PG-Fe^0 composite were added to each solution, solutions were then shaken in a water bath shaker at constant temperature of 298K. When equilibrium was established, the concentration of LEV, an aliquot of 5ml each solution was taken for subsequent UV-Vis analysis. LEV concentration in each solution was then calculated using the previously constructed calibration curve (i.e., that shown in Figure 2.1).

2.5.3-Effect of Adsorbent Dose

To evaluate the optimum amount of adsorbent dose needed for LEV adsorption, 100 mL of 25 ppm LEV solution was applied to each dose of PG-Fe^0 composite (i.e., 0.1, 0. 3, 0.5, and 1 g PG-Fe^0). At a temperature of 298K and a pH of 6.5, the mixtures were put in a shaking water tank. After equilibrium was established, the samples were filtered, and the final LEV concentrations were measured in all studied solutions.

2.5.4-Effect of temperature

The removal amount of LEV was investigated as a function of times for 20 ppm of LEV solution at different temperatures 278, 288, 298, and 308K.

At each temperature, a 0.5 g of PG-Fe^0 composite was added to the corresponding LEV solution (i.e., 100 mL of 20 ppm LEV kept at the required temperature). The solutions were shaken in a thermostat shaker at 120 rpm. Samples from each solution were collected at different time intervals (particularly, at 5,10,15,20,30,40, 80, and 320 min) the collected samples were filtered by double filtered through the syringe filter 0.45μm, and the absorbance of each sample was measured, and LEV concentrations were calculated using the equation of the straight line shown in Figure 2.1

2.6- nZVI as a Fenton Catalyst

The LEV removal kinetics were also studied using a Fenton-like reaction, by exposing 0.5g of PG-Fe^0 composite to 90.0 mL of 10 mg/L LEV solution, and 10 mL of freshly prepared 10% (v/v) H_2O_2. Then the solution was kept in a thermostatic shaking water bath at 298 K for two hours, then the absorbance of the separated LEV solution was measured.

2.7-Antimicrobial activity

The well-agar diffusion method was used to examine the antimicrobial activity of PG-Fe^0-LEV. In order to study the activity of PG-Fe^0-LEV against different types of gram-positive and gram-negative bacteria, PG-Fe^0-LEV composite was prepared by adding 0.5g of PG-Fe^0 composite to 100 mL of 25 ppm of LEV solution and left for 300 min under continuous shaking conditions at 120 rpm. Upon completion of the adsorption process after 300min, the nanoparticles were collected back by an external magnetic field and dried. The adsorbed LEV concentration was measures using UV–vis spectrophotometric analysis as described earlier. The optimum concentrations of PG-Fe^0 -LEV, PG-Fe^0 composite and LEV were tested, Milli-Q water was taken as a negative control. Various types of gram-Positive bacteria (E. faecalis, S. epidermidis, and S. aureus) and gram-negative bacteria (E. coli, K. pneumonia, and P. Mirabilia) were used to study the antibacterial activity for PG-Fe^0-LEV via Agar-well diffusion method. A certain number of bacterial strains were spread over the entire surface of the Mueller-Hinton agar plate. A 6 mm hole was pierced with a sterile head, 50 µl of antimicrobial agent was injected into the well. The plates were incubated at 310Kfor 24 hours. The samples were copied and, the average diameter of the final inhibition zone was calculated.

Chapter Three

Result and Discussion

3.1-Characterization of PG-Fe^0 composite.

Generally, the iron oxide form is thermodynamically stable, while nZVI is unstable and very easily oxidized in the presence of oxygen. The high chemical reactivity of metal-metal iron particles gives it a high ability to convert various pollutants into less toxic forms. [139-140]

nZVI reveals a typical core-shell structure, which forms zero-valent or metallic iron (Fe^0), and the shell is formed due to the oxidation of nanoparticles and is composed of mixed-valent iron [Fe (II) and Fe (III)] Oxide. Moreover, the showed that nZVI has special electron donor characteristics, which makes it a resource-rich repair material.[139] Through its core-shell structure, nZVI can fix pollutants through redox mechanisms and adsorption mechanisms.[141] The core forms an electron source for redox reactions with several organic and inorganic pollutants, while the oxide shell provides a location for chemical adsorption.[139]

Since ZVI's magnetic dipoles are solid, it forms chain-like aggregates. If the nanoparticles agglomerate, they have a permanent oxide coating but the metallic cores are cut into thinner interfacial oxide layers. The iron oxide layer

is amorphous and distorted and results in extremely small nanoparticle radiation that impedes the formation of crystalline and prevents further oxidation of the core of nanoparticles. [142-143]

During the process of charge transfer from the nanoparticle to a sequestrated contaminant on the outside surface, the core layer is helps to transfer contaminants.[139] It has semiconductor properties[144], and a relatively low load transfer due to its limited thickness and due to the presence of non-working areas to reduce contaminants. [145]

In this study, PG was utilized as a Fe^0 supporter to prevent further oxidation of the sites, as well as to improve the surface area of Fe^0 by promoting dispersion and lowering aggregation.

Different techniques were used to characterize the surface and morphology of NPs and composite such as SEM, TEM, EDS.XRD, and FTIR.

3.1.1-TEM characterization

As shown in Figure 3.1, Transmission electron microscopy (TEM) was used to characterize the adsorbents morphology of PG, Fe^0, and spherical PG-Fe^0 composite. Figure 3.1(a, b) shows the TEM, and SEM images of Fe^0 NPs opening line aggregator chain, with an average diameter of about 60 nm. The drake area indicates the presence of iron, while the light area indicates the iron oxide on the surface shell. The core-shell composition of Fe^0 NPs is well known. The core is composed of Fe in the (0) valence state, and the shell is composed of iron oxide and oxyhydroxide. Figure 3.1(c) shows SEM images of grinded pencil graphite, which appeared like bonded sheets and flakes. Figure 3.1(d) shows an SEM image of the PG-Fe^0 composite. The image showed the Fe^0 NPs stick and dispersed area on the PG surface.

The Fe^0 NPs were lightly bonded to the PG, and not separated when exposed to extreme magnetic, this makes the separation of the composite simple,and the ability to reuse the composite is more applicable.

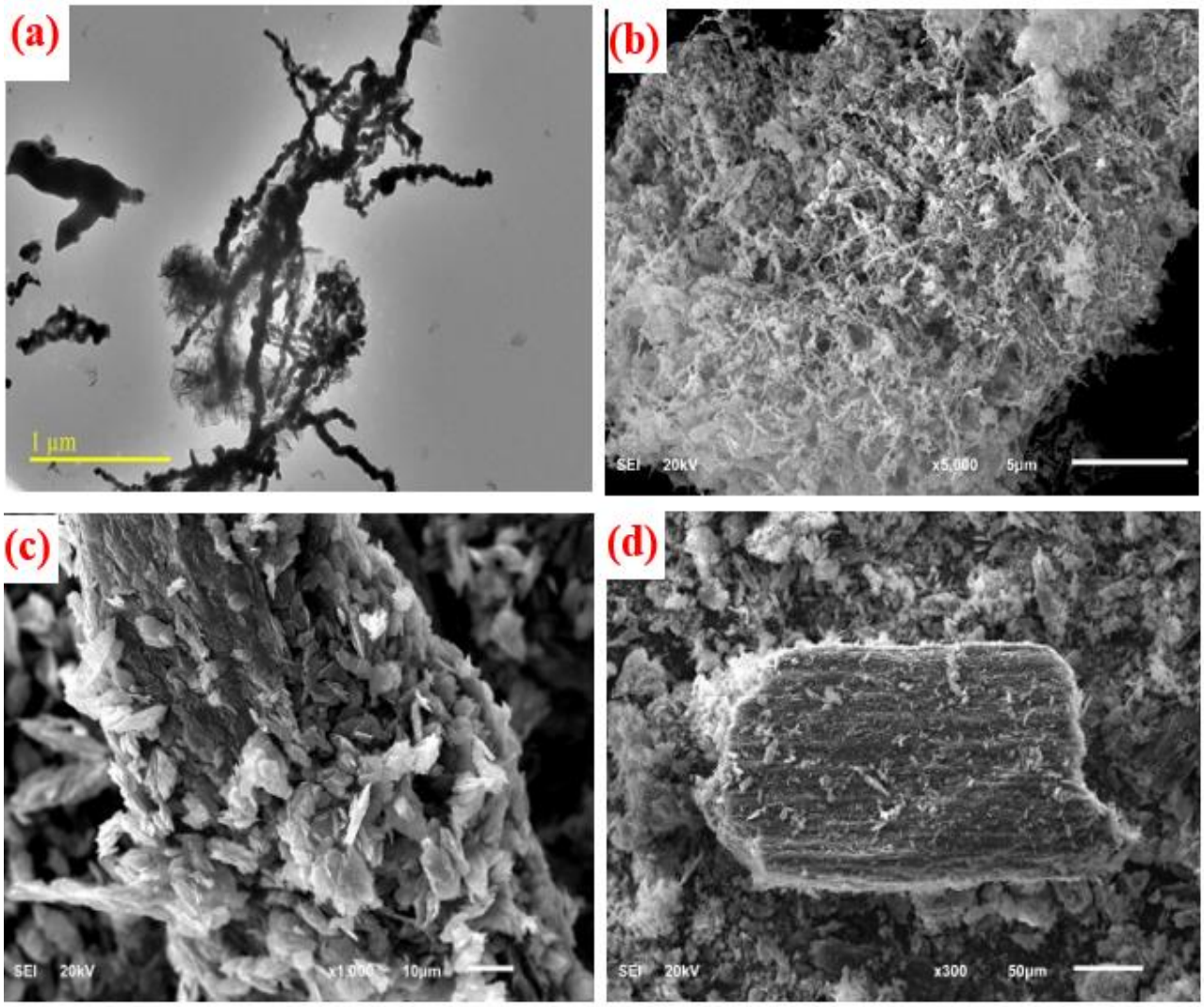

Figure 3.1:(a) TEM (b) SEM images of Fe^0, (c) SEM image of grinded PG (d) SEM image of PG-Fe^0 composite.

3.1.2-EDS characterization

Energy-dispersive X-ray spectroscopy (EDS) analysis was used to evaluate the surface element of composition of PG, Fe^0 and PG-Fe^0 composite. The EDS spectra of PG, Fe^0 and PG-Fe^0 composite are shown in Figures 3.2, 3.3, and 3.4, respectively.

As shown in Figure 3.2, and table 3.1 (EDS results), the weight percentage composition of C was about 79.5%, O was ~ 7.8%, and Si was ~ 12.7%. The element analysis illustrated by the EDs spectrum revealed the absence of Fe. The coating is the only source of auto element, the fiction conductivity.

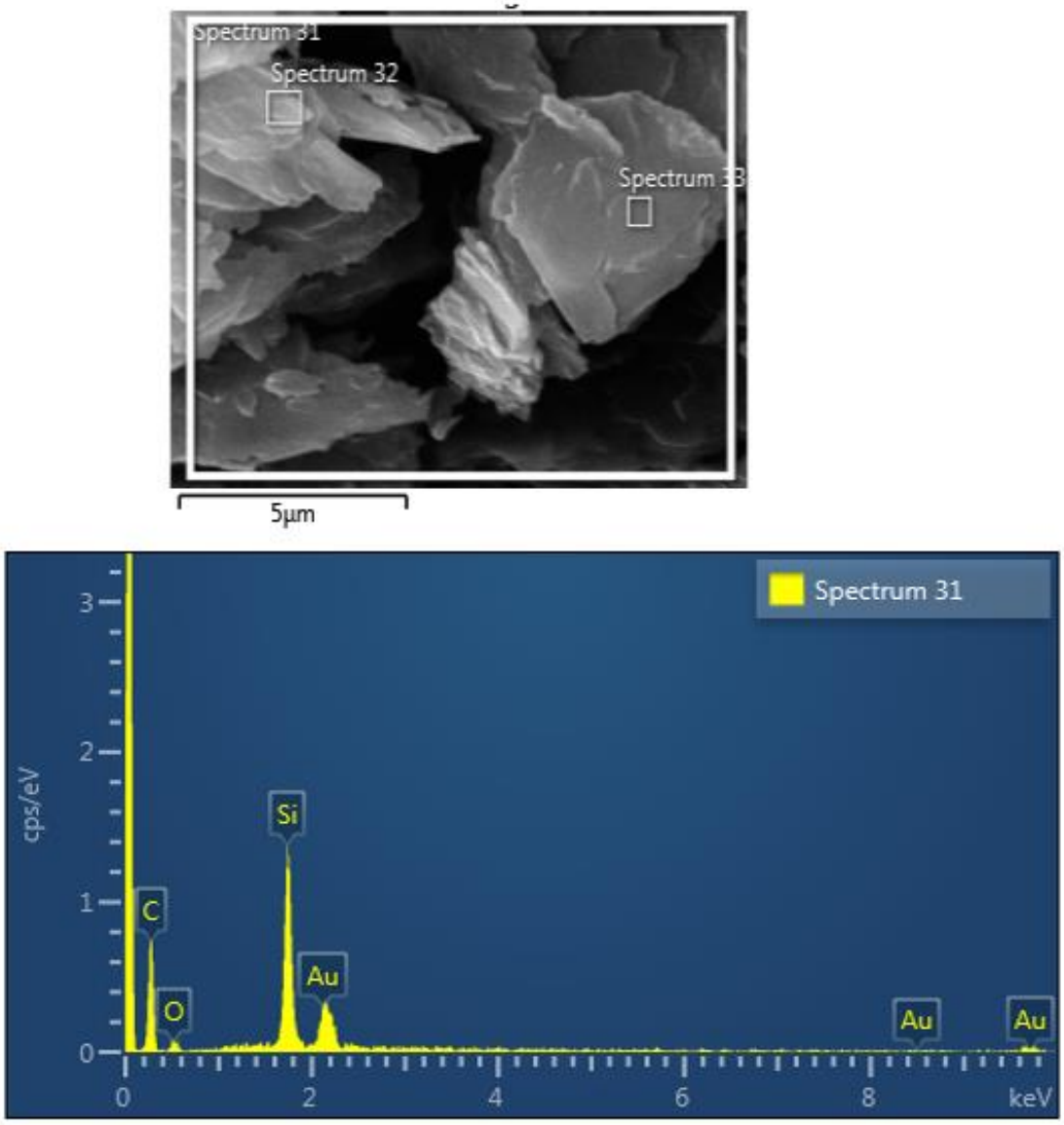

Figure 3.2: EDS spectrum for a selected area of PG.

Table 3.1: Element's analysis of pencil graphite.

Element	Line Type	Apparent Concentration	k Ratio	Wt%	Wt% Sigma	Standard Label	Factory Standard
C	K series	17.12	0.17116	79.48	1.60	C Vit	Yes
O	K series	2.16	0.00726	7.79	1.59	SiO_2	Yes
Si	K series	14.96	0.11857	12.73	0.65	SiO_2	Yes
Total:				100.00			

As shown In Figure 3.3, and table 3.2, EDS analysis verified the integrated mode's percentage composition by showing Fe^0 composition approximately 56.1 5%, oxygen 23.07%, and Carbon 20.17%.

Selected area of EDS analysis was used to distinguish between dark and light areas (where in back-scattered SEM mode, the light areas stand for high atomic number elements and the dark ones for lighter elements). The Fe^0 composition in the light area appeared to be higher than the average, and vice versa in the dark area (, Figure 3.3). [143] The concept of having several degrees of oxidation on the nZVI surface was supported by the obtained results.

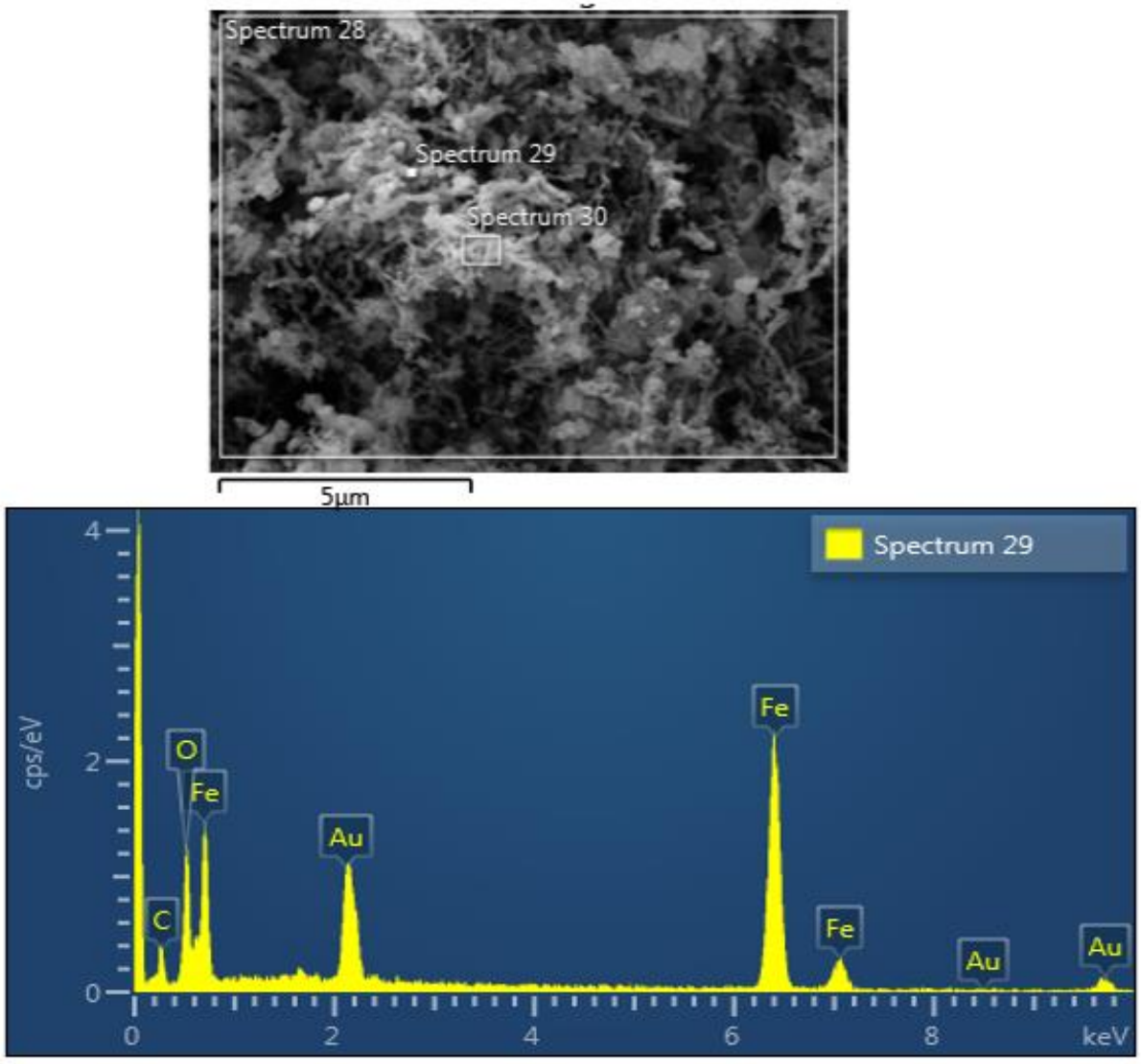

Figure 3.3: EDS spectrum for a selected area of Fe^0.

Table 3.2: Elemental analysis of Fe^0.

Element	Line Type	Apparent Concentration	k Ratio	Wt%	Wt% Sigma	Standard Label	Factory Standard
C	K series	3.26	0.03260	20.78	1.76	C Vit	Yes
O	K series	18.19	0.06123	23.07	0.97	SiO_2	Yes
Fe	K series	53.31	0.53313	56.15	1.43	Fe	Yes
Total:				100.00			

Figure 3.4 and table 3.3 show EDS elemental analysis of PG-Fe^0 composite, the results indicated that the weight percentage composition of C was about 71.79%, O was about 17.34%, and Si was about 2.38%. In addition, the EDS spectrum confirmed the presence of Fe^0 with a percentage of ~ 8.49.

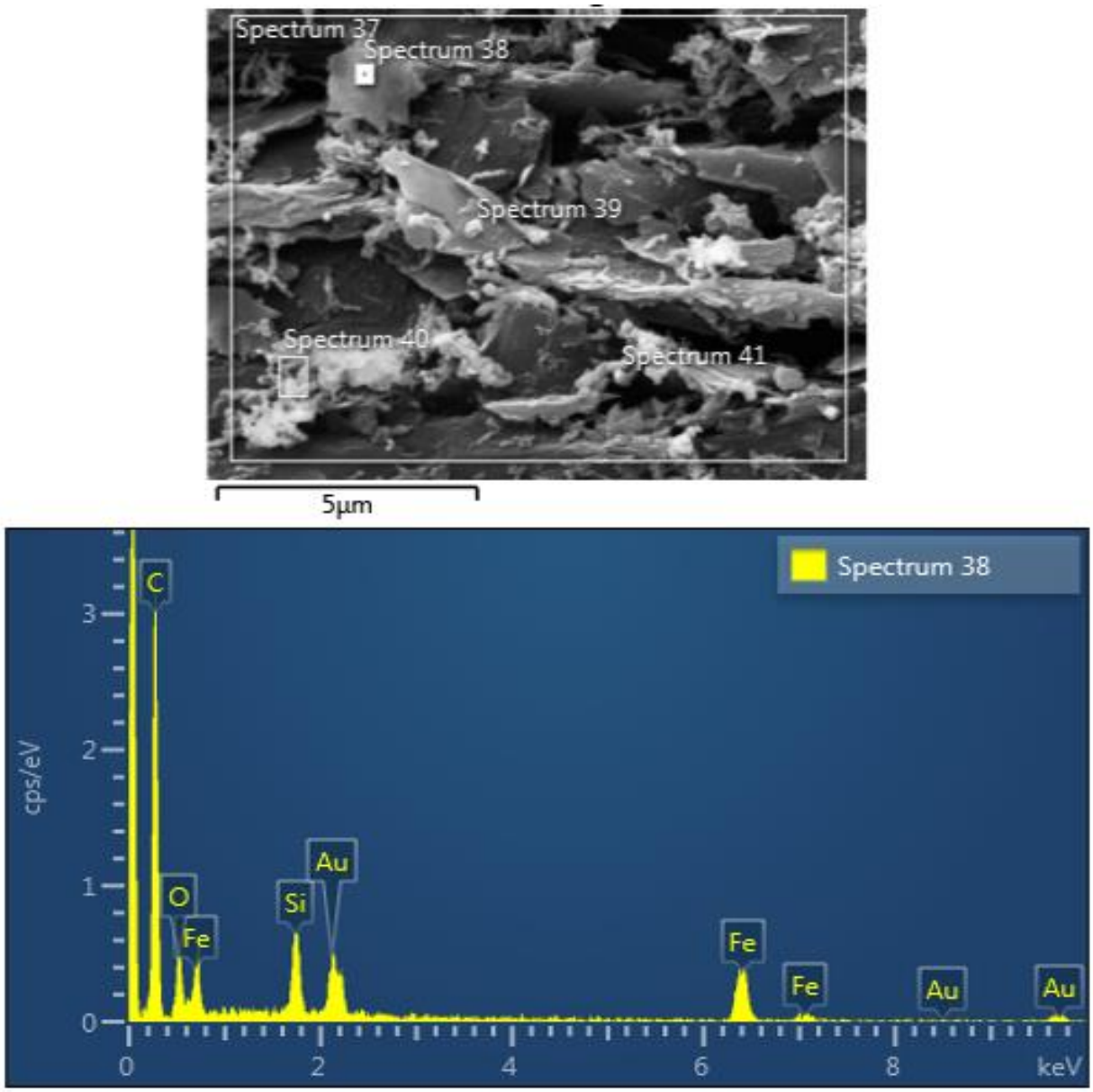

Figure 3.4: EDS spectrum for a selected area of PG-Fe^0 composite.

Table 3.3: Element analysis of PG-Fe^0 composite.

Element	Line Type	Apparent Concentration	k Ratio	Wt%	Wt% Sigma	Standard Label	Factory Standard
C	K series	47.96	0.47964	71.79	1.41	C Vit	Yes
O	K series	11.55	0.03885	17.34	1.43	SiO_2	Yes
Si	K series	4.96	0.03928	2.38	0.18	SiO_2	Yes
Fe	K series	15.54	0.15540	8.49	0.51	Fe	Yes
Total:				100.00			

3.1.3-XRD characterization.

X-ray powder diffraction (XRD) was used to determine the structure and crystal morphology of PG, Fe^0 and PG-Fe^0 composites. Results of XRD are shown in Figure 3.5. In the X-ray diffraction pattern (XRD), graphite showed characteristic peaks at $2\theta = 26.7^0$ and $2\theta = 55^0$ as shown in Figure 3.5 (a). XRD was used to characterize the structure of Fe^0 to provide evidence about the presence of crystalline zero-valent iron in the sample. As shown in (Figure 3.5 (b)), the basic reflection of metallic iron zero at $2\theta = 44.9°$ (110 reflection); the reflection peak of iron oxide was very weak, indicating that nZVI is the main composition of iron nanoparticle materials.[146]

(Figure 3.5 (c)) shows the (XRD) spectrum of PG-Fe^0 composite the main at diffraction angles occurred at (2θ) 26.70, 44.9° and 55, respectively, these might be attributed to the reflections of (002), (110) and (004), respectively.

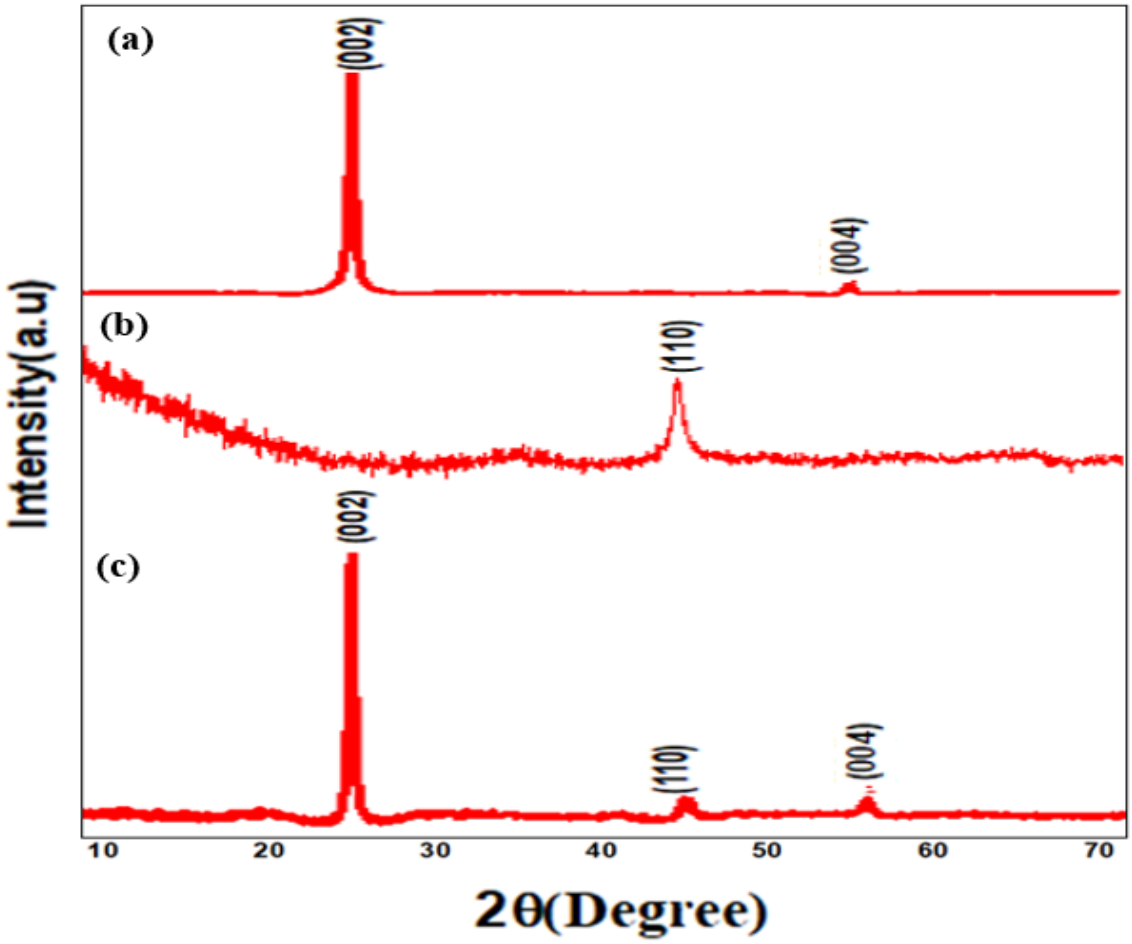

Figure 3.5: XRD patterns of (a) PG (b) Fe^0 (c) PG-Fe^0 composite.

3.1.4-FT-IR characterization.

The adsorption of LEV on the surface of synthesized PG-Fe^0 composite was characterized by FTIR spectroscopy (Figure 3.6). FTIR spectra of (a) LEV (b) PG-Fe^0, and (c) PG-Fe^0 - LEV composite was obtained in the range of 4000-400 cm^{-1}. The spectrum of LEV in Figure 3.6 (a) showed a prominent band at 3264 cm^{-1}, corresponding to –COOH group, in addition to bands at 3031 cm^{-1} (–CH– stretching), 1724 cm^{-1} (–C=O), 1291 cm^{-1} (C–N), and 1085 cm^{-1} for fluorine. The IR absorbance bands of PG-Fe^0 composite are illustrated in Figure 3.6 (b). The stretching bands of Fe-O on the iron oxide thin layer occurred at 800 and1200 cm^{-1} [147-148]. Therefore, these results were compatible with the oxidation bands appeared in the spectrum of PG-Fe^0composite after adsorption of LEV. This supports the partial oxidation of nZVI on the composite's surface, as shown in Figure 3.6 (c).

Additionally, the same characteristic peaks of LEV were observed in the spectrum but with lower intensity, e.g., (V_{as}, COO) at 1500 cm^{-1}. Figures 3.6 (b) and 3.6 (c) depicted the characteristic peaks at 1200 cm^{-1} which belong to the presence of Fe-O stretching mode. In addition, by comparing the relative intensities of distinct Fe-O and C-O bands, it was observed that the enhancement in signal intensity of Fe-O stretching and decrease in the intensity of C-O stretching (1282 cm^{-1}) after adsorption is due to the

formation of a surface complex, which supports the sorption phenomenon between adsorbent and adsorbate (Fig.3.6 c). Moreover, the spectra show two distinct peaks indicating the presence of the O-H group on the surface of magnetite nanoparticles. These strong bands appeared at 3420 cm^{-1}, and 1629 cm^{-1}, respectively; these bands correspond to O-H stretching and bending, respectively [149].

The most distinct peaks of LEV appeared in the spectra (a, c). The stretching vibrations of the C-H methyl band were detected at 2500–3600 cm^{-1}, the C-C ring bend at 707 cm^{-1}, and the C-C ring stretch at 1623 cm^{-1}. The asymmetric and symmetric stretching vibrations of O-C-O appeared ~ 1542 cm^{-1} and 1472 cm^{-1}, respectively. While, C-O stretch appeared at 1729 cm^{-1}, and C-N stretch band appeared at 1294 cm^{-1}.[150]

The peaks observed in the 1100 cm^{-1} to 1400 cm^{-1} range suggested the existence of C-H group. In the FTIR, overall modifications appeared; adsorption of LEV through PG-Fe^0 composite was shown by spectra.

Furthermore, some peaks were shifted, like C–C stretching vibration, which was found shifted to 468 cm^{-1}, suggested that the F atom participated in the adsorption process.

These changes indicated that the oxygen atoms of the carboxylate group (-COO-) were merged into the interaction between LEV and PG-nZVI composite after adsorption. Additionally, the presence of hydrogen acceptors like (-NH) and a hydrogen donor (OH groups) on the surface of PG-Fe^0 composite favored the formation of H bonds with adsorbents LEV.

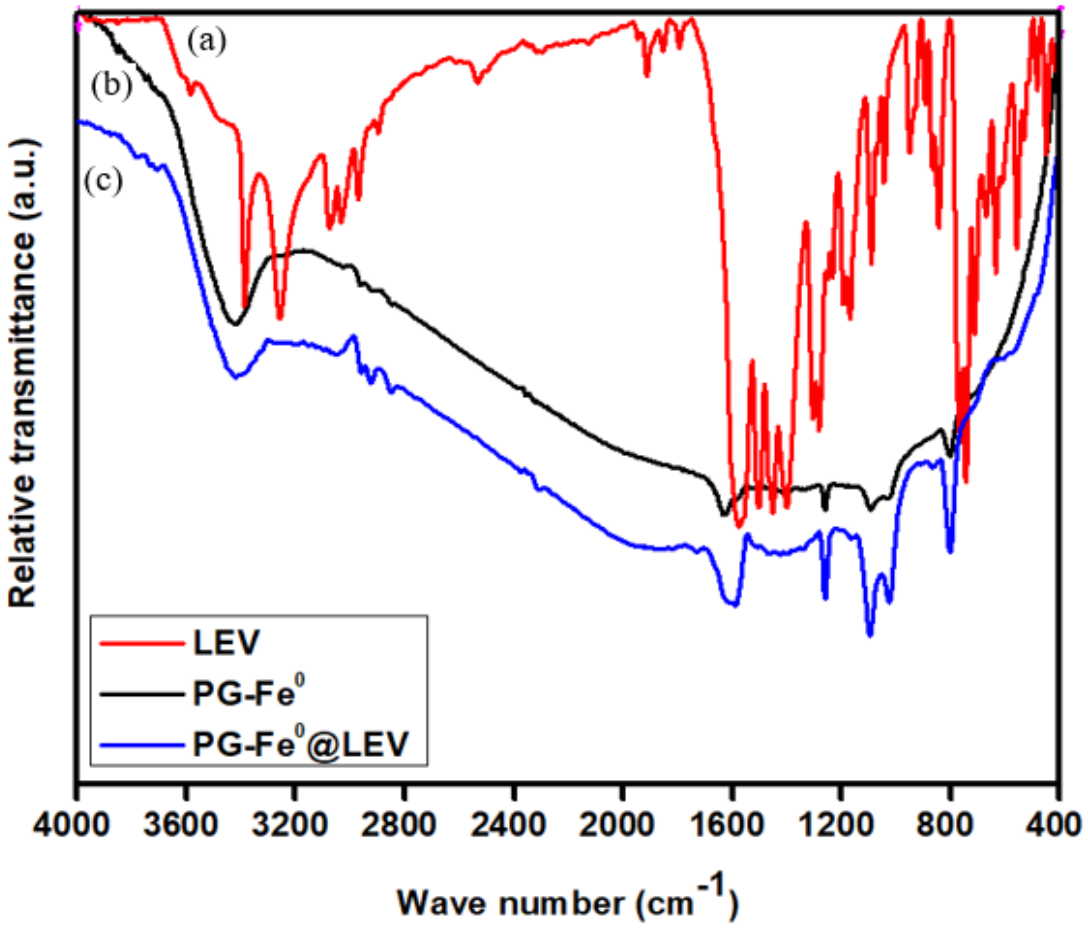

Figure 3.6: FTIR spectra of (a) LEV, (b) PG-Fe^0 composite (c) PG-Fe^0-LEV compos

3.2-Effect of Adsorbent Type

Different types of adsorbents were used in this research of PG-Fe_3O_4 composite, Fe^0, and PG-Fe^0 composites were used to study the removal of LEV from aqueous solution. The experimental results showed that at 298K, at pH of 3.0 and =8.0. The composite of PG-Fe_3O_4 showed no removal efficiency towards LEV at both pH shows in Figure 3.7(a,b).

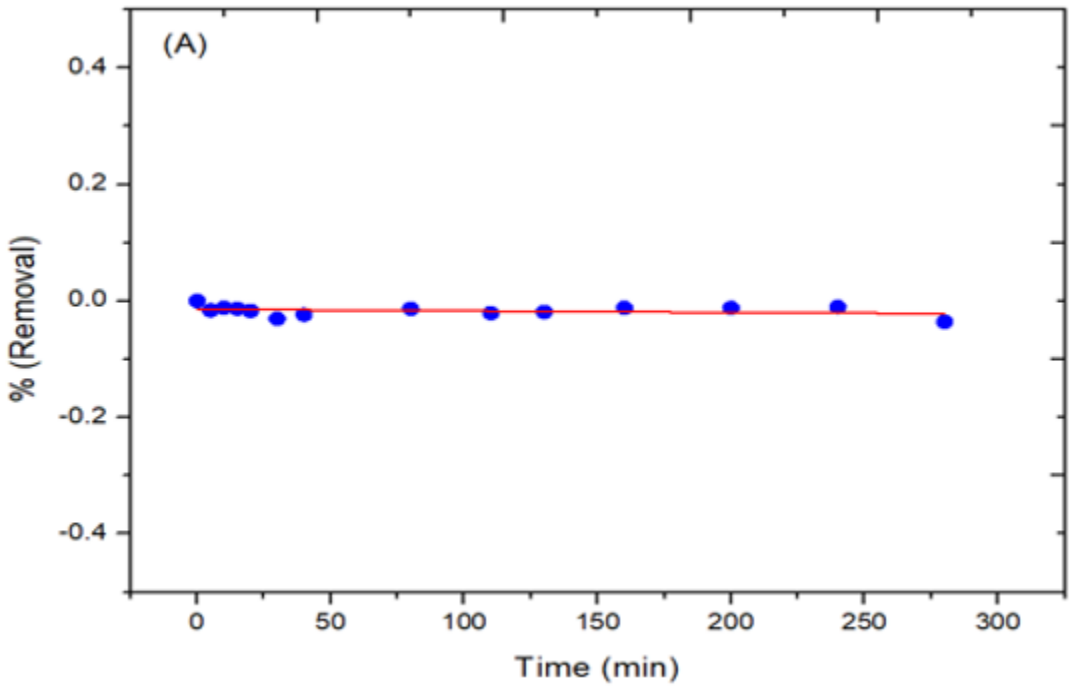

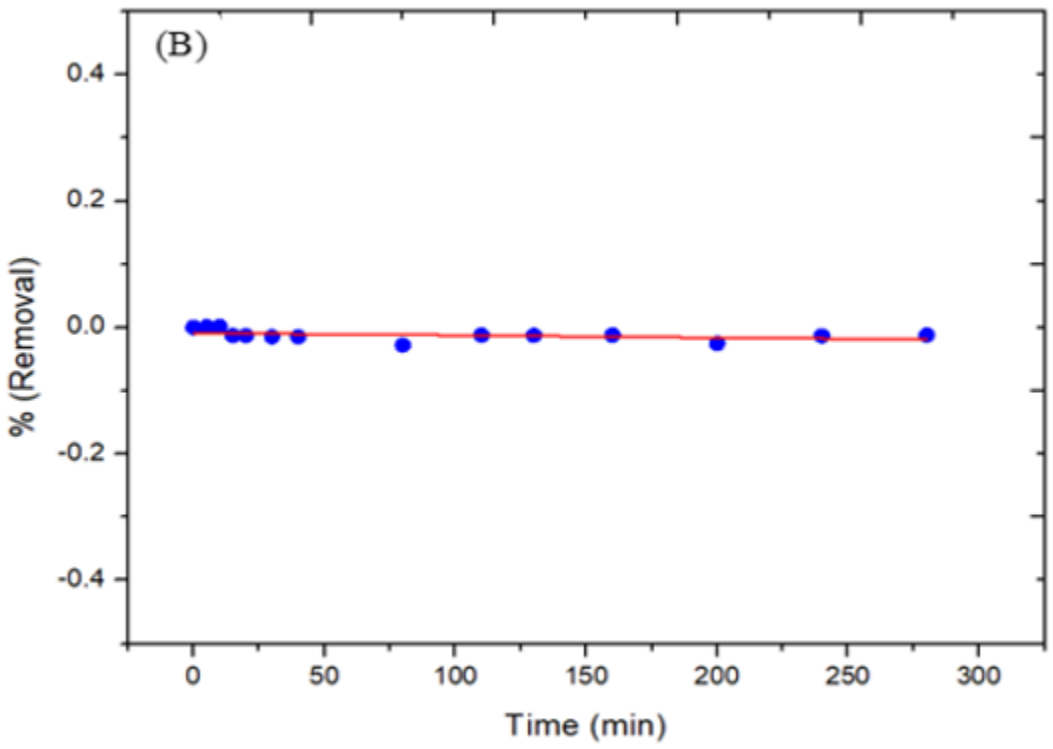

Figure 3.7: Percentage removal of LEV via 0.5g of PG-Fe_3O_4 composite, a) pH=3 b) pH=8 (Initial conc.:10 mg/L, 298K).

The PG-Fe_3O_4 composite was no removal efficiency of LEV, the removal is about~ 0% for 280 minutes, at 298 K, at pH of 3.0, and =8.0. As shown in figure 3.7(a,b).

The experimental results at 298K, PG-Fe^0composite showed better removal efficiency for LEV compared to that obtained with the adsorbent Fe^0 NPs. Figure 3.8 showed the removal percentage of LEV via different synthesis adsorbents.

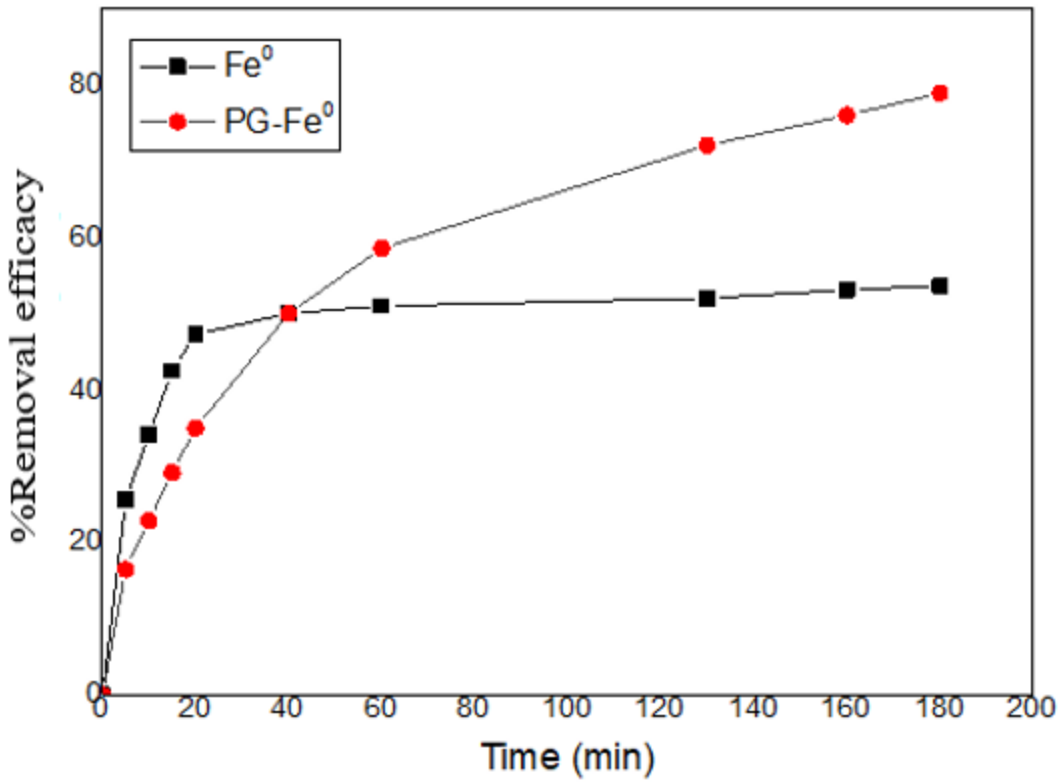

Figure 3.8: The percentage removal of LEV two types of adsorbents, a) Fe^0NPs b) PG-Fe^0 composite (initial conc.:10 mg/L, 298K, pH=6.5).

PG-Fe^0 composite removal efficiency for LEV was about 78% for 180 minutes, compared to ~53% via Fe^0 NPs. However, the removal efficiency was attributed to Fe^0 in composite, and the PG had no capacity for LEV and. It works as a support for Fe^0.

3.3-LEV Removal kinetics

Kinetic experiments were performed to study the adsorption rate and the kinetic mechanism of the adsorption process. The experimental condition was applied at 298K at 20.0 mg/L, the adsorption time of LEV. The mass balance equation (eq.1) was used to calculate the amount of LEV adsorbed via the PG-Fe^0 composite surface.[151]

$$Q = (C_0 - Ce)\frac{V}{m} \ldots\ldots\ldots\ldots (1)$$

Where Q is the concentration of LEV removal by adsorbent (mg/g).

C_0 is the initial concentration of LEV (mg/L).

C_e is the LEV concentration in solution at a given time.

V is the volume of solution (L)

m is the mass of adsorbent(mg)

Figure 3.9 demonstrates the impact of contact time on removal LEV concentrations by using PG-Fe^0 composite at pH=6.5,8.

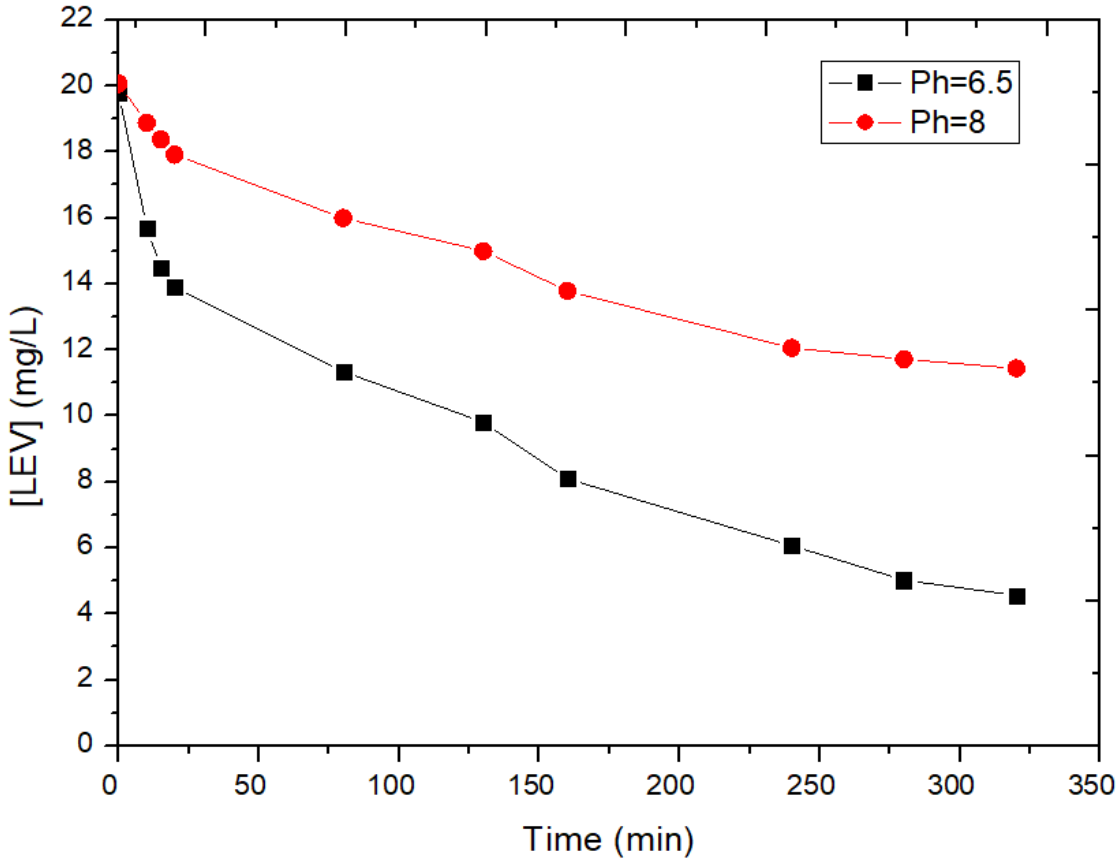

Figure 3.9: Effect of contact time on the removal of LEV using PG-Fe^0 composite. (At concentration: 20 mg/L, pH=6.5, and 8. 298K).

As illustrated in Figure 3.9, the concentration of LEV in an aqueous solution decrease over time, but its adsorption on two pH increases. As a result, LEV's removal efficiency rises for a short time before becoming practically unchanged once equilibrium is established.

The percentage for LEV removal was determined using the following equation:[152]

$$\%\ Removal = \frac{C_0 - C_e}{C_o} * 100\% \ldots\ldots\ldots\ldots (2)$$

Where C_0 is the initial concentration of LEV in the solution (mg/L),

C_e is the equilibrium concentration of LEV in the solution (mg/L).

Also, the removal percentage is demonstrated in figure 3.10.

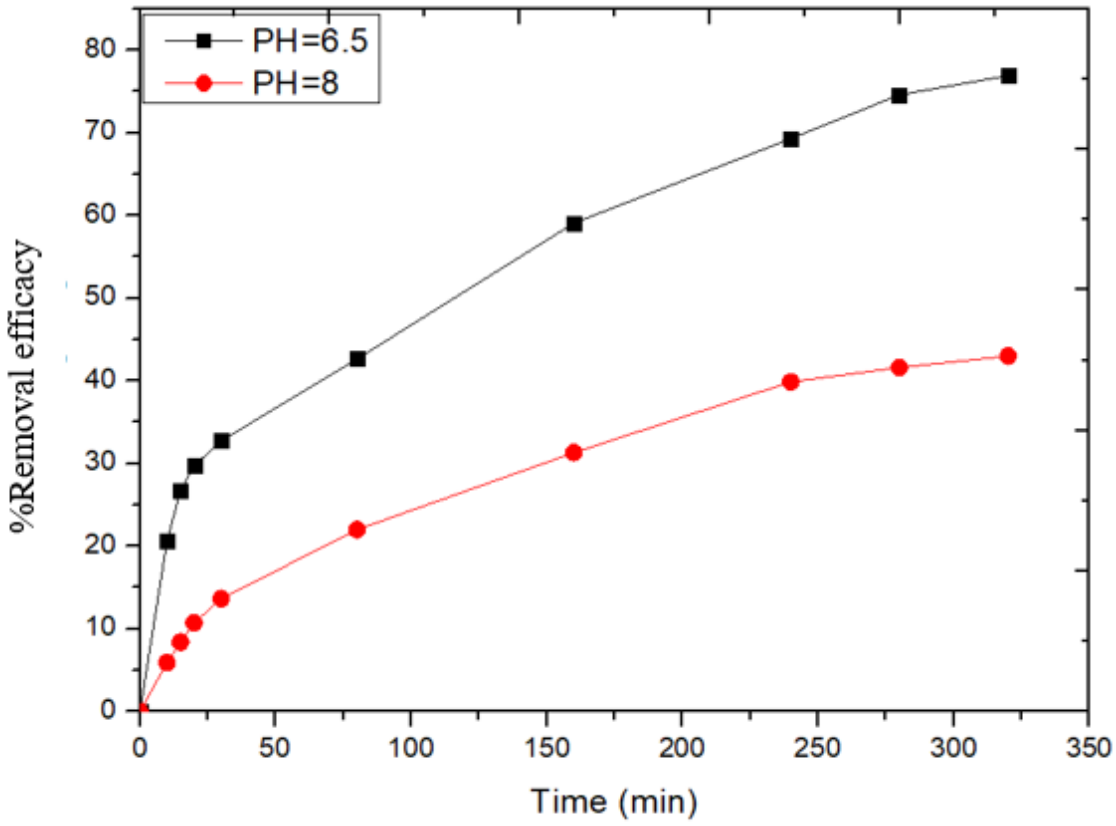

Figure 3.10: Effect of contact time on the adsorption of LEV by using PG-Fe^0 composite. (At concentration 20 ppm, pH=6.5,8 .298K).

As shown in Figures 3.10, the elimination of both pH LEV increased with increasing contact time until 180 minutes, from 0% to 60% at pH=6.5 and

from 0% to 35% at pH=8.0, then the removal gradually increased until equilibrium was reached at 320 minutes.

In addition, the removal efficiency for PG-Fe^0composite was greater at pH=6.5 (removal efficiency of ~78%) compared to that obtained at a pH of ~ 8.0 (where removal efficiency was ~40%). This difference in removal efficiency might be attributed to the different electrostatic attraction between the adsorbent and adsorbent acidic and basic medium; however, more explanations are presented at the next section.

The following methods were used to study the adsorption mechanism: pseudo-first-order kinetic model, pseudo-second-order kinetic model and intra-particle diffusion model. [153-154]

The experimental data of LEV adsorption by PG-Fe^0 composite shown in Figures 3.11and 3.12 were tested by Lagergren pseudo first-order and pseudo-second-order models. [155-156.]

The linear Lagergren pseudo-first-order model represented as:[157]

$$Ln(q_e-q_t) = lnq_e-K_1t \ldots\ldots\ldots\ldots (3)$$

Where q_e and q_t are the amount of LEV adsorbed by the adsorbent at equilibrium and at any time (mg/g), respectively.

k_1: is the first-order rate constant (min^{-1})

t: contact time (min).

The relationship was obtained by plotting ln (qe-qt) Vs contact time. The results of this relationship are plotted in Figure 3.11and Figure 3.12, where the values of k_1 and q_e were obtained from the slope and intercept, respectively.

Furthermore, Shahwan (2015) also attempted using an updated Lagergren equation. Q_e is replaced in this form with q_m[158]

$$\ln (Q_{max} - Q) = lnQ_{max} - kt \ldots\ldots\ldots\ldots\ldots (4)$$

Q_{max} can be calculated by:

$$Q_{max} = (V/m) * C_0 \ldots\ldots\ldots\ldots\ldots\ldots (5)$$

Where:

V is the volume of solution (L).

m is the mass of adsorbent(mg)

C_0 is the initial concentration of LEV (mg/L).

The kinetic data of the PG-Fe^0 composite case were plotted using the two equations as shown in Fig 3.11. and Fig 3. 12. Both equations (original and modified Lagergren equations) yielded similar results as could be seen in Table 3.4.

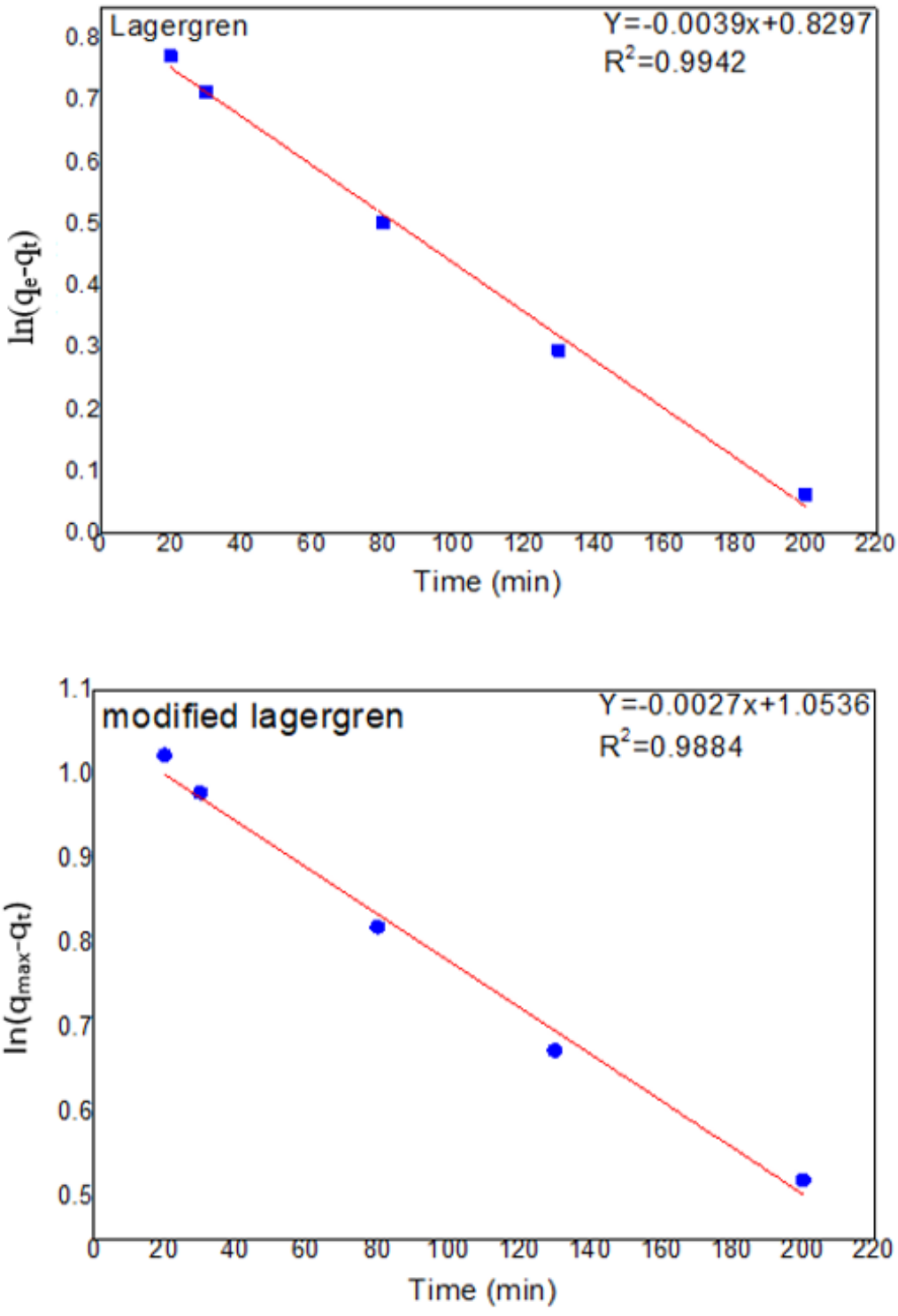

Figure 3.11: Pseudo-first-order linear fit for PG-Fe^0 composite using original Lagergren equation and modified Lagergren equation at pH=6.5.

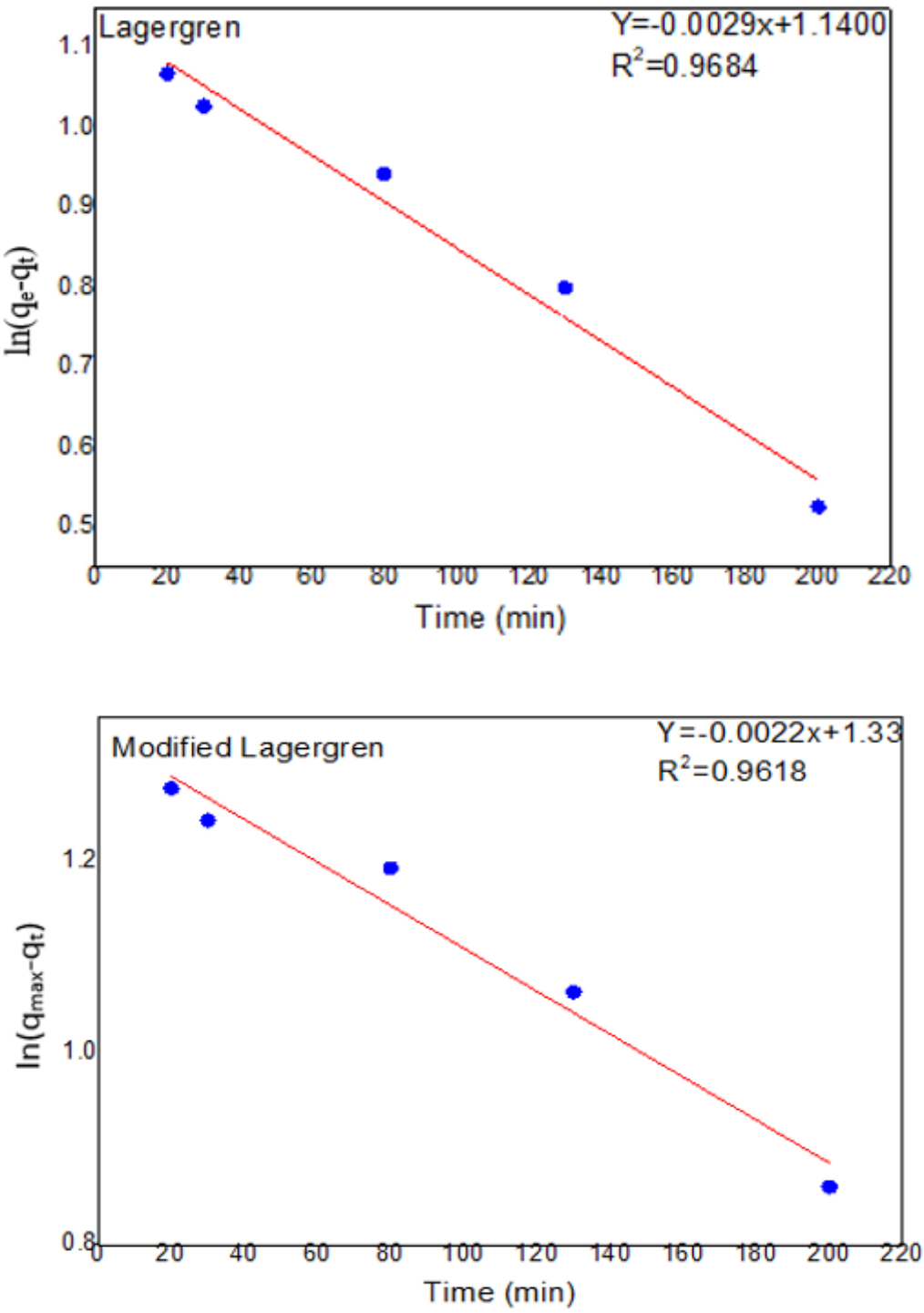

Figure 3.12: Pseudo-first-order linear fit for PG-Fe^0 composite using original Lagergren equation and modified Lagergren equation. at pH=8.

The extracted parameters from Figure 3.11 and Figure 3.12 were tabulated in table 3.4.

Table 3.4: Kinetic parameters for LEV adsorbents using PG-Fe^0 composite.

PH=6.5	Modified Lagergren Equation	Original Lagergren Equation
Slope	-0.0027	-0.0039
Intercept	1.0536	0.8297
Coefficient of determination, r^2	0.9884	0.9942
Rate constant, k (min^{-1})	0.0027	0.0039
Experimental Q_e (or Q_m) (mg/g)	3.956827	3.3400133
Model value of Qe (or Q_m) (mg/g) 0.5g of PG-Fe^0 composite	2.867	2.292
Effective mass Q_{max} 80mg	17. 91	14.325
pH=8	Modified Lagergren Equation	Original Lagergren Equation
Slope	-0.0022	-0.0029
Intercept	1.33	1.1400
Coefficient of determination, R^2	0.9618	0.9684
Rate constant, k (min^{-1})	0.0022	0.0029
Experimental Q_e (or Q_m) (mg/g)	4.013004	3.34001336
Model value of Q_e (or Q_m) (mg/g) 0.5g of PG-Fe^0 composite	3.781	3.126
Effective mass Q_{max} 80mg	23.63	19.53

Table 3.4 provides the Kinetic parameters extracted from Figures 3.11 and 3.12. Table 3.4. R^2 values were higher at pH of 6.5 when Lagergren equation was used (R^2 were 0.9942, and 0.9689) compared to those obtained at a pH of 8.0 when Eq. (4) was used (R^2 were 0.9884, and 0.9618).

Based upon these results, the two equations appeared to be yielding similar outcomes as the percentage of LEV elimination increased. The results showed that the Lagergren equation was better linked to a higher-level Extent of sorption.[159] This is sensible because the Q_e value was closer to the Q_{max} value when the extent of the sorting grows.[159]

Another kinetic model was studied to fit with the experimental data; the linearized pseudo-second-order model as given by H_o:[160]

$$\frac{t}{Q} = \frac{1}{k_2\, Q_e^2} + \frac{1}{Q_e}\, t \ldots\ldots\ldots\ldots\ldots (6)$$

Where Q is the amount of the LEV adsorbed on the adsorbent (mg/g).

Q_e: is the amount of the LEV adsorbed on the adsorbent at equilibrium (mg/g).

$k_{2:}$ is the rate constant of the pseudo-second-order adsorption (g .mg^{-1} min^{-1}).

t: is the contact time (min).

The linear fits obtained by pseudo-second-order kinetics is shown in Figures 3.13 and 3.14, respectively.

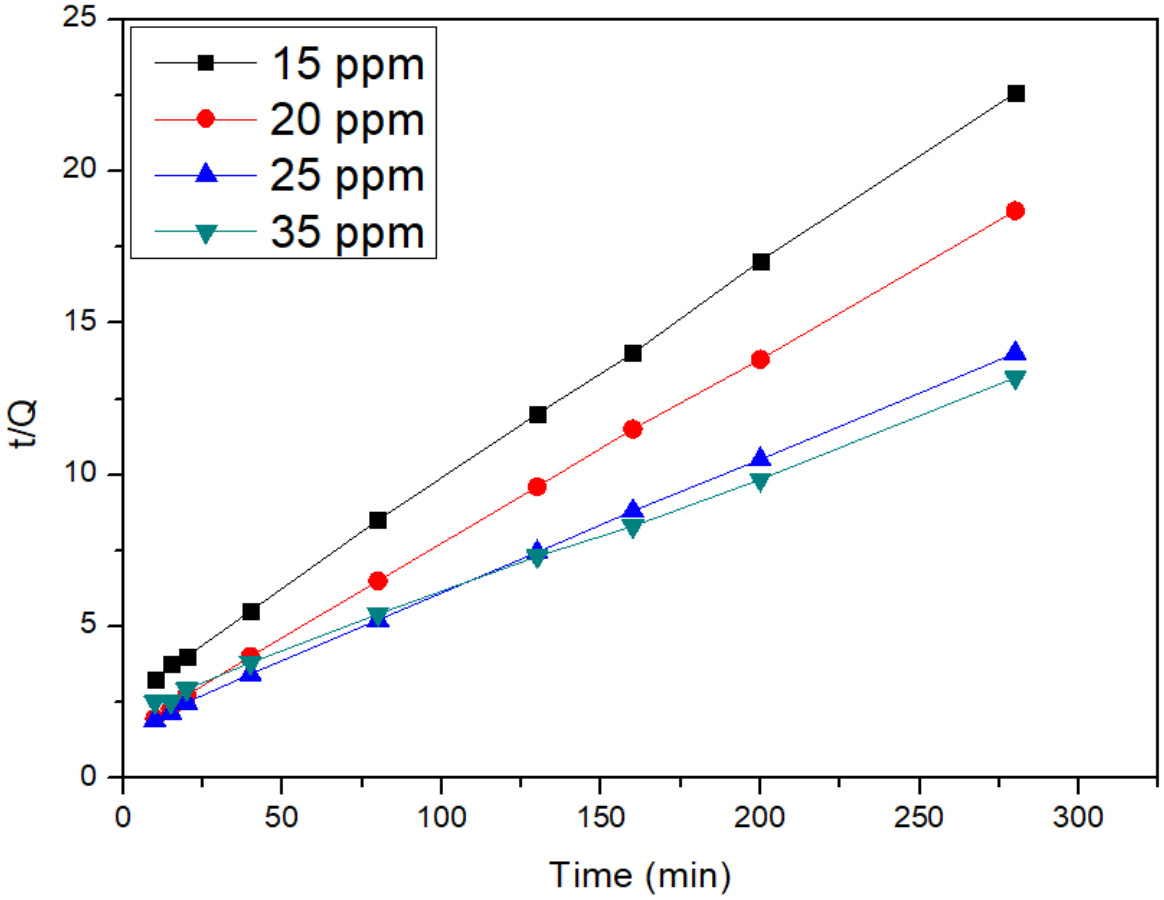

Figure 3.13: Pseudo-second-order linear fits for the removal of LEV byPG-Fe^0 composite at pH=6.5

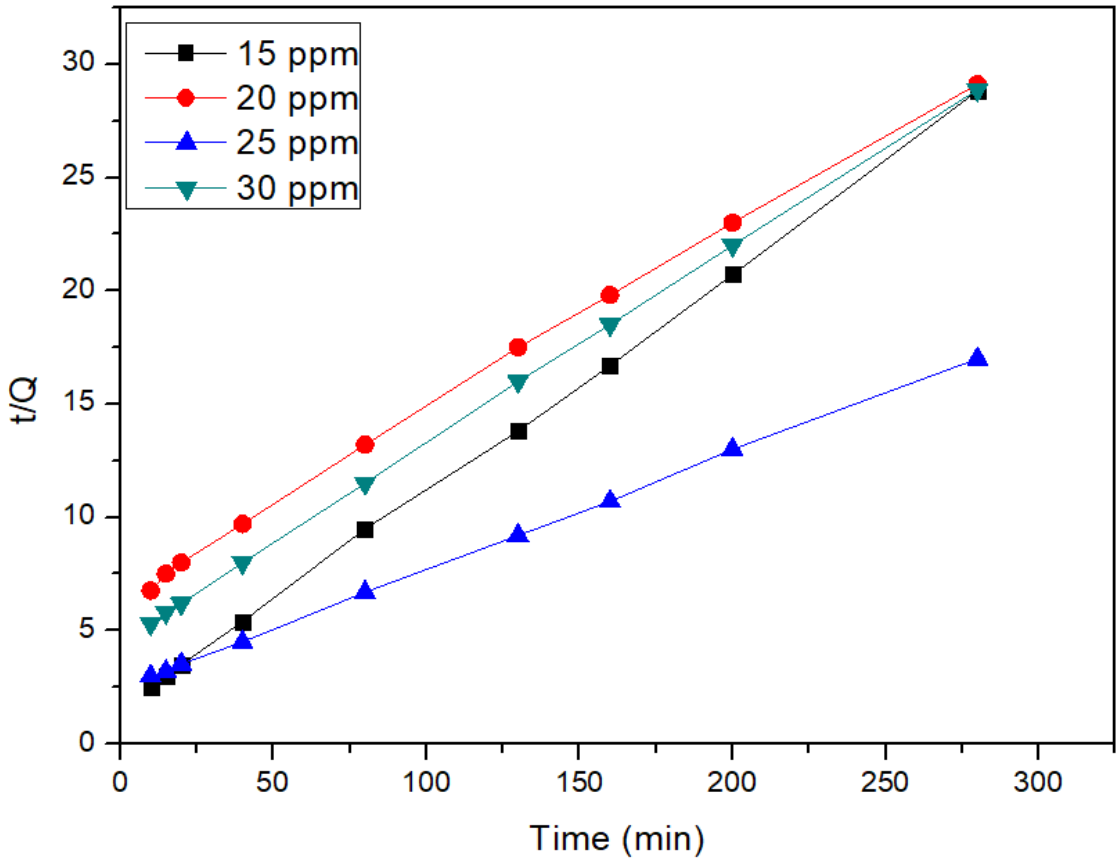

Figure 3.14: Pseudo-second-order linear fits for the removal of LEV byPG-Fe^0 composite at pH=8.

The extracted parameters from Figure 3.13 and Figure 3.14 were tabulated in Table 3.5.

Table 3.5: Kinetic parameters of LEV adsorption using PG-Fe^0 composite at 298K

pH=6.5	**Pseudo-second-order**			
Concentration mg/L	K_2 (g/(mg.min))	Qe (exp) (mg/g)	Q_{cal} (mg/g)	R^2
15	0.001652846	12.39678154	14.36781609	0.9998
20	0.001315397	17.96261378	19.08396947	0.9997
25	0.001225532	20.64255526	23.14814815	0.9971
35	0.000416207	24.50585176	30.76923077	0.9951
pH=8	**Pseudo-second-order**			
Concentration mg/L	K_2 (g/(mg.min))	Qe (exp) (mg/g)	Q_{cal} (mg/g)	R^2
15	0.003931671	9.71765153	10.72961373	0.9965
20	0.000973385	9.617197664	12.37623762	0.9816
25	0.00076889	19.17896618	21.64502165	0.9764
30	0.002470054	9.45058518	10.88139282	0.9825

Table 3.5 provides the kinetic parameters extracted from Figures 3.13 and 3.14 the data was more fitted with pseudo-second-order model than the pseudo-first-order model. Table 3.5 shows that R^2 values were greater than 0.99 at pH of 6.5, but lower than 0.99 at pH of 8.0.

At all concentrations, Q_{cal} was greater than Q_{exp}. At pH=6.5 and 8.0, the Q climbed from 15 ppm to 25 ppm, then declined to 30 ppm, according to the retrieved data. At pH 6.5, however, the Q increased from 15 to 35 ppm.

In liquid solid adsorption system, the relationship between Q and t can be clarified using different kinetic models. This study used the pseudo second-order rate equation defined by H_o Equation and Shahwan Equation. These two equations were derived using two separate methods. Although these two equations look identical, they are different in the way they explain the Q_e or Q_m, as well as in the method of determination of the rate constant (k).

The nonlinear form of the H_o equation is [161]

$$Q = \frac{k.t.Q_e^2}{1 + k.Q_e.t} \dots\dots\dots\dots\dots\dots\dots\dots (7)$$

Where Q_e is the experimental value of Q at the equilibrium, and k is the rate constant.

On the other hand, the nonlinear and linearized forms of the Shahwan equation are given as:

$$Q = \frac{Q_m C_0 k_2 t}{C_0 k_2 t + 1} \dots\dots\dots\dots\dots\dots\dots (9)$$

It could be linearized to;

$$\frac{t}{Q} = \frac{1}{Q_m C_0 k_2} + \frac{1}{Q_m}\, t \ldots\ldots\ldots\ldots\ldots (10)$$

Where Q_m is the maximum amount of solute that would be sorted if the sorption reaction goes to completion (equals to V/ m multiplied by C_0), and k is the rate constant.

The data used in the plots correspond to the pre-equilibrium stage of the experiments. Fundamentally, the kinetic analysis applies to the variation of concentration with time, which occurs during the initial stage of the experiment.[162]

Linear regression is the most commonly used method to obtain the parameters involved in the kinetic equations and also in predicting the best fitting kinetic expression.

The calculated kinetic rate constants. The corresponding coefficients of determinations (r^2) and theoretical Q values are given in Table 3.6.

Table 3.6: The kinetic parameters for adsorption LEV by using PG-Fe^0 composite of the pseudo-second-order linear fits using equations 6 and 10 at a PH=6.5, 8 and different concentrations at 298K.

PH=6.5	Concentration			
Ho Equation	15 ppm	20 ppm	25 ppm	35 ppm
Slope	0.0696	0.0524	0.0432	0.0325
R^2	0.9998	0.9997	0.9971	0.9951
intercept	2.9308	2.0874	1.5228	2.5378
k_2 ($g.mg^{-1}.min^{-1)}$	0.001652846	0.00131	0.0012	0.00041
$Q_{e\,(cal)}$ (mg/g)	14.36781609	19.08	20.6	24.5
$Q_{e\,(exp)}$ (mg/g)	12.39678154	17.9	23.1	30.7
Shahwan Equation	15 ppm	20 ppm	25 ppm	35 ppm
Slope	0.0696	0.0524	0.0432	0.0325
R^2	0.9998	0.9997	0.9971	0.9951
Intercept	2.9308	2.0874	1.5228	2.5378
k_2 ($L.mg^{-1}.min^{-1}$)	0.00465	0.00253	0.00173	0.00093
$Q_{m\,(cal)}$ (mg/g)	14.36781609	19.08	20.6	24.5
$Q_{m\,(exp)}$ (mg/g)	12.39678154	17.9	23.1	30.7
PH=8	Concentration			
Ho Equation	15 ppm	20 ppm	25 ppm	30 ppm
Slope	0.0932	0.0808	0.0462	0.0919
R^2	0.9965	0.9816	0.9764	0.9825
intercept	2.0903	6.7071	2.7764	3.419
k_2 ($g.mg^{-1}.min^{-1)}$	0.0039	0.00097	0.00077	0.0025
$Q_{e\,(cal)}$ (mg/g)	10.73	12.37	21.64	10.88
$Q_{e\,(exp)}$ (mg/g)	9.71	9.617	19.17	9.45
Shahwan Equation	15 ppm	20 ppm	25 ppm	30 ppm
Slope	0.0932	0.0808	0.0462	0.0919
R^2	0.9965	0.9816	0.9764	0.9825
Intercept	2.0903	6.7071	2.7764	3.419
k_2 ($L.mg^{-1}.min^{-1}$)	0.0062	0.004	0.0018	0.003
$Q_{m\,(cal)}$ (mg/g)	10.73	12.37	21.64	10.88
$Q_{m\,(exp)}$ (mg/g)	9.71	9.617	19.17	9.45

Since the linear plots of H_o and Shahwan equations are the similar, the slope and the intercept are identical.

As shown in Table 3.6, the results indicated that the rate constant of LEV removal by PG-Fe^0 composite at pH of 6.5 was higher than the that observed a pH of 8.0, suggesting a faster removal process by PG- Fe^0 composite at pH of 6.5.

The calculated value of k using H_o equation was less than that calculated using the Shahwan equation. To check which of the two equations provide a better correlation with the experimental results, the calculated k and Q values were substituted in the nonlinear equations 7 and 9, respectively, and the calculated Q (or the model prediction) values were plotted against the experimental values. As shown in Figure 3.15 a,b and Figure 3.16 a,b for PG-Fe^0 composite kinetic experiment, the nonlinear fit using Shahwan equation fitted the experimental data better than the H_o equation.

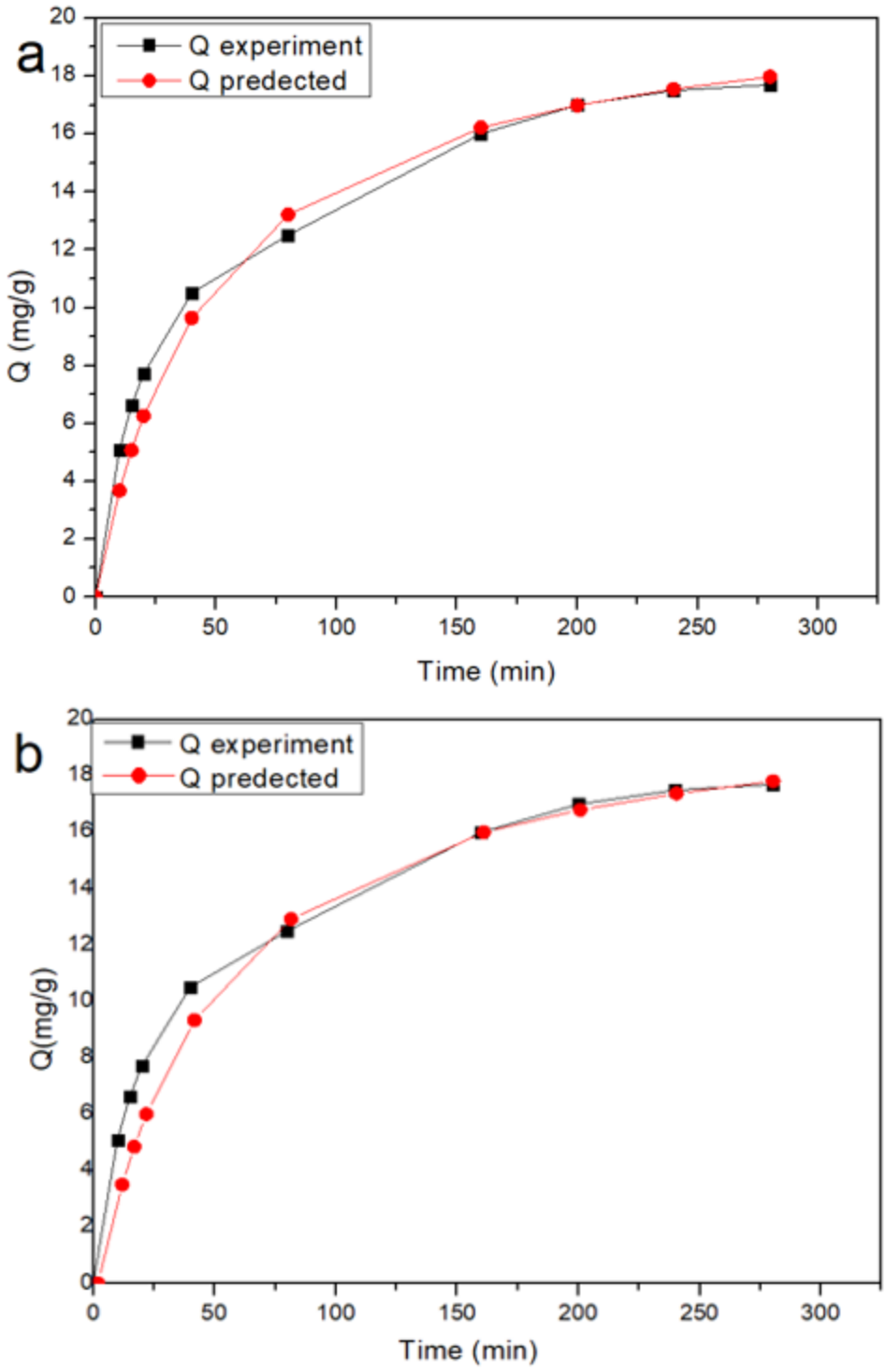

Figure 3.15: Nonlinear fits of the kinetic data of LEV removal by PG-Fe^0composite; at pH of 6.5 (a) using Ho equation (b) using Shahwan equation.

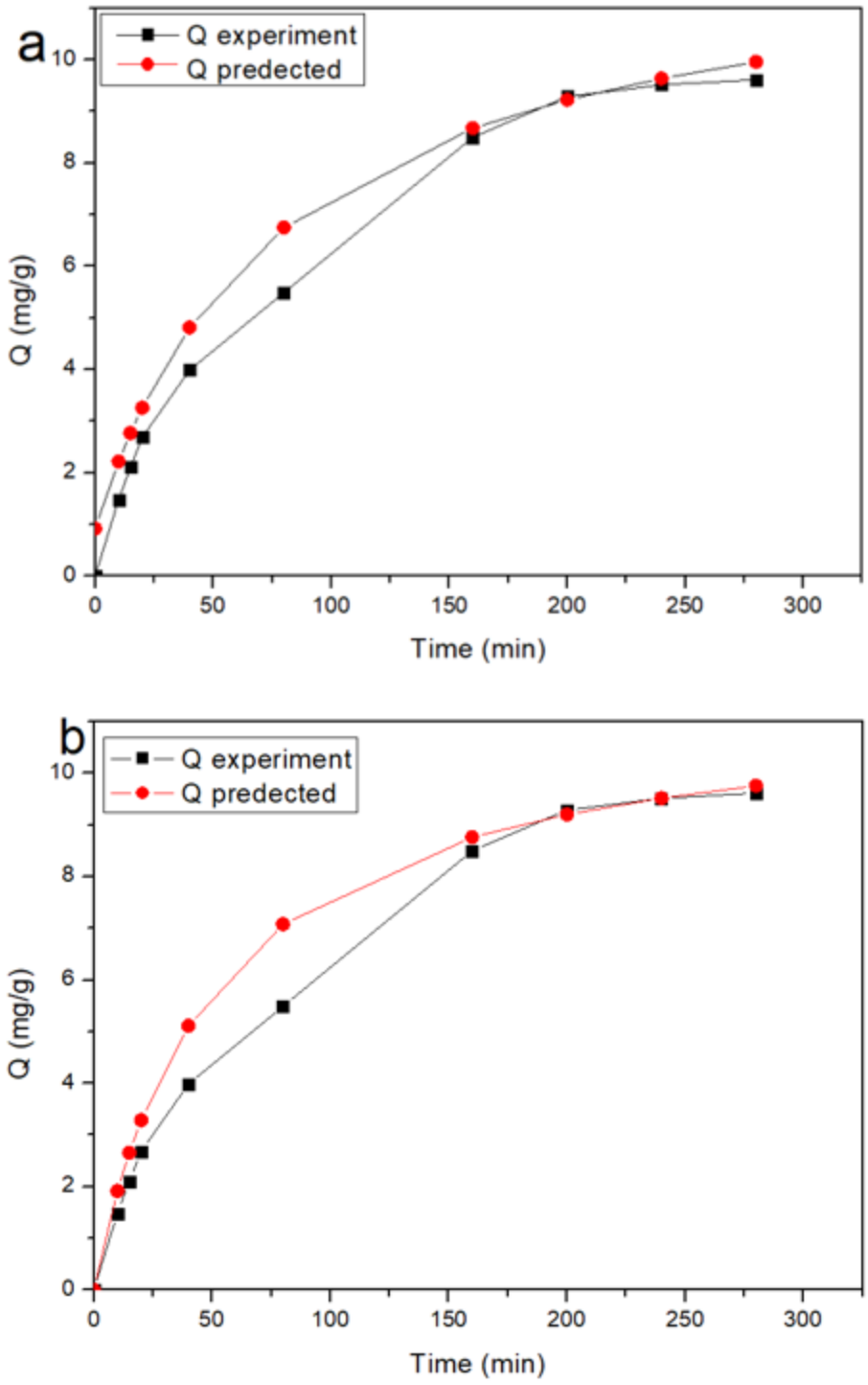

Figure 3.16: Nonlinear fits of the kinetic data of LEV removal by PG-Fe^0 composite; at pH of 8.0(a) using Ho equation (b) using Shahwan equation.

As a further test of the correlation, the Chi test was performed. For this purpose, the following equation was used:

$$\chi^2 = \sum_{1}^{n} \frac{(Q_{exp} - Q_{model})^2}{Q_{model}} \ldots\ldots\ldots\ldots\ldots\ldots\ldots (11)$$

The Chi test results express the compatibility between the experimental and predicted value of Q. The smaller the value of χ^2 indicates that the difference between experimental and predicted values is small.

Table 3.7 shows the values of χ^2 for the two models (i.e., Shahwan and H_o using PG-Fe^0composite at pH of 6.5, and 8.0 for LEV removal kinetics by using PG-Fe^0 composite). The Chi test results indicated that the Q values predicted by H_o equation were more compatible to the experimental values compared to the results of the compatibility test between the Q values predicted by Shahwan equation and the experimental values. Moreoer, the Chi test for the LEV removal kinetics using PG-Fe^0 composite at pH of 6.5 exhibited similar trend.

Table 3.7: Values of Q obtained from Experimental Q values, values of Q_m values predicted by Shahwan model, and values of Q_e values predicted by H_o model, and the Chi-test results values obtained at for the two different studied-pH values (i.e., pH of 6.5 and 8.0).

at 20 ppm	PH=6.5				
Time (min)	Q (mg/g)	Q_m (mg/g)	Chi test (Shahwan model)	Q_e (mg/g)	Chi test (Ho model)
0	0	0	-	0	-
10	5.094278	3.674697	0.726207	3.674697	0.548402
15	6.612484	5.068581	0.643793	5.068581	0.470277
20	7.7	6.25488	0.481667	6.25488	0.333879
40	10.50634	9.638823	0.147422	9.638823	0.078079
80	12.5	13.21299	0.013851	13.21299	0.038474
160	16	16.22032	0	16.22032	0.002993
200	17	16.9939	0.002381	16.9939	2.19E-06
240	17.5	17.55195	0.000838	17.55195	0.000154
280	17.7	17.97354	0.000784	17.97354	0.004163
		X^2	2.016943	X^2	1.476422
at 20 ppm	PH=8				
Time (min)	Q (mg/g)	Q_m (mg/g)	Chi test (Shahwan model)	Q_e (mg/g)	Chi test (Ho model)
0	5.19E-09	0	-	0	-
10	1.479194	1.916667	0.099852	1.420528	0.002423
15	2.103381	2.653846	0.114178	2.017514	0.003655
20	2.685306	3.285714	0.109715	2.55423	0.006726
40	3.985696	5.111111	0.247805	4.250266	0.016469
80	5.487646	7.076923	0.356907	6.362724	0.120351
160	8.5	8.761905	0.007829	8.466799	0.00013
200	9.287061	9.2	0.000824	9.066431	0.005369
240	9.514629	9.517241	7.17E-07	9.515709	1.22E-07
280	9.617198	9.757576	0.00202	9.864883	0.006219
		X^2	0.939129	X^2	0.161342

Intraparticle diffusion model

The Weber–Morris method was utilized to test if intraparticle diffusion was the rate-controlling step of this adsorption using the following Equation:

$$\mathbf{q_t = K_{id} t^{1/2} + Z} \quad \ldots\ldots\ldots\ldots (12)$$

Where.

K_{id}: is the intraparticle diffusion average stability (mg/ g. $min^{1/2}$).

Z (mg/g): provides information about the thickness of the boundary layer.

The results obtained upon plotting q_t vs. $t^{1/2}$ (forcing the line to pass through the origin) indicated that intraparticle diffusion was indeed the major rate-controlling step (please refer to Figures 3.17 and 3.18).

When qt (the quantity of adsorption at any given time) is plotted against $t^{1/2}$ (the square root of time), a straight line is compelled to pass through the origin [163]. Multi-linearity is considered in the qt vs. t1/2 plot (two or three steps are required to follow the entire process) [164].

The first step is external surface adsorption, also known as instantaneous adsorption; the second step is gradual adsorption, in which intraparticle diffusion is controlled; and the third step is final equilibrium, in which the solute slowly moves from larger pores to micropores, resulting in a slow

adsorption rate.[165] The time it takes to complete the second phase is usually determined by system variables (such as solute concentration, temperature, and adsorbent particle size), which are difficult to forecast or control.[166]

A straight line is obtained by plotting q_t against $t^{1/2}$, but it does not necessarily pass through the origin; that is, there is an intercept [167]

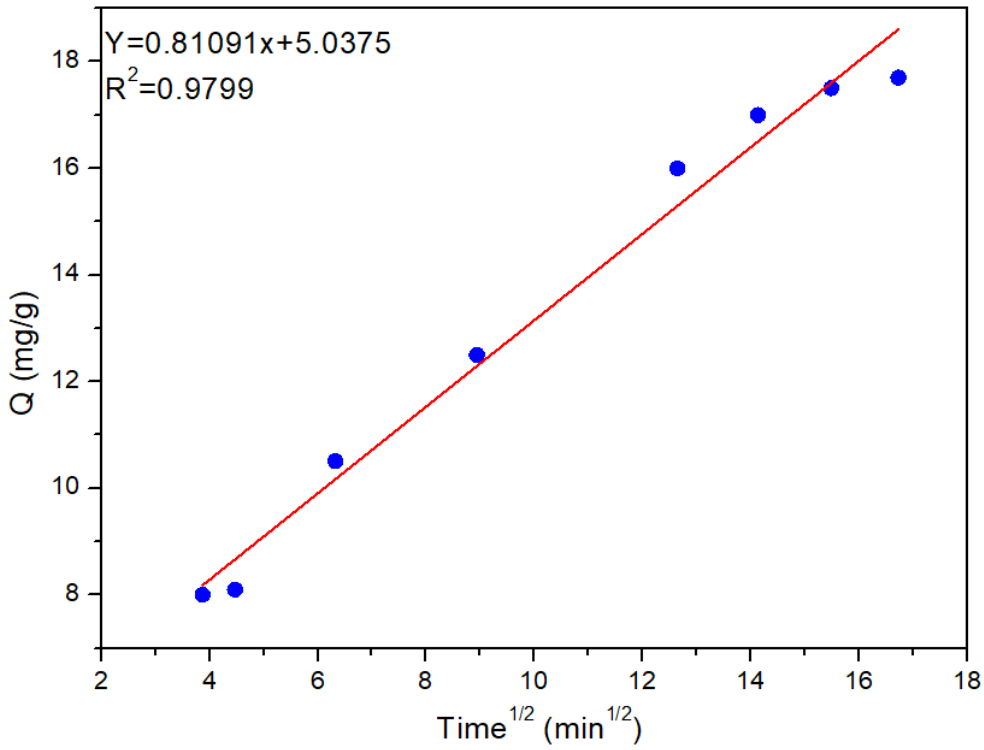

Figure 3.17: The intraparticle diffusion of LEV on PG-Fe^0 composite. (Temperature was 298K, and pH was 6.5,).

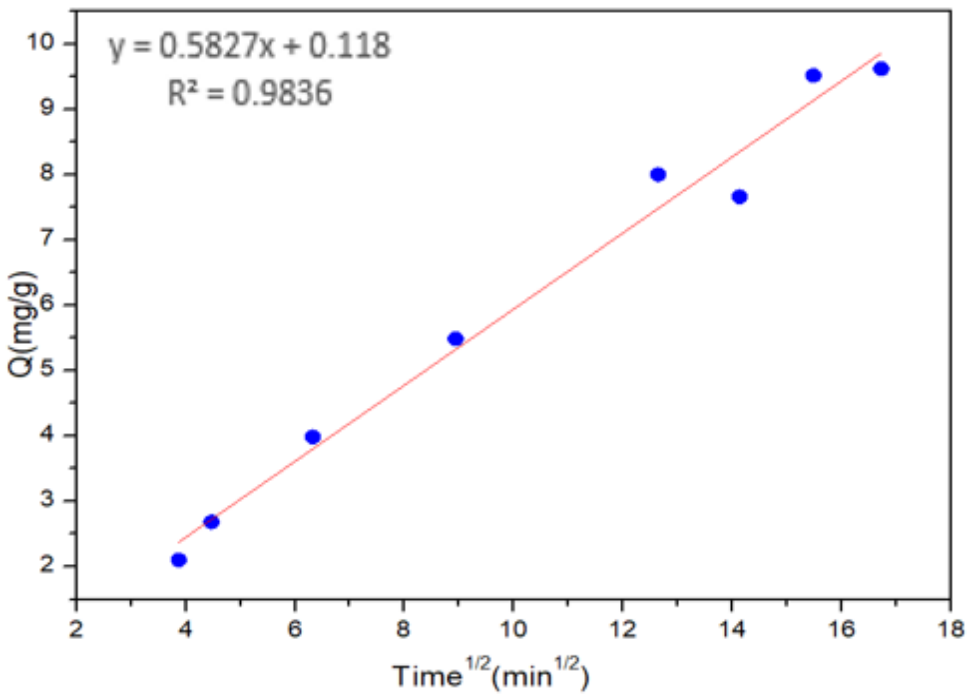

Figure 3.18: The intraparticle diffusion of LEV on PG-Fe^0 composite. (Temperature was 298K, and pH was8.0, solution Volume was 100 mL, adsorbent dose was 0.5 g).

As shown in Figures 3.17and 3.18, The Intercept and slope for pH=8.0 are smaller than for pH=6.5, indicating that the rate of intraparticle diffusion and the initial amount of adsorption rise as the yield of PG-Fe^0composite for the adsorption of bigger molecules LEV decreases. Because the correlation coefficient (R2) ranges from 0.9799 to 0.9836, the IPD model is acceptable for describing the current data. All of the straight lines have a large intercept but none of them travel through the origin. This is due to the vast range of pore sizes found in the activated carbons investigated. The IPD model's kinetic parameters are listed in Table 3.8.

Table 3.8: The intraparticle diffusion of LEV using PG-Fe^0composite.

Intraparticle diffusion model		
pH=6.5		
Z	K	R^2
5.0375	0.8109	0.9799
pH=8		
Z	K	R^2
0.188	0.5827	0.9836

As shown in Table 3.8, a difference in the R^2 values at pH of 6.5 and pH of 8.0 was observed. When LEV was adsorbed utilizing PG-Fe^0 composite, and intercept (Z), the value of the rate constant obtained by the intraparticle diffusion model (k) at a pH of 8.0 was less than that obtained at a pH of 6.5. The diffusion rate or adsorption rate observed at the surfaces decreased at pH of 8.0. indicating that the adsorption rate at the surface increased with decreasing pH; this might be explained by the decrease in the diffusion encountered at the boundary layer.

3.4-Adsorption isotherm

The adsorption isotherms were used when equilibrium is reached (the partitioning of LEV between the liquid and solid phases). Langmuir and Freundlich isotherms were fitted well with the adsorption data of LEV on PG-Fe^0 composite. At equilibrium, the adsorbed amount of LEV (q_e in mg/g was determined by the equation of mass balance as given below:

$$Q = (C_0 - C)\frac{V}{m} \ldots\ldots\ldots\ldots (13)$$

The adsorption isotherm of the nonlinear Langmuir is given as:

$$Q_e = \frac{Q_m K_L C_e}{1 + K_L C_e} \ldots\ldots\ldots\ldots\ldots\ldots\ldots\ldots (14)$$

Where C_e is the equilibrium concentration of the LEV solution (in mg/L).

Q_e is the amount of LEV adsorbed per gram of the adsorbent at equilibrium (expressed in mg/g).

Q_m is the maximum amount of LEV (mg) adsorbed per gram of adsorbents for complete monolayer coverage.

k_L is the Langmuir constant related to the energy of adsorption (L/mg).

All of the four models of Langmuir isotherm fitted with the experimental data of LEV adsorption on PG-Fe^0 composite. Table 3.19 shows R^2 values of the four linear Langmuir models using PG-Fe^0 composite at different pH. According to the R^2 values, the R^2 value of the linear Langmuir form (I) was higher than that obtained by the other linear Langmuir forms. This indicated that the linear form of Langmuir (I) is suitable for the experimental results.

Table 3.9: correlation coefficients (R^2) values of linear Langmuir form at 298 K.

pH	Number	Linear Langmuir forms	R^2 **PG-Fe^0**
6.5	**I**	$\frac{C_e}{Q_e} = \frac{1}{Q_m} k_L + \frac{C_e}{Q_m}$	0.9808
	II	$\frac{1}{Q_e} = \frac{1}{Q_m} + \frac{1}{Q_m k_L C_e}$	0.9710
	III	$Q_e = Q_m - \frac{Q_e}{k_L C_e}$	0.9354
	IV	$\frac{Q_e}{C_e} = k_L Q_m - k_L Q_e$	0.9354
pH	Number	Linear Langmuir forms	R^2 **PG-Fe^0**
8	**I**	$\frac{1}{Q_e} = \frac{1}{Q_m} + \frac{1}{Q_m k_L C_e}$	0.9218
	II	$\frac{C_e}{Q_e} = \frac{1}{Q_m} k_L + \frac{C_e}{Q_m}$	0.9877
	III	$Q_e = Q_m - \frac{Q_e}{k_L C_e}$	0.7533
	IV	$\frac{Q_e}{C_e} = k_L Q_m - k_L Q_e$	0.7533

The linear Langmuir adsorption isotherm was used to fit the experimental data as shown in the following equation:

$$\frac{C_e}{Q_e} = \frac{1}{Q_m K_L} + \frac{C_e}{Q_m} \ldots\ldots\ldots\ldots\ldots\ldots (15)$$

Were

C_e is the equilibrium concentration of the LEV solution (mg/L)

Q_e is the amount of LEV adsorbed per gram of the adsorbent at equilibrium (mg/g).

Q_m is the maximum amount of LEV (mg) adsorbed per gram of adsorbents for complete monolayer coverage.

k_L is the Langmuir constant related to the energy of adsorption (L/mg).

The adsorption parameters Q_m and k_L were obtained from the slope and intercept of the linear plot of C_e/q_e Vs. C_e as shown in Figure 3.19 and

Figure 3.20.

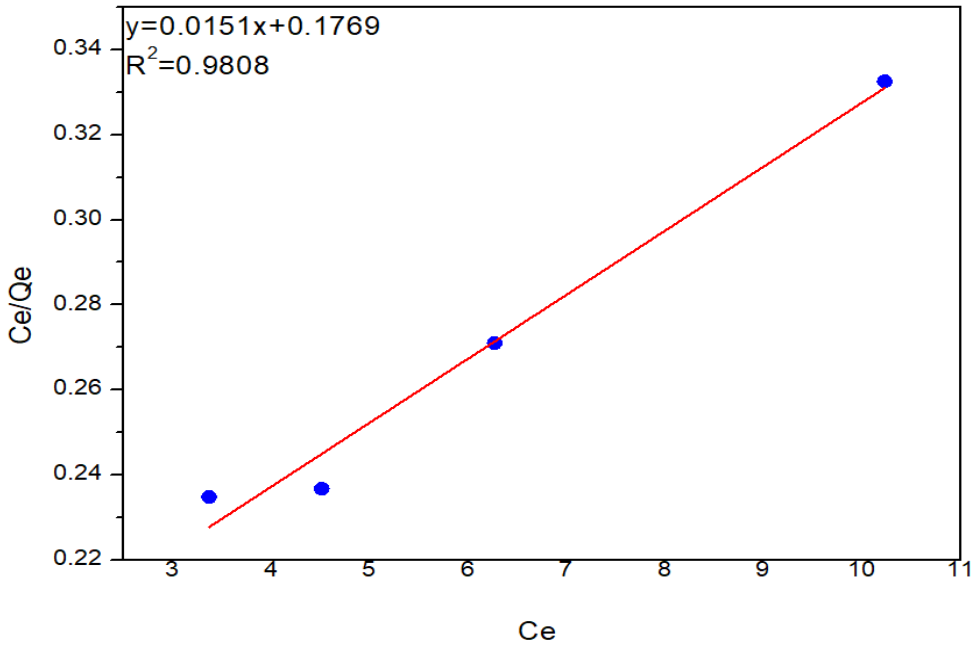

Figure 3.19: Linear plots of Langmuir isotherm model of LEV adsorption onto PG-Fe^0composite at 298K. pH of 6.5.

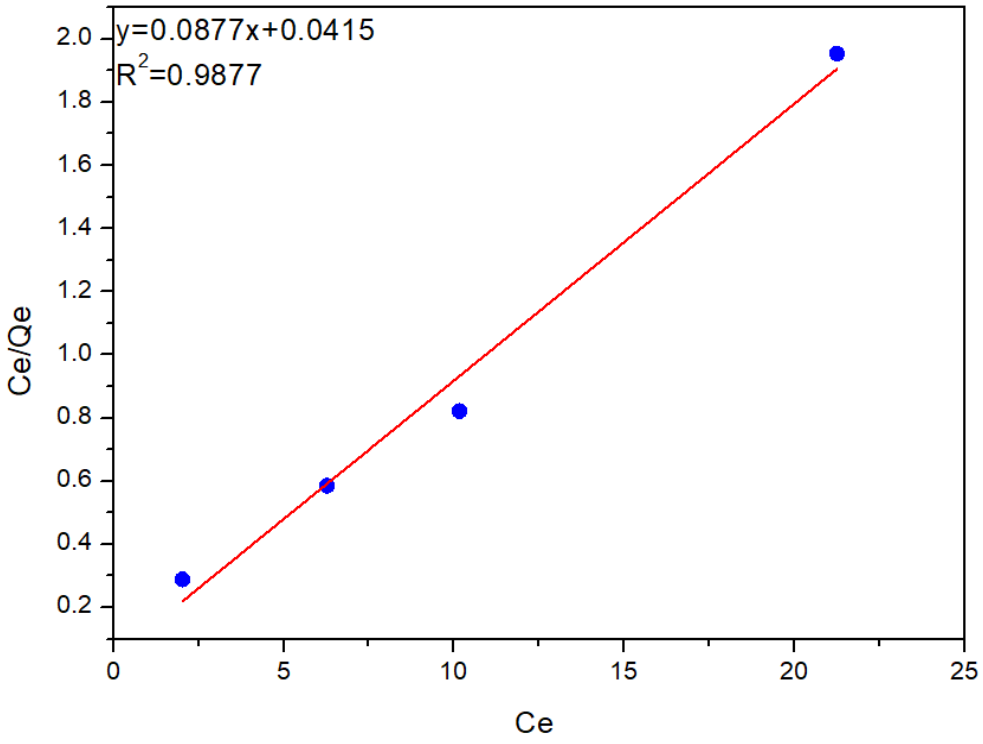

Figure 3. 20: Linear plots of Langmuir isotherm model of LEV adsorption onto PG-Fe^0 composite at 298K. pH of 8.0.

Another commonly used adsorption model is the Freundlich isotherm, which allows multilayer adsorption and can be used for heterogeneous adsorbent surfaces with different sites of varying adsorption energy.[168-169]

The experimental data of adsorption LEV onto the adsorbent were analyzed using the Freundlich isotherm model.

The nonlinear form of Freundlich isotherm model is given as:

$$Q_e = k_f \, C_e^{\frac{1}{n}} \ldots\ldots\ldots\ldots\ldots\ldots\ldots\ldots\ldots (16)$$

The linearized form of the Freundlich isotherm model is represented by this equation:

$$lnQ_e = lnk_f + \left(\frac{1}{n}\right) lnC_e \ldots\ldots\ldots\ldots . (17)$$

Where Ce is the equilibrium concentration of the LEV solution (mg/L), and Q_e is the amount of LEV adsorbed per gram of the adsorbent at equilibrium (mg/g). k_f is the Freundlich constant, which reflects the adsorption affinity, and n is the Freundlich constant related to the adsorption linearity.

The isotherm parameters k_f and 1/n of Freundlich for adsorption of LEV onto PG-Fe^0 composite could be calculated from the intercept and slope of the linear plot of ln Q_e vs ln C_e, the corresponding plots is shown in Figures 3.21 and 3.22, respectively.

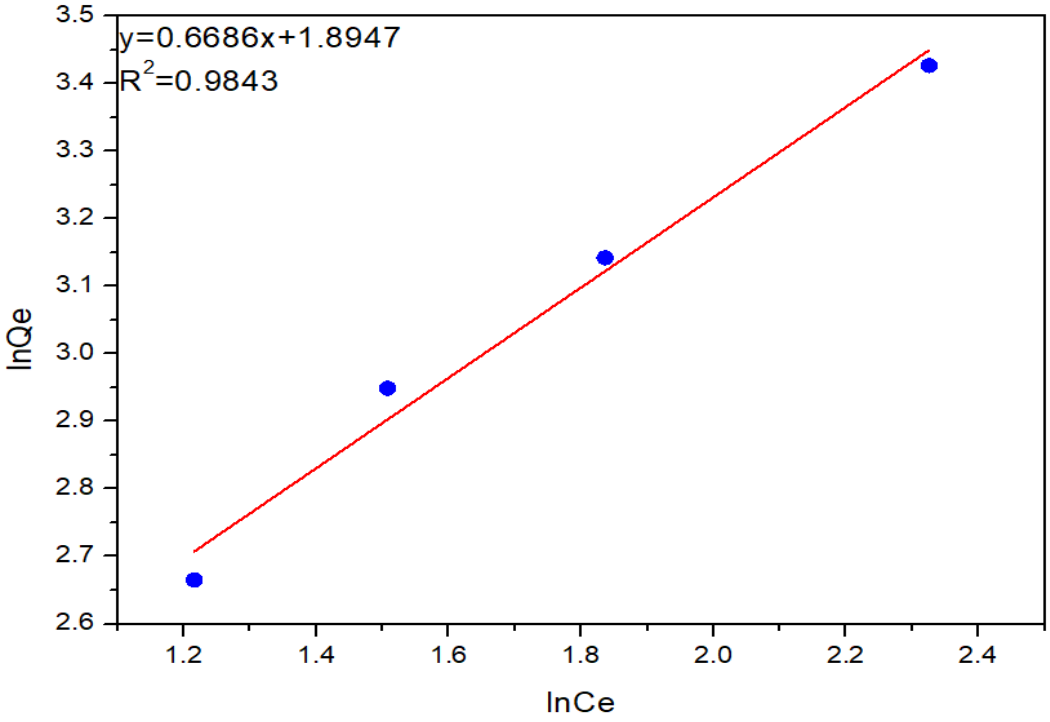

Figure 3.21: Linear plots of Freundlich isotherm model of LEV adsorption on PG-Fe^0 composite at 298K.pH of =6.5.

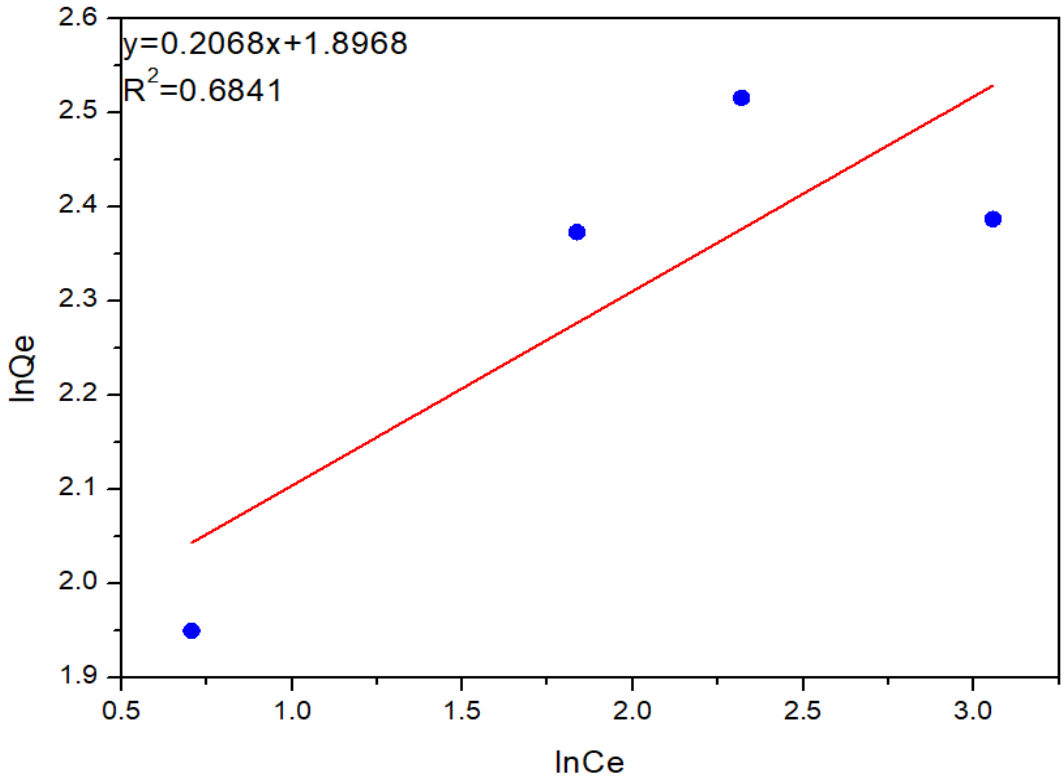

Figure 3.22: Linear plots of Freundlich isotherm model of LEV adsorption on PG-Fe^0composite at 298K. pH of =8.

The Parameters of Langmuir and Freundlich models are shown in table 3.10 below.

Table 3.10: Parameters of Langmuir and Freundlich models for LEV adsorption using PG-Fe^0composite.

Langmuir Isotherm			**Freundlich Isotherm**		
pH=6.5			**pH=6.5**		
R^2	K (L/mg)	$Q_{(max)}$	R^2	K_F ((mg/g) (L/mg)1/n)	n
0.9808	0.0853	66.22	0.9877	0.6390	1.49
pH=8			**pH=8**		
R^2	K (L/mg)	$Q_{(max)}$	R^2	K_F ((mg/g) (L/mg)1/n)	n
0.9843	2.113	11.40251	0.6841	0.640	4.835

Langmuir is based on the kinetic principle and represents the adsorption of a monolayer surface on a solid with specific sites strongly identical. According to equation (15), the values of Q_m and K are worked out from slope and the intercept of Langmuir plot C_e/Q_e Vs C_e, which are shown in Figure 3.19 and Figure 3.20. Langmuir adsorption-desorption equilibrium constant (K_L) and regression constant (R^2) were determined and values are shown in Table 3.10.

The adsorption at the site of the supporting surface depends on various relationship or on the surface of heterogeneous solution, Freundlich model includes interaction between the adsorbed molecules and represents the non-

ideal adsorption that includes heterogeneous surface energy system as described in equation (16). The linear form of this equation could be written as shown in equation (17). The constants K_F (L /mg) and 1/n (i.e., the adsorption intensity), were determined from a graph of ln (Q_e) vs. ln (C_e) as shown in Figures 3.21 and 3.22, respectively. The value of 1/n < 1 in the Freundlich model is indicative of a normal adsorption process. The significance of 1/n values and the utility of Freundlich regression the 1/n number generated from the Freundlich equation describes the linearity of adsorption or, alternately, the degree of curvature of the isotherms over the concentration range investigated.1/n values typically range from 1 to 0. A score of 1 indicates that the chemical's relative adsorption (adsorption partition) was the same across the whole range studied (C-type isotherm), which is unusual (especially in the two-order-of-magnitude concentration range commonly utilized in regulatory studies), but not unheard of.

The R^2 values shown in Table 3.10 indicated that the experimental data were interpreted by both Langmuir and Freundlich isotherms. It should be noted however, that Langmuir isotherm model described the data better than Freundlich isotherm.

The Langmuir isotherm model showed that the adsorption increased with increasing LEV concentration until it reaches the saturation point.

This described the adsorption process which occurred by the formation of monolayer to LEV molecules on the surface of the adsorbent, and after that, no further adsorption occurred.[170] All sites on the surface of the adsorbent were occupied by LEV molecules so any further increase in LEV concentration would not cause an increase in adsorbed LEV.

To examine which of the two isotherm models provide better correlation with the experimental results, the calculated Q_m and k_L values were inserted in the nonlinear (equation 14), the calculated k_f and n values were inserted in the nonlinear (equation 16), then from the calculated Q values the model prediction was obtained. The experimental and predicted data of Q at the two studied pH values (i.e., 6.5, and 8.0) were plotted as shown in the Figures 3.23 and 3.24.

As shown in Figure 3.24, for PG-Fe^0 composite at pH of 8.0, the nonlinear fit using the Langmuir isotherm model yielded a better correaltion (R^2 =0.9843) with the experimental data compared to that obtained with using the Freundlich isotherm model (R^2 =0.6841).

Results of PG-Fe^0 composite at pH of 6.5 are shown in Figure 3.23. Here, the two models (Langmuir, and Freundlich) yielded similar correlations (R^2 = 0.9808 for Langmuir, and R^2 = 0.9877 for Freundlich).

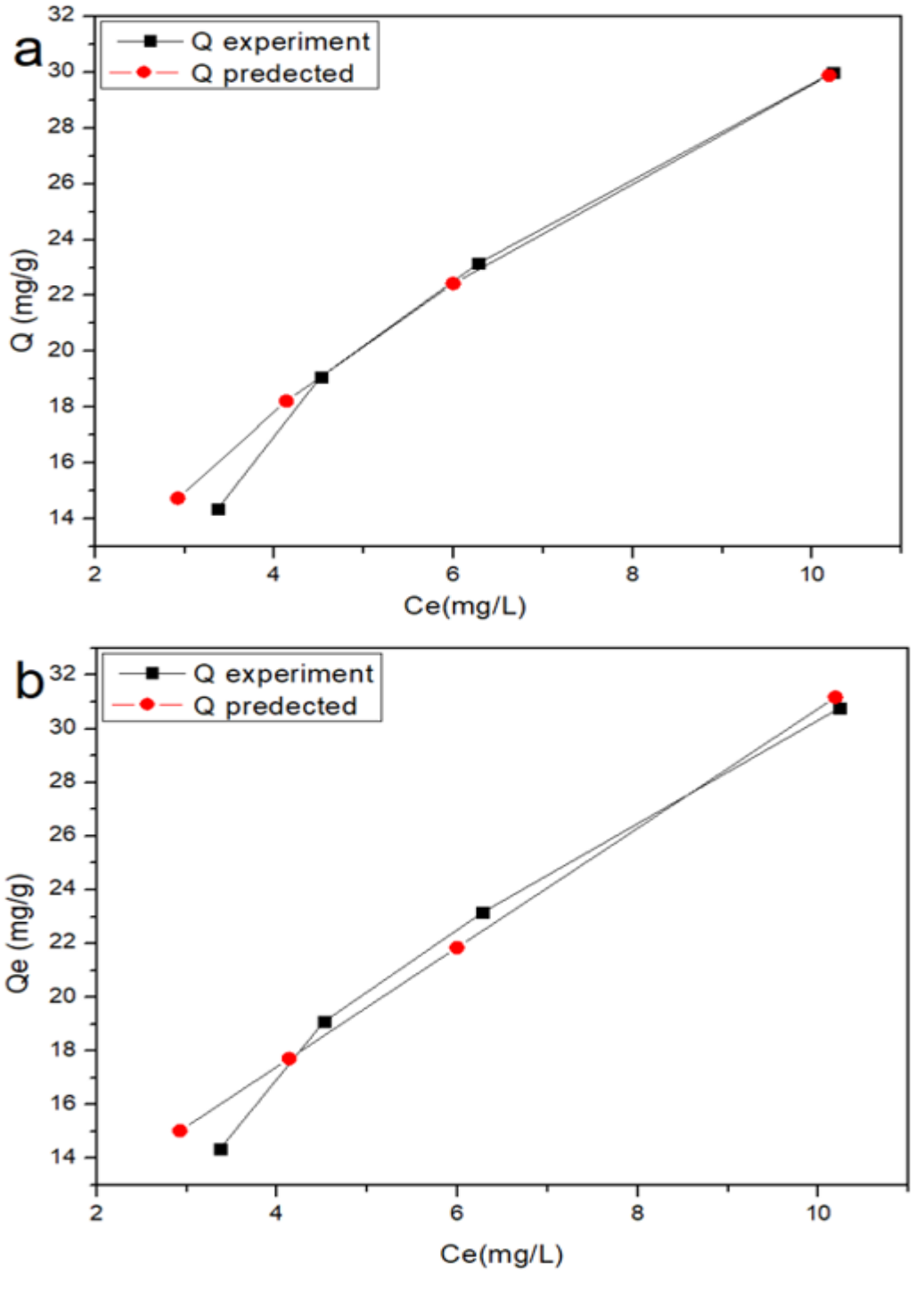

Figure 3.23: Nonlinear fits of the kinetic data of LEV removal by PG-Fe^0composite; (a) using Langmuir model (b) using Freundlich model at pH of =6.5

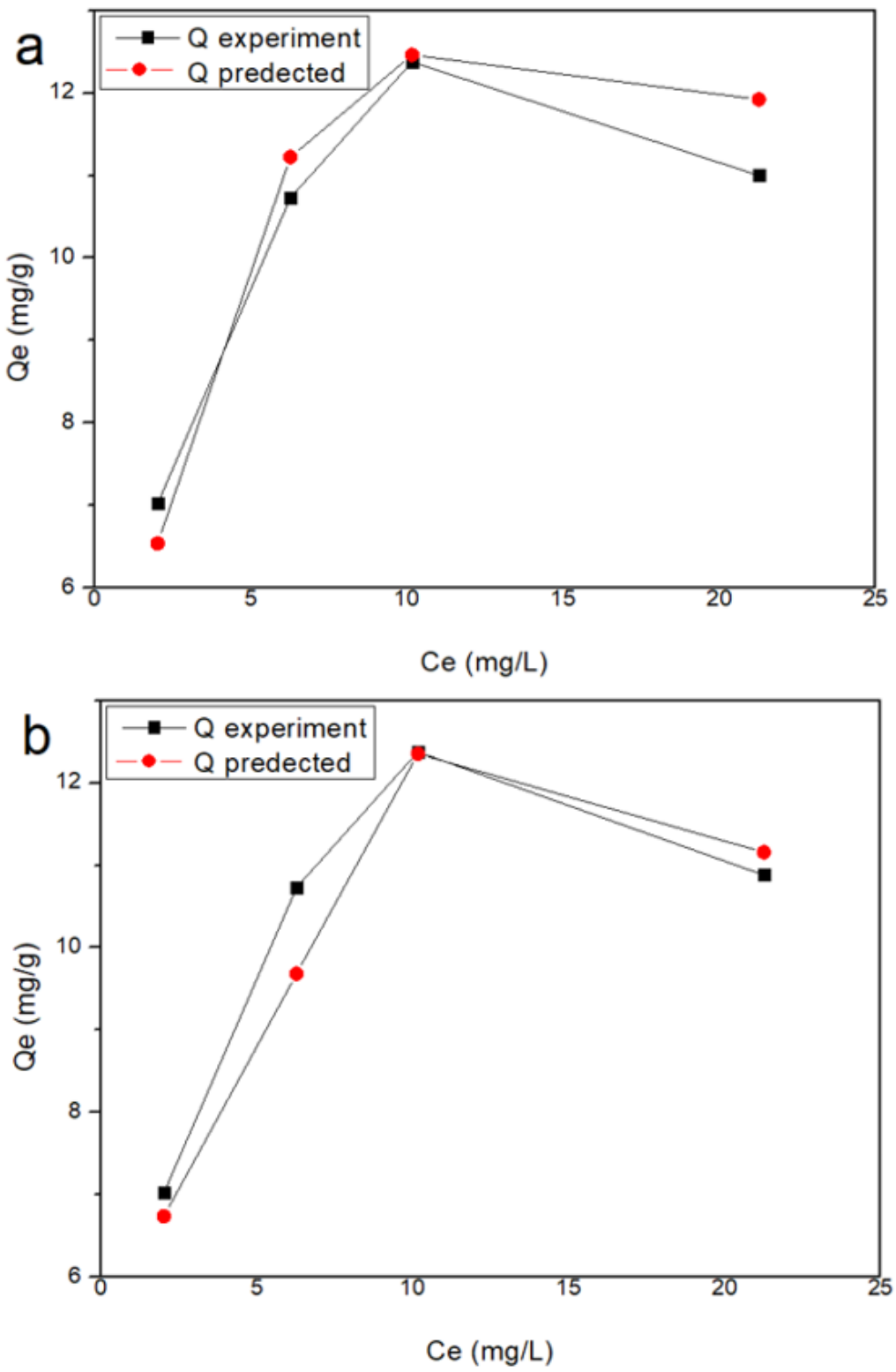

Figure 3.24: Nonlinear fits of the kinetic data of LEV removal by PG-Fe^0composite; (a) using Langmuir model (b) using Freundlich model at pH of =8.0

In addition, Chi test was performed using equation (11) to examine the correlation and to study the compatibility between the experimental value and the predicted value of Q.

Table 3.11 shows the χ^2 values of the Langmuir and Freundlich models using PG-Fe^0 composite. In the Chi test results at pH of 6.5 and 8.0, the Q values predicted by the Langmuir model correlated better with the experimental values compared to the correlation between the Q values predicted by the Freundlich model and the experimental Q values.

Table 3.11: Values of Q obtained from the experiment, values of Q predicted by equations (14 and 16), and the Chi–test values for the sorption systems of PG-Fe^0 composite at 298 K.

C_e (mg/L)	**Q_{exp}** (mg/g)	**Q_{pre}** (mg/g)	**Chi test** (Langmuir model)	**Q_{pre}** (mg/g)	**Chi test** (Freundlich model)
pH=6.5					
3.373107	14.36782	15.64446	0.104179	16.7204	0.331011
4.51696	19.08397	18.94004	0.001094	19.0081	0.000303
6.273419	23.14815	22.92778	0.002118	22.52102	0.017463
10.23377	30.76923	30.00000	0.019724	30.44172	0.003524
		χ^2	0.127114929	X^2	0.352301
pH=8					
2.025901	7.022472	8.034238	0.127414	8.0000	0.119445
6.275867	10.72961	10.35071	0.01387	10.0000	0.053234
10.16403	12.37624	10.92512	0.192743	11.81275	0.026879
21.25847	10.88139	11.46088	0.0293	13.0000	0.345269
		χ^2	0.363327	χ^2	0.544827

Temkin Adsorption Isotherm

This isotherm contains a factor reflecting the adsorbent-adsorbate interactions and suggests that, because of these interactions, the heat of adsorption of all the molecules in the layer decreases linearly with the coverage. The model is given by the following equation.[171-175]

$$Q_e = BlnC_e + BlnA$$

Where:

$B = \frac{RT}{b}$, and

b is the Temkin constant related to the heat of sorption (J/mol);

A is the Temkin isotherm constant (L/g),

R the gas constant (8.314 J/mol K) and T the absolute temperature (K).

Q_e is the amount of LEV adsorbed in mg/g on the surface of PG-Fe^0.

C_e is the equilibrium concentration in mg/L

According to the above equation, a plot of Q_e Vs ln C_e was constructed as shown in Figures 3.25 and 3.26, respectively, from which, the constants, A, B and b were calculated. All parameters and correlation coefficient are listed in Table 3.12 below.

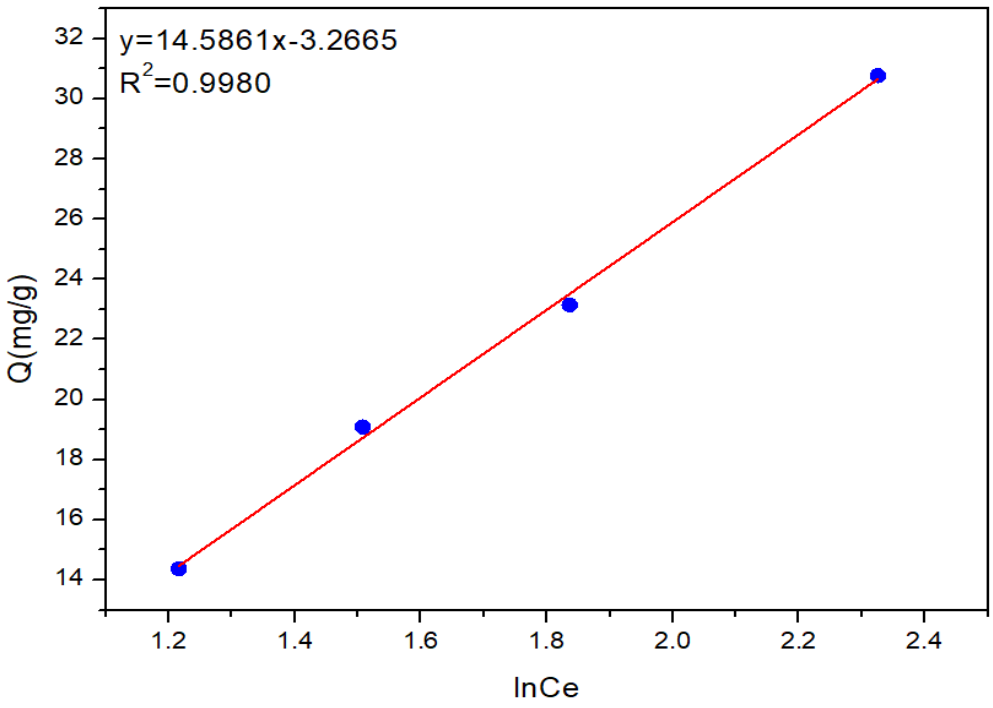

Figure 3.25: Temkin plot for LEV adsorption on PG-Fe^{0}composite. (Temp.= 298K, pH= 6.5).

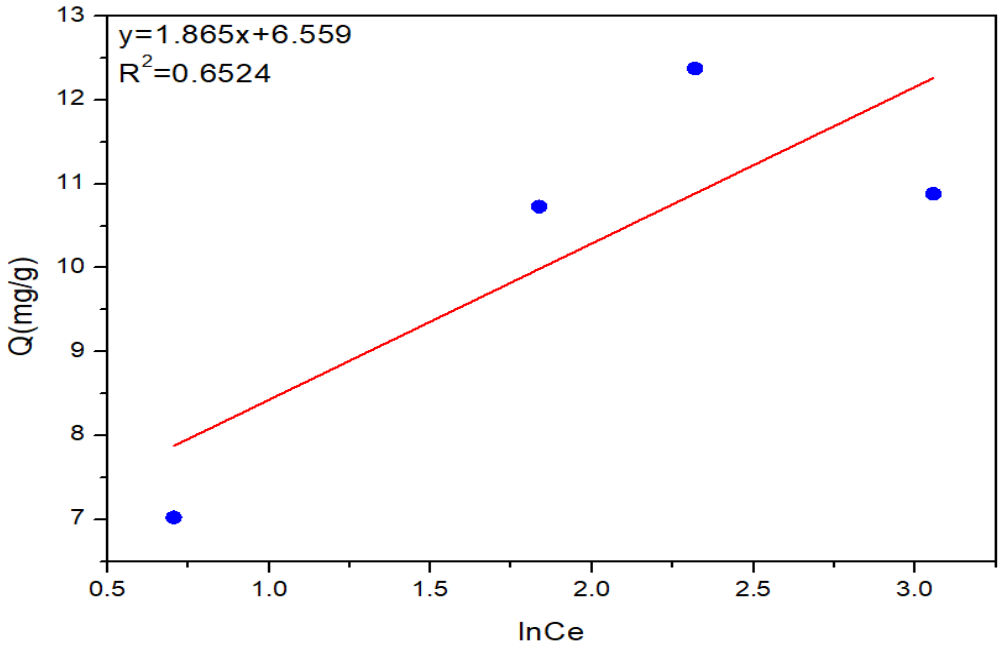

Figure 3.26: Temkin plot for LEV adsorption on PG-Fe^{0}composite. (T= 298K, pH= 8.0)

The extracted parameters from Figure 3.25 and Figure 3.26 were tabulated in table 3.12.

Table 3.12: Temkin isotherm model parameters and correlation coefficient for adsorption of LEV on PG-Fe^0composite.

Temkin isotherm model parameters				
pH=6.5	Parameters			
	A(L/g)	b(J/mol)	B	R^2
	1.249	169.8	14.586	0.9980
pH=8	Parameters			
	A(L/g)	b(J/mol)	B	R^2
	33.67	1328.4	1.865	0.6524

The value range found for the Temkin model is low when compared to the Freundlich and Langmuir models, as shown in (Table 3.12). As a result, it stands. The Temkin model is not appropriate for these adsorption experiments. And that the sequence is followed by the applicability; Langmuir > Freundlich > Adsorption model of Temkin.

3.5-Effect of Amount of Adsorbent

To investigate the effect of the adsorbent dose on the removal of LEV on the surface of the PG-Fe^0 composite, various experiments were performed using different doses of PG-Fe^0 composite. The dose amounts range from 0.1 to 1 g, as shown in Figure 3.27 below this experiment was studied using 25 mg/L solutions of LEV and pH = 6.5 at 298K.

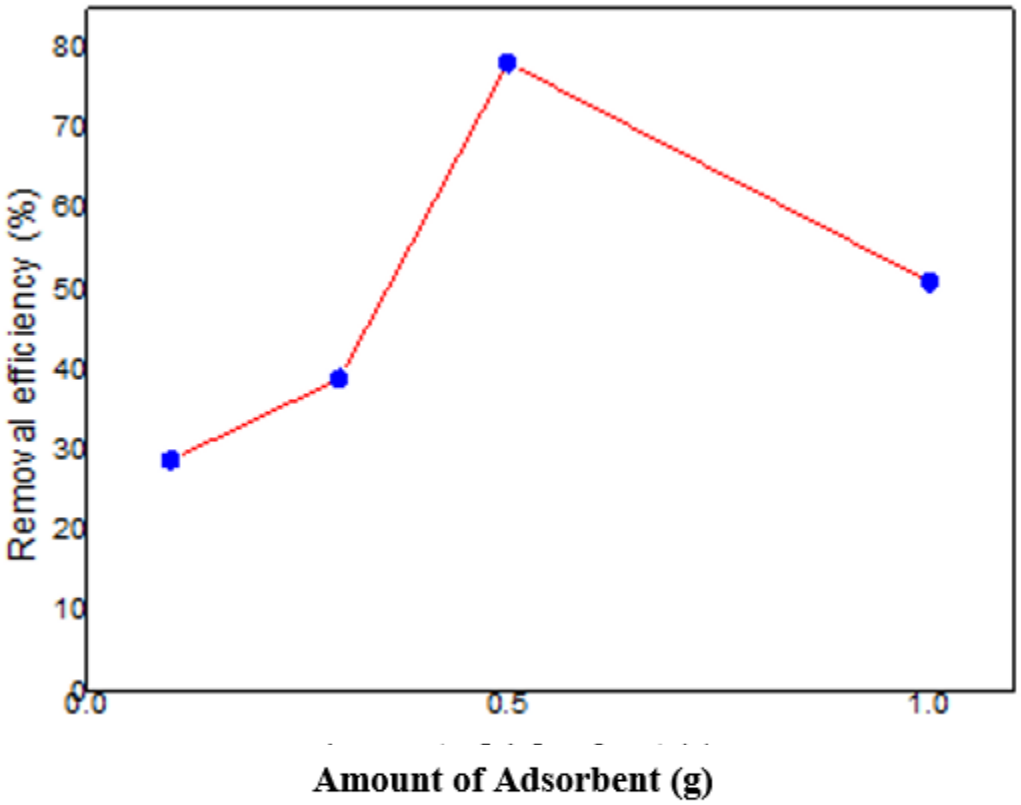

Figure 3.27: Effect of amount of adsorbent on the removal of LEV (298K, pH= 6.5, concentration of LEV= 25 mg/L).

As shown in Figure 3.27, the efficiency of adsorption increases as the dose increases, from ~30%to ~80%, and this is due to an increase in adsorption sites (i.e., more surface area) which is triggered by the availability of vacant locations and the instauration of adsorption locations.

The adsorption efficiency also showed a declining percentage of removal at 1 g from~80%to~52%, which indicates that the vacant sites are almost saturated with LEV ions the no exchangeable sites on the adsorbent surface area in addition due to electrostatic repulsion between similar charges. However, performance augmentation occurs only after a specific amount of adsorbent dose has been added, and after that, performance becomes constant and does not increase much. Increased adsorbent dosage means more accessible surface area for adsorption and more adsorption sites. Because there are fewer binding sites available for adsorption when the adsorbent dosage is below the optimal value, LEV removal is poor. For this purpose, we selected to use an adsorbent dose of 0.5 g

3.6- Effect of Adsorbate Concentration.

Adsorption was observed at pH ~ 6.5 by using a PG-Fe^0 composite adsorbent, and the maximum removal efficiency reached 100%. Increasing the concentration of LEV from 2.5 to 20 mg. L^{-1} causes a decrease in the LEV

adsorption with a removal efficiency of ~55%. The effect of the initial concentration of LEV on the adsorption capacity was studied and the results are shown in Figure 3.28.

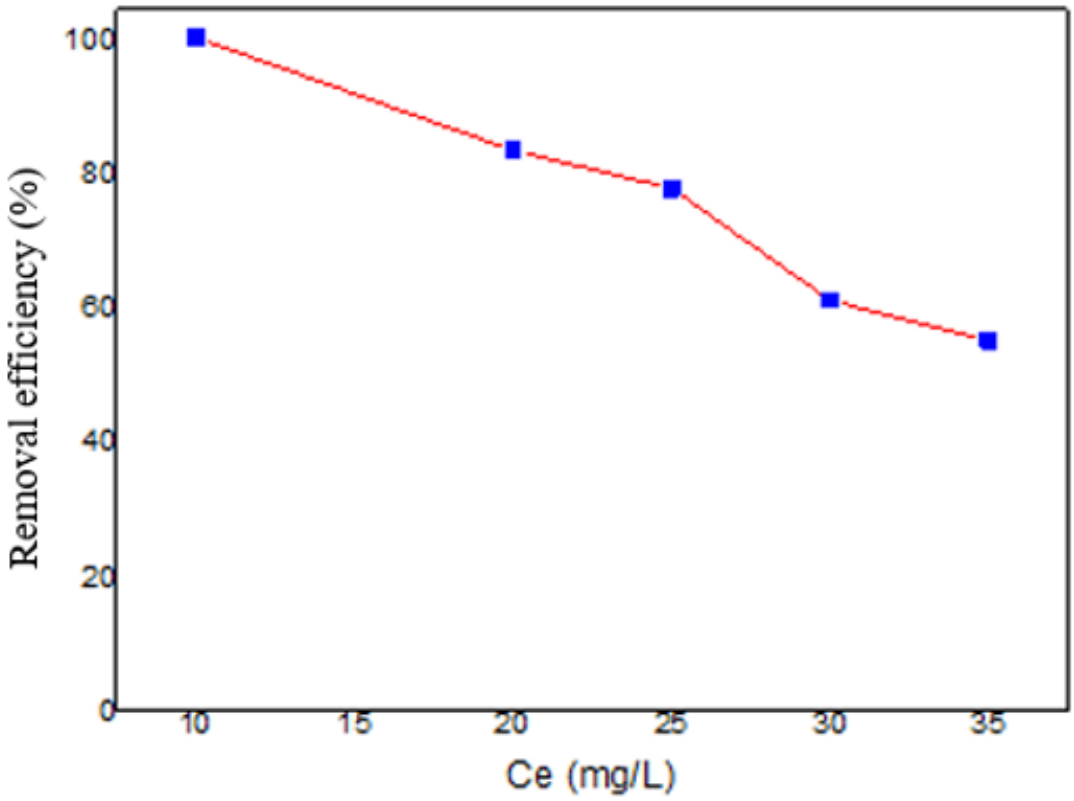

Figure 3.28: Effect of LEV concentration on % removal by using PG-Fe^0 composite at pH:6.5, 298K.

Figure 3.28 shows the effect of initial LEV concentration on percentage removal of LEV at equilibrium. The increase of concentration lowers the LEV removal percentage. As LEV concentration increases from 10mg/L to 35mg/L, the percentage removal decreases from 100% to 55%.

3.7-Effect of pH on the removal of LEV.

The pH value is an important parameter that affects the adsorption of LEV using PG-Fe^0 composite. The extent removal of LEV was studied at pH from 3 to 10 using 0.5g of adsorbate, with shaking speed 120 rpm for 320 min. The pH of 100 ml 20 mg/L LEV solution was adjusted by 0.1 M HCl / 0.1 M NaOH solution, using a pH meter (827 pH laboratory, Metrohm) to reach the corresponding pH value. The effect of pH on the adsorption of LEV in an aqueous solution with nanoparticle adsorbent is shown in Figure 3.29. The maximum adsorption of LEV on pure PG-Fe^0 composite occurs at (pH neutral) pH~ (6-6.5). At this pH, LEV exists as a neutral/zwitterion. As the pH increases or decreases due to electrostatic repulsion between similar charges[176] the removal efficiency decreases. In addition, the affinity of some cationic and anionic adsorbates to the adsorbent metal ions is poorer than their neutral/zwitterionic equivalents and may be attributable to higher or lower pH value ranges. [177-178]

Figure 3.29 shows that with an increase in pH from 3.0 to 6.5, the removal of LEV increases. In the range of pH 3.0-6.5 LEV molecules occurring in cationic form LEV+, as pH increases the cationic form of LEV+ gradually decreases and LEV molecules are converted to LEV+− (zwitter ionic form).

As the pH of LEV solution increases from 7.0 and becomes alkaline a gradual decrease in LEV removal takes place. At alkaline pH LEV molecules in solution exists in the anionic form (LEV−). The aspect for maximum exclusion of LEV molecules at pH < 7 or at pH = 7 may be owing to cationic interchange.[179-180]

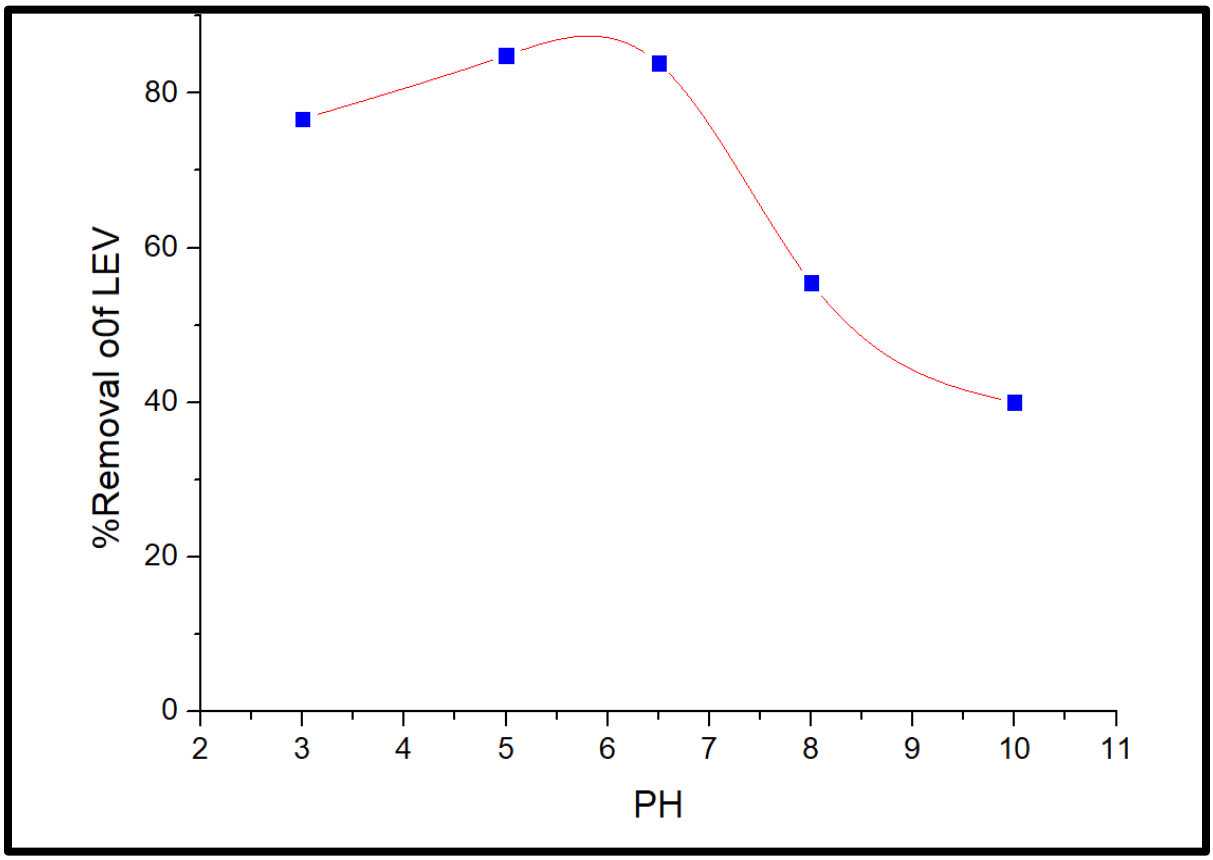

Figure 3.29: Effect of pH on the removal of LEV.

3.8- Effect of Temperature.

The effect of temperature on LEV sorption was investigated using PG-Fe^0 composite at various temperatures of 278, 288, 298, and 308 K, as illustrated in Figure 3.30. The absorption process is more acceptable at 298K temperature, as shown below. This is due to the low surface activity, implying that the absorption between the LEV and the PG-Fe^0composite combination is a thermal reaction. The effect of temperature on the adsorption process was investigated using PG-Fe^0 composite at initial LEV concentrations of 20 mg/L with shaking speed 120 rpm for 320 min.

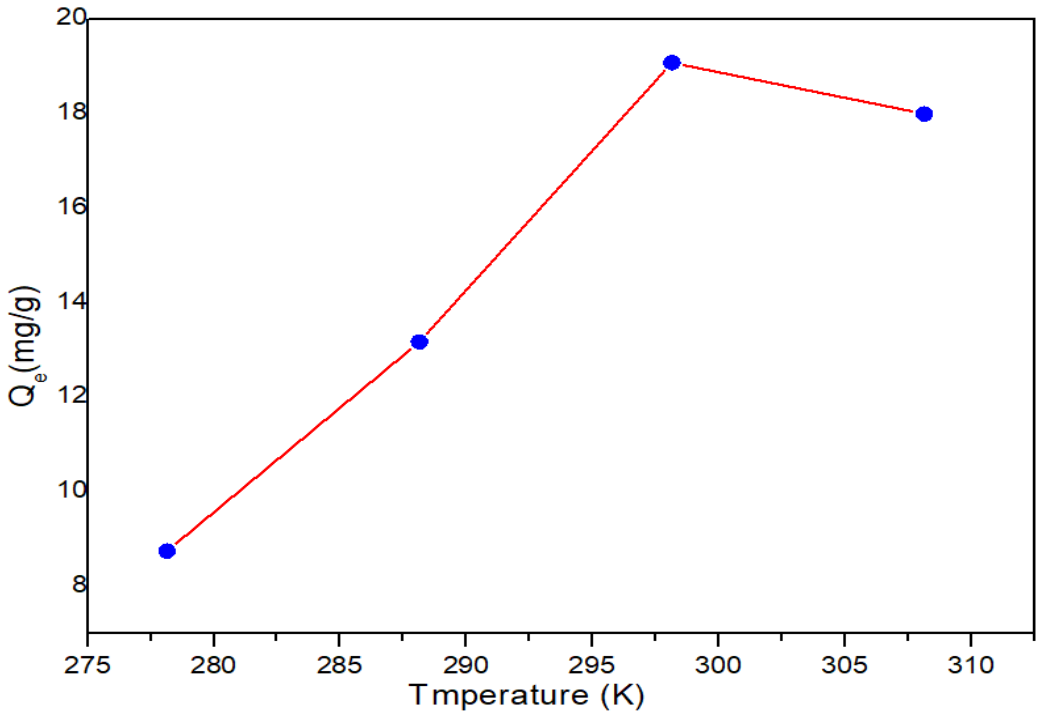

Figure 3.30: Effect of temperature on the adsorption of LEV onto PG-Fe^0 composite at pH=6.5.

Figure 3.30 clearly shows that the temperature rise hurts the adsorption mechanism, as the temperature rises adsorption capacity decreases. The increase in temperature from 298 K to 308K causes the adsorption ability to decrease. The temperature increase confirms that the physical forces between the LEV and the adsorbent are destabilized.

Table 3.13: Amount of LEV adsorbed via PG-Fe^0 composite at different temperatures at 20mg/L

T(K)	Qe (mg/g)
278.15	8.748906
288.15	13.17523
298.15	19.08397
308.15	18.76173

From data in Table 3.13, the concluded, main results were that the amounts of LEV sorption on nanoparticles decrease at the highest temperature due to the change in the equilibrium toward desorption, and when the temperature decreases the Q value decreases.

From the kinetics data obtained at different temperature, the activation energy of adsorption LEV onto PG-F^0 composite were calculated using the Arrhenius equation: [181]

$$ln\, k_2 = ln\, A - \frac{E_a}{R\,T} \ldots\ldots\ldots\ldots\ldots\ldots (19)$$

Where k_2 is the rate constant of pseudo-second-order (g mg^{-1} min^{-1}).

A is the pre-exponential factor.

E_a is the activation energy (kJ mol^{-1}).

R is the gas constant (8.314 J K^{-1} mol^{-1}).

T is the absolute temperature (K).

The value of E_a was calculated from the slope of the linear plot of lnk_2 versus 1/T as shown in Figure 3.31.

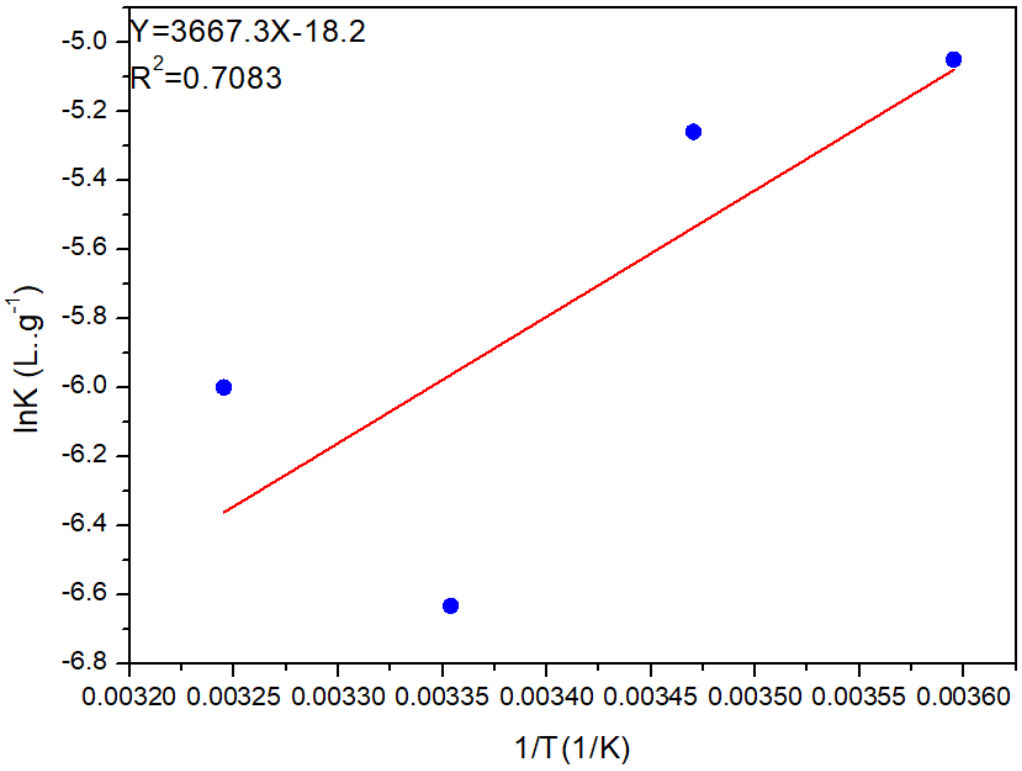

Figure 3.31: Arrhenius equation graph of LEV adsorption on PG-Fe^0composite.at pH=6.5.

The magnitude of the activation energy can be used to indicate whether the adsorption mechanism is physisorption (in the range 5 to 40 kJ mol−1) or chemisorption (in the range 40 to 800 kJ mol−1).[181-183]

The value of the activation energy barrier in the adsorption process of PG-Fe^0 composite was calculated to be 30.48 (KJ mol^{-1}). This means that the adsorption is a physisorption process. Moreover, it is also concluded that the value of the rate constant increases with decreasing the value of activation energy as shown in Table 3.14.

Table 3.14: Activation energy and rate constant values of adsorbed LEV onto PG-Fe^0 composite at the different initial temperatures.

Temperature		1/T K^{-1}	C_0 (ppm)	C_e (ppm)	Q_e (mg/g)	K_c (L/g)	LnK_c (L/g)
C^o	K						
5	278.15	0.003595	19.79713914	12.798014	8.748906	0.006414	-5.04934
15	288.15	0.00347	20.02990897	9.48972452	13.17523	0.005199	-5.25932
25	298.15	0.003354	19.7841	4.51695967	19.08397	0.001315	-6.63362
35	308.15	0.003245	19.942783	4.93340197	18.76173	0.0025	-6.001

3.9-Adsorption thermodynamics.

The effect of temperature on the adsorption of LEV by using PG-Fe^0 composite was studied at 278, 288, 298, and 308 K. To investigate the activation energy (E_a) of the adsorption process, the Arrhenius relation was applied using Eq. 19. Other thermodynamic parameters such as heat of adsorption (standard enthalpy change(ΔH^0), standard entropy change (ΔS^0) , and standard Gibbs free energy change (ΔG^0) were estimated). The following thermodynamic Eqs. 20-21 were applied to evaluate the presented parameters.

In the previous section, the effect of temperature on the adsorption process was studied and the data were analyzed to determine the thermodynamic parameters, including Gibbs free energy change ΔG^0, change in standard enthalpy (ΔH^0), and change in standard entropy ΔS^0

The ΔH° and ΔS° values were determined using van't Hoff equation:[182]

$$ln\,K = \frac{\Delta S^\circ}{R} - \frac{\Delta H^\circ}{R\,T} \ldots\ldots\ldots..(20)$$

The value of Gibbs free energy change (ΔG°) was obtained from the following equations:

$$\Delta G^\circ = \Delta H^\circ - T\Delta S^\circ \ldots\ldots\ldots\ldots(21)$$

$$G = -RT\ lnK \ldots\ldots\ldots\ldots\ldots\ldots\ldots\ldots..(22)$$

Where ΔG° change in Gibbs free energy (kJ mol^{-1}), ΔH° change in enthalpy (kJ mol^{-1}), ΔS° change in entropy (kJ mol^{-1} K^{-1}), R is the ideal gas constant

(8.3145 J/mol K), T is the temperature in Kelvin, and K is the apparent equilibrium constant expressed as $\left(\frac{Q_e}{C_e}\right)$.

The values of ΔH° and ΔS° were calculated from the slope and y-intercept obtained from the linear plot of ln K versus 1/T, as shown in Figure 3.32. The thermodynamic parameters were calculated and tabulated in Table 3.15.

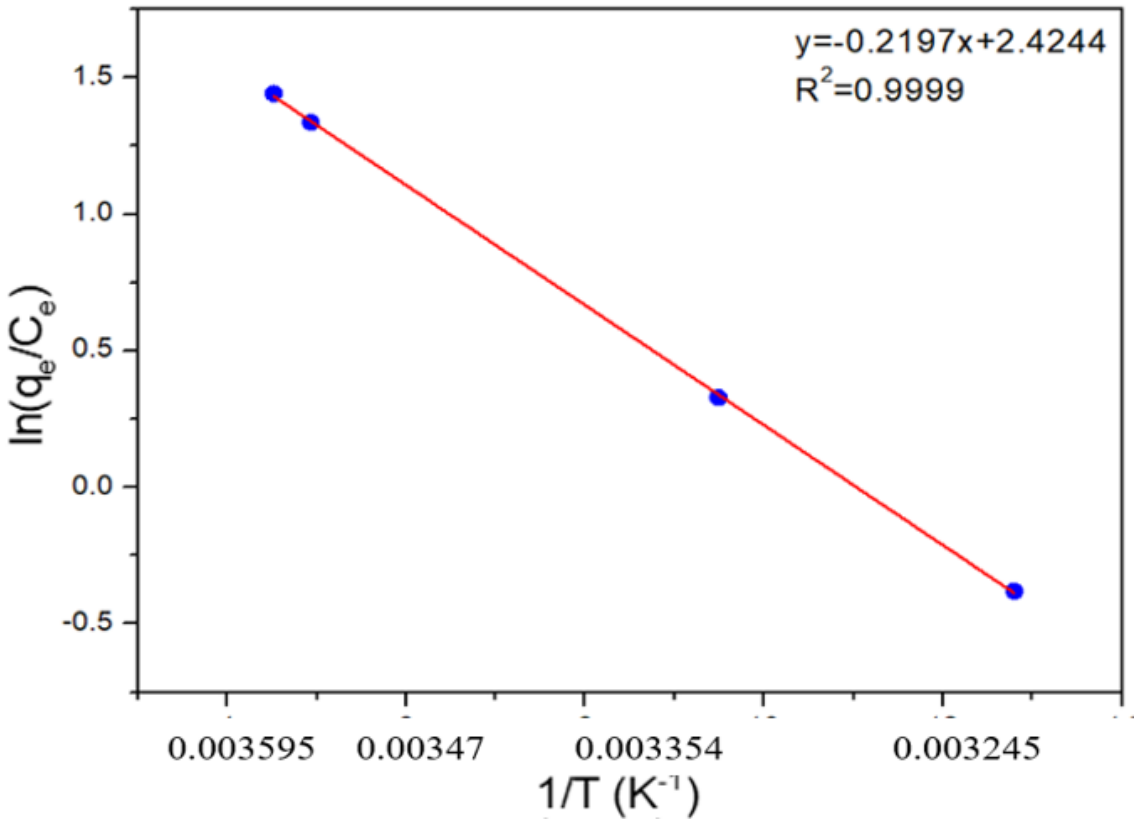

Figure 3.32: Determination of thermodynamic parameters of LEV adsorbed onto PG-Fe^0 composite.

Table 3.15: Thermodynamic parameters of LEV adsorbed using PG-Fe^0 composite

ΔH^o (J/mol)	ΔS^o (J/mol.K)	ΔG^o (kJ/mol)			
1.812452	19.97106	278K	288K	298K	308K
		-5.553	-5.752	-5.952	-6.152

The conclusion drawn from previous studies is that the negative value of Gibbs free energy (ΔG^o) indicates that the adsorption process is spontaneous. Moreover, the increase in the magnitude of ΔG^o with the increase in temperature indicates that the adsorption process is spontaneous, and that it becomes more spontaneity at the higher temperature. In addition, the type of adsorption can be known through the value of ΔG^o. If it lies in the range of -20 to 0 kJ mol^{-1}, it is considered to be a physical adsorption process, and it is a chemical adsorption process if it lies between -50 to -400 kJ mol^{-1}. The enthalpy value of the adsorption process can be used to distinguish between exothermic and endothermic processes.[181-183]

In this study, the negative value of ΔG^o indicates that LEV is naturally adsorbed by the adsorbent, and the value of ΔG^o increases with the increase of temperature, so the adsorption of LEV at low temperature is more favorable. The positive value of ΔH^o indicates that the adsorption process is endothermic.

3.10. Removal of LEV by a Fenton-like process.

In this section, nZVI was used as a Fenton-like catalyst in the removal of LEV. The experiments were conducted by introducing 0.5g of PG-Fe^0composite to 90.0 mL of 10 mg/L LEV solution, and 10 mL of freshly prepared 10% (v/v) H_2O_2. Other experiments were conducted introducing 80mg of Fe^0 to 90.0 mL of 10 mg/L LEV solution, and 10 mL of freshly prepared 10% (v/v) H_2O_2.

One of the most powerful instruments for the degradation of organic contaminants is chemical oxidation. The hydroxyl radical ($OH^{\cdot}$) Fenton reagent can be generated in an aqueous solution from the interaction between Fe^{2+} and H_2O_2. On the other hand, a Fenton-like reaction occurs when the ferrous ions are replaced by nZVI or iron oxides and oxyhydroxides.

The hydroxyl radicals are created by the reactions during a cycle like a Fenton in which nZVI is employed as a source of Fe^{2+} ions:[184-185]

(i) $Fe^0 + 2H_2O_2 \rightarrow Fe^{2+} + 2OH^{\cdot} + 2OH^-$

(ii) $Fe^{2+} + 2H_2O_2 \rightarrow Fe^0 + 2OOH' + 2H^+$

$OH^{\cdot}$ can then destroy the organic pollutants.

The results of related experiments are shown in Figure 3.33. The figure shows that $Fe^0 + H_2O_2$ forms are the closest simulator to the Fenton cycle, which

leads to LEV degradation. Under the research conditions, this oxidation method seems to have no advantage over the direct use of nZVI toward LEV removal.

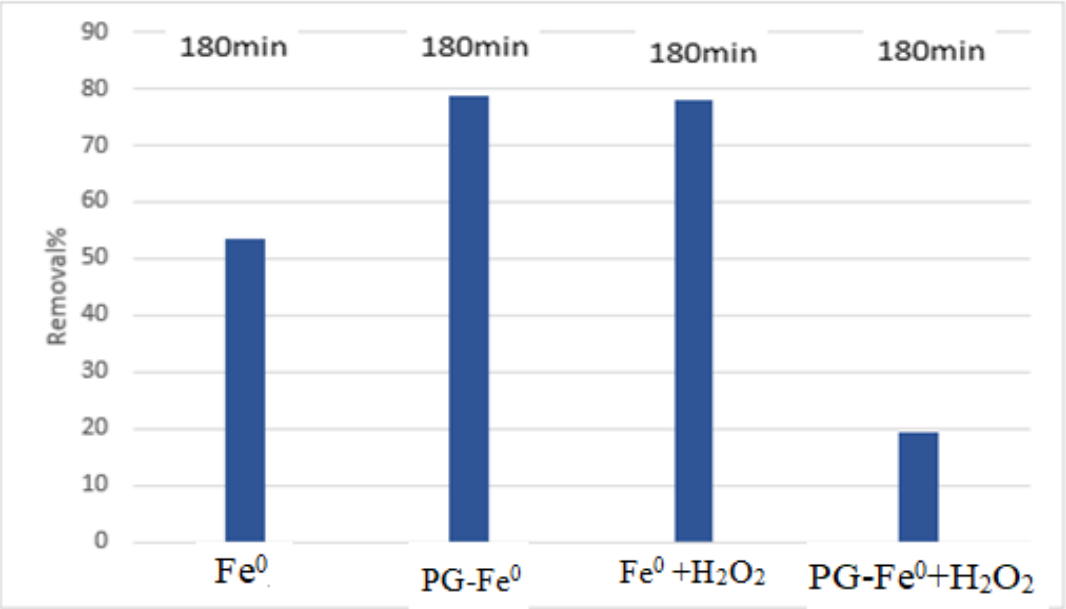

Figure 3.33: % Removal of LEV with ZVI as a Fenton-like catalyst.

The reaction is very fast; 2 hours are enough for a Fenton-like reaction to complete with no significance.

3.11-Antibacterial activity

PG-Fe^0-LEV NPs have tested antibacterial activity against different bacteria. In addition to its reusability, health, and environmental safety, it has also researched multidrug-resistant pathogens to explore its possible future biomedical applications. The lack of growth of bacteria or microorganisms is observed in the area around the hole called the inhibition zone, which indicates the efficacy of the LEV antibiotic at the required concentration in the four types of bacterial strains used in our study (Figures 3.34 and 3.35). Compared with pure LEV, bacterial strain types (Klebsiella pneumonia, Escherichia coli, Staphylococcus aureus, and Staphylococcus aureus), PG-Fe^0-LEV was the practice in more than four bacteria to achieve the better antibacterial activity. The remaining activity of the bacteria exceeds two varieties (Enterococcus faecalis, Staphylococcus epidermidis).

Although PG-Fe^0 composite magnetic nanoparticles have not yet detected any antibacterial activity in all tested samples. Tables 3.16 and 3.17 provide the calculated suppression zone diameter. The results show that, after being adsorbed on the surface of the PG-Fe^0 composite, LEV activity was the same as pure LEV drug. It will not destroy the bacterial inhibition mechanism of LEV antibiotics, because the active LEV carboxylate and the PG-Fe^0composite surface of the nanoparticles have a new combination. Therefore,

there is a major opportunity for the recovery and recycling of a large number of antibiotics in the synthesized PG-Fe^0 composite. The future of these types of nanoparticles can be used to reduce environmental pollution and control the release of antibiotics in drug delivery systems.

Figures 3.34 and 3.35 show the Antibacterial activity of PG-Fe^0 composite, LEV, PG-Fe^0-LEV, and negative control (water) in terms of zone inhibition via the agar-well diffusion method at pH=6.5 and 8.

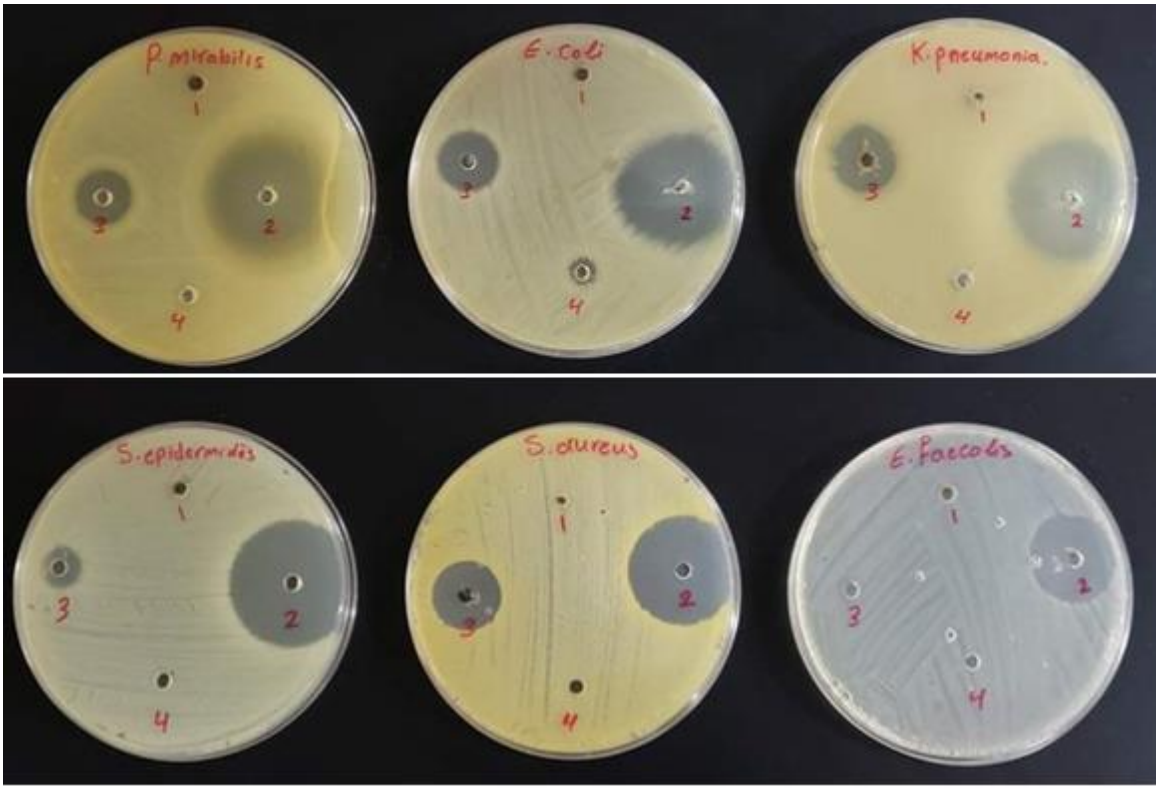

Figure 3.34: Photographs of Petri plates utilized in agar-well diffusion method; (1) PG-Fe^0composite, (2) LEV, (3) PG-Fe^0-LEV, and (4) negative control (water). At pH=6.5

Table 3.16: Antibacterial activity of PG-Fe^0 composite, LEV, PG-Fe^0-LEV, and negative control (water) in terms of zone inhibition via agar-well diffusion method.at pH=6.5

Type of bacteria	Diameter of inhibition zone (mm)			
	PG-Fe^0 composite	Levofloxacin (LEV)	PG-Fe^0-LEV	Negative control (Water)
E.Coli	6	45.35	25.73	6
K.pneumoniae	6	45.9713	28.826	7
P.mirabilis	6	40.7	24.104	6
S.epidemidis	6	46.233	15.04	6
S.aureus	6	44.12	21.826	6
E.faecalis	6	34.356	6	6

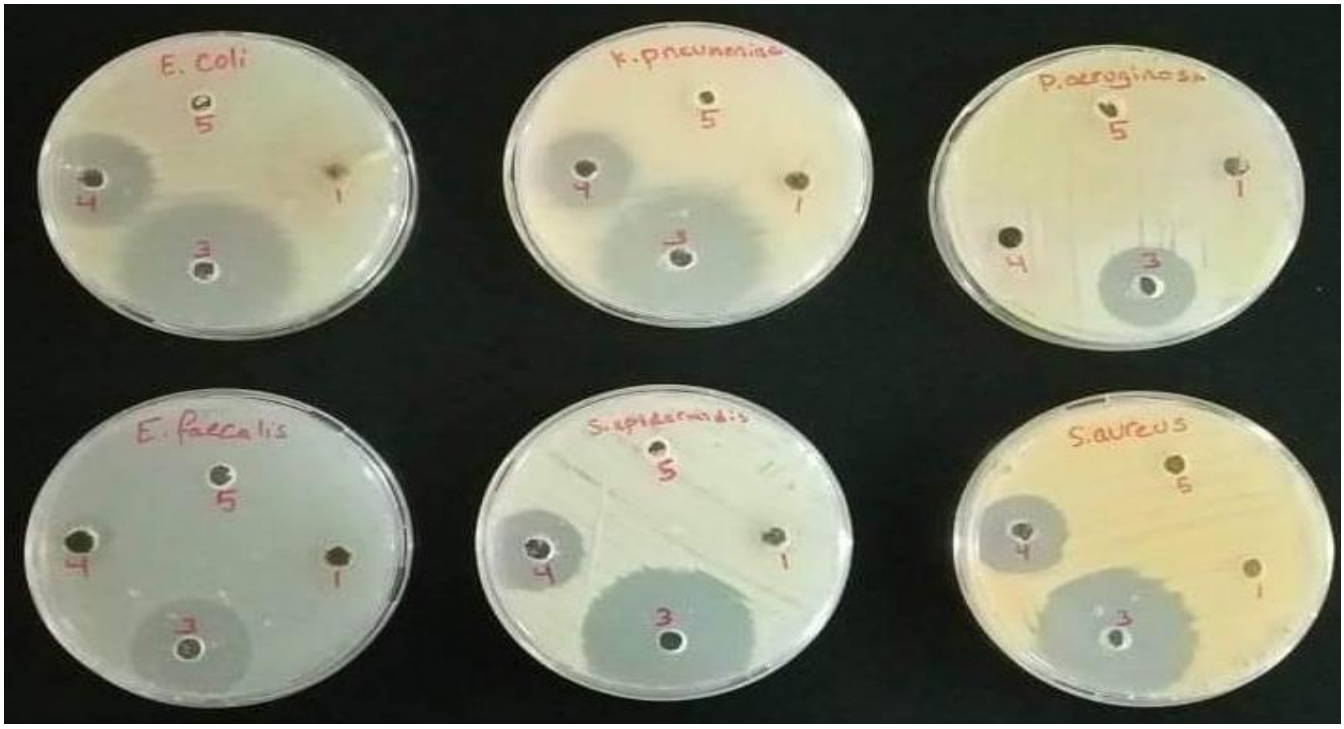

Figure 3.35: Photographs of Petri plates utilized in agar-well diffusion method; (1) PG-Fe^0composite, (2) LEV, (3) PG-Fe^0-LEV, and (4) negative control (water). At pH=8

Table 3.17: Antibacterial activity of PG-Fe^0 composite, LEV, PG-Fe0-LEV, and negative control (water) in terms of zone inhibition via agar-well diffusion method. (LEV=1.2mg)

Type of bacteria	Diameter of inhibition zone (mm)			
	PG-Fe^0 composite	Levofloxacin (LEV) (1.2 mg)	PG-Fe^0-LEV	Negative control (Water)
E.Coli	6	42.05	27.6	6
K.pneumoniae	6	39.645	23.065	6
P.aeruginosa	6	23.405	6	6
S.epidemidis	6	39.435	20.35	6
S.aureus	6	35.24	20.70	6
E.faecalis	6	34.84	11.5	6

Chapter Four

Conclusions

In this study, it was found that the new nanoparticles have good thermal and chemical stability, so they can be used as a good adsorbent for LEV from groundwater. PG-Fe^0 composite was successfully used to remove LEV from the aqueous solution. According to the findings, PG-Fe^0 composite was able to rapidly extract LEV with high removal efficiency within 320 minutes at pH around 6.5, 298K temperature, 0.5 g dose weight, and an initial concentration of 20 mg/L of 100 mL LEV solution. At the same condition, about 78 percent LEV removal efficiency was achieved after 320 minutes.

Langmuir's maximum adsorption capacity Q_m and Freundlich model parameters (values of 1/n and n) indicate that the adsorption of LEV on PG-Fe^0composite is favorable.

The amount of LEV adsorbed per unit mass PG-Fe^0 composite obtained by the Lagergren pseudo-second-order model Q_e (calc.) is consistent with the experimental value. Q_e (exp.) indicates that chemical adsorption may be the rate-limiting step, and the valence is determined by the adsorption of the electron, sharing or exchange between the agent and the adsorbate.

negative values of ΔG^o indicate that adsorption at these temperatures is favorable and spontaneous. ΔH^o indicates that positive adsorption is an endothermic process, and points out that low-temperature adsorption is preferred and that adsorption is a Physical process. A small positive value of $\Delta S°$ indicates that some structural changes have occurred on the adsorbent, and in the adsorption system, the entropy at the solid/liquid interface is increased through the adsorption process.

PG-Fe^0 composite is a good and effective adsorbent for removing LEV from wastewater. PG-Fe^0 composite can provide a convenient method for the effective treatment of industrial wastewater, which has a low LEV concentration at a temperature of about 25^0C and can remove more than 78%.

The maximum diameter 25.7, 28.8, 24.1, and 21.8 mm of inhibition zones were observed for PG-Fe^0-LEV against E. coli, K. pneumonia, P.mirabilis, and S. aureus, respectively. Studies have shown that PG-Fe^0-LEV nanoparticles can potentially be used to reduce environmental pollution and control the delivery of antibiotics.

Chapter Five

Recommendations

1- Further research needs to investigate the mechanism of using this adsorbent or other adsorbents to remove levofloxacin.

2- Further research needs to investigate how metal ions in aqueous media affect the adsorption of levofloxacin.

3- Further research needs to investigate the ability of nanoparticles to remove other contaminants.

4- Further research needs to investigate and compare the removal of levofloxacin efficiency with synthetic nanoparticles.

5- Further research needs to investigate the real concentration of levofloxacin in wastewater, and use the nanoparticles to remove it.

6- Further research needs to investigate using materials other than pencil-shaped graphite-supported magnetic nanoparticles PG-Fe^0, such as charcoal.

7- A small experimental station can be established to test the method's effectiveness.

References

1. Yunus, I. S., Harwin, Kurniawan, A., Adityawarman, D., & Indarto, A. (2012). Nanotechnologies in water and air pollution treatment. Environmental Technology Reviews, 1(1), 136-148.
2. Alrumman, S. A., El-kott, A. F., & Keshk, S. M. A. S. (2016). Water pollution: Source and treatment. American Journal of Environmental Engineering, 6(3), 88-98.
3. Lützhøft, H. C. H., Birch, H., Eriksson, E., & Mikkelsen, P. S. (2011). Comparing chemical analysis with literature studies to identify micropollutants in a catchment of Copenhagen (DK).
4. Pan, S., Li, J., Noonan, O., Fang, X., Wan, G., Yu, C., & Wang, L. (2017). Dual-functional ultrafiltration membrane for simultaneous removal of multiple pollutants with high performance. Environmental science & technology, 51(9), 5098-5107.
5. Brame, J., Li, Q., & Alvarez, P. J. (2011). Nanotechnology-enabled water treatment and reuse: emerging opportunities and challenges for developing countries. Trends in Food Science & Technology, 22(11), 618-624.
6. Shannon, M. A., Bohn, P. W., Elimelech, M., Georgiadis, J. G., Marinas, B. J., & Mayes, A. M. (2008). Science and technology for water purification in the coming decades. Nature 452, 301e310.
7. Bradl, H. (2005). Heavy metals in the environment: origin, interaction, and remediation. (2005).
8. Haseena, M., Malik, M. F., Javed, A., Arshad, S., Asif, N., Zulfiqar, S., & Hanif, J. (2017). Water pollution and human health. Environmental Risk Assessment and Remediation, 1(3), 16-19.
9. Bartolomeu, M., Neves, M. G. P. M. S., Faustino, M. A. F., & Almeida, A. (2018). Wastewater chemical contaminants: Remediation by advanced oxidation processes. Photochemical & Photobiological Sciences, 17(11), 1573-1598.
10. Lapworth, D. J., Baran, N., Stuart, M. E., & Ward, R. S. (2012). Emerging organic contaminants in groundwater: a review of sources, fate, and occurrence. Environmental pollution, 163, 287-303.

11. Adams, C., Wang, Y., Loftin, K., & Meyer, M. (2002). Removal of antibiotics from the surface and distilled water in conventional water treatment processes. Journal of environmental engineering, 128(3), 253-260.
12. Alum, A., Yoon, Y., Westerhoff, P., & Abbaszadegan, M. (2004). Oxidation of bisphenol A, 17β-estradiol, and 17α-ethynyl estradiol and byproduct estrogenicity. Environmental Toxicology: An International Journal, 19(3), 257-264.
13. Kümmerer, K. (2009). The presence of pharmaceuticals in the environment due to human use–present knowledge and future challenges. Journal of environmental management, 90(8), 2354-2366.
14. Kolpin, D. W., Furlong, E. T., Meyer, M. T., Thurman, E. M., Zaugg, S. D., Barber, L. B., & Buxton, H. T. (2002). Pharmaceuticals, hormones, and other organic wastewater contaminants in US streams, 1999− 2000: A national reconnaissance. Environmental science & technology, 36(6), 1202-1211.
15. Yuan, F., Hu, C., Hu, X., Qu, J., & Yang, M. (2009). Degradation of selected pharmaceuticals in aqueous solution with UV and UV/H2O2. Water Research, 43(6), 1766-1774.
16. Kümmerer, K. (2001). Drugs in the environment: emission of drugs, diagnostic aids, and disinfectants into wastewater by hospitals with other sources–a review. Chemosphere, 45(6-7), 957-969.
17. Daughton, C. G., & Ternes, T. A. (1999). Pharmaceuticals and personal care products in the environment: agents of subtle change? Environmental health perspectives, 107(suppl 6), 907-938.
18. Tambosi, J. L., Yamanaka, L. Y., José, H. J., Moreira, R. D. F. P. M., & Schröder, H. F. (2010). Recent research data on the removal of pharmaceuticals from sewage treatment plants (STP). Química Nova, 33(2), 411-420.
19. Kalyva, M. (2017). The fate of pharmaceuticals in the environment-A review.
20. Geissen, V., Mol, H., Klumpp, E., Umlauf, G., Nadal, M., Van der Ploeg, M., ... & Ritsema, C. J. (2015). Emerging pollutants in the environment: a challenge for water resource management. International soil and water conservation research, 3(1), 57-65

21. de Andrade, J. R., Oliveira, M. F., da Silva, M. G., & Vieira, M. G. (2018). Adsorption of pharmaceuticals from water and wastewater using nonconventional low-cost materials: a review. Industrial & Engineering Chemistry Research, 57(9), 3103-3127.
22. Padhi, B. S. (2012). Pollution due to synthetic dyes toxicity & carcinogenicity studies and remediation. International Journal of Environmental Sciences, 3(3), 940.
23. Kurniawan, T. A., Chan, G. Y., Lo, W. H., & Babel, S. (2006). Physicochemical treatment techniques for wastewater laden with heavy metals. Chemical engineering journal, 118(1-2), 83-98.
24. Kabbout, R., & Taha, S. (2014). Biodecolorization of textile dye effluent by biosorption on fungal biomass materials. Physics Procedia, 55, 437-444.
25. Kaushik, P., & Malik, A. (2009). Fungal dye decolorization: recent advances and future potential. Environment International, 35(1), 127-141.
26. Schwarzenbach, R. P., Egli, T., Hofstetter, T. B., Von Gunten, U., & Wehrli, B. (2010). Global water pollution and human health. Annual review of environment and resources, 35, 109-136.
27. Deblonde, T., Cossu-Leguille, C., & Hartemann, P. (2011). Emerging pollutants in wastewater: a review of the literature. International journal of hygiene and environmental health, 214(6), 442-448.
28. Mompelat, S., Le Bot, B., & Thomas, O. (2009). Occurrence and fate of pharmaceutical products and by-products, from resource to drinking water. Environment International, 35(5), 803-814.
29. Halling-Sørensen, B. N. N. S., Nielsen, S. N., Lanzky, P. F., Ingerslev, F., Lützhøft, H. H., & Jørgensen, S. E. (1998). Occurrence, fate, and effects of pharmaceutical substances in the environment-A review. Chemosphere, 36(2), 357-393.
30. Velagaleti, R. (1997). The behavior of pharmaceutical drugs (human and animal health) in the environment. Drug information journal: DIJ/Drug Information Association, 31(3), 715-722.
31. Jørgensen, S. E., & Halling-Sørensen, B. (2000). Drugs in the environment. Chemosphere, 40(7), 691-699.

32. Petrović, M., Gonzalez, S., & Barceló, D. (2003). Analysis and removal of emerging contaminants in wastewater and drinking water. TrAC Trends in Analytical Chemistry, 22(10), 685-696.
33. Zuccato, E., Castiglioni, S., Fanelli, R., Reitano, G., Bagnati, R., Chiabrando, C., ... & Calamari, D. (2006). Pharmaceuticals in the environment in Italy. Environmental Science and Pollution Research, 13(1), 15-21.
34. Kim, S. D., Cho, J., Kim, I. S., Vanderford, B. J., & Snyder, S. A. (2007). Occurrence and removal of pharmaceuticals and endocrine disruptors in South Korean surface, drinking, and wastewaters. Water Research, 41(5), 1013-1021.
35. Pinkston, K. E., & Sedlak, D. L. (2004). Transformation of aromatic ether-and amine-containing pharmaceuticals during chlorine disinfection. Environmental science & technology, 38(14), 4019-4025.
36. Summers, R. S., Haist, B., Koehler, J., Ritz, J., Zimmer, G., & Sontheimer, H. (1989). The influence of background organic matter on GAC adsorption. Journal-American Water Works Association, 81(5), 66-74.
37. Saravia, F., & Frimmel, F. H. (2008). Role of NOM in the performance of adsorption-membrane hybrid systems applied for the removal of pharmaceuticals. Desalination, 224(1-3), 168-171.
38. Fono, L. J., & Sedlak, D. L. (2005). Use of the chiral pharmaceutical propranolol to identify sewage discharges into surface waters. Environmental science & technology, 39(23), 9244-9252.
39. Kobya, M., Demirbas, E., Senturk, E., & Ince, M. (2005). Adsorption of heavy metal ions from aqueous solutions by activated carbon prepared from apricot stone. Bioresource Technology, 96(13), 1518-1521.
40. Deegan, A. M., Shaik, B., Nolan, K., Urell, K., Oelgemöller, M., Tobin, J., & Morrissey, A. (2011). Treatment options for wastewater effluents from pharmaceutical companies. International Journal of Environmental Science & Technology, 8(3), 649-666.
41. Song, W., Xie, B., Huang, S., Zhao, F., & Shi, X. (2020). Aerobic membrane bioreactors for industrial wastewater treatment. Current Developments in Biotechnology and Bioengineering, 129-145.

42. Esplugas, S., Bila, D. M., Krause, L. G. T., & Dezotti, M. (2007). Ozonation and advanced oxidation technologies to remove endocrine-disrupting chemicals (EDCs) and pharmaceuticals and personal care products (PPCPs) in water effluents. Journal of hazardous materials, 149(3), 631-642.
43. Moreira, F. C., Soler, J., Alpendurada, M. F., Boaventura, R. A., Brillas, E., & Vilar, V. J. (2016). Tertiary treatment of municipal wastewater toward pharmaceuticals removal by chemical and electrochemical advanced oxidation processes. Water Research, 105, 251-263.
44. Trovó, A. G., Nogueira, R. F., Agüera, A., Fernandez-Alba, A. R., Sirtori, C., & Malato, S. (2009). Degradation of sulfamethoxazole in water by solar photo-Fenton. Chemical and toxicological evaluation. Water Research, 43(16), 3922-3931.
45. Dias, I. N., Souza, B. S., Pereira, J. H., Moreira, F. C., Dezotti, M., Boaventura, R. A., & Vilar, V. J. (2014). Enhancement of the photo-Fenton reaction at near-neutral pH through the use of ferrioxalate complexes. Chemical Engineering Journal, 247, 302-313.
46. Zupanc, M., Kosjek, T., Petkovšek, M., Dular, M., Kompare, B., Širok, B., ... & Heath, E. (2013). Removal of pharmaceuticals from wastewater by biological processes, hydrodynamic cavitation, and UV treatment. Ultrasonics sonochemistry, 20(4), 1104-1112.
47. Gadipelly, C., Pérez-González, A., Yadav, G. D., Ortiz, I., Ibáñez, R., Rathod, V. K., & Marathe, K. V. (2014). Pharmaceutical industry wastewater: a review of the technologies for water treatment and reuse. Industrial & Engineering Chemistry Research, 53(29), 11571-11592.
48. Rosal, R., Rodríguez, A., Perdigón-Melón, J. A., Petre, A., García-Calvo, E., Gómez, M. J., ... & Fernández-Alba, A. R. (2010). Occurrence of emerging pollutants in urban wastewater and their removal through biological treatment followed by ozonation. Water research, 44(2), 578-588.
49. Kaya, Y., Ersan, G., Vergili, I., Gönder, Z. B., Yilmaz, G., Dizge, N., & Aydiner, C. (2013). The treatment of pharmaceutical wastewater using in a submerged membrane bioreactor under different sludge retention times. Journal of Membrane Science, 442, 72-82.

50. Clara, M., Strenn, B., Gans, O., Martinez, E., Kreuzinger, N., & Kroiss, H. (2005). Removal of selected pharmaceuticals, fragrances, and endocrine-disrupting compounds in a membrane bioreactor and conventional wastewater treatment plants. Water Research, 39(19), 4797-4807.
51. Sui, Q., Zhao, W., Cao, X., Lu, S., Qiu, Z., Gu, X., & Yu, G. (2017). Pharmaceuticals and personal care products in the leachates from a typical landfill reservoir of municipal solid waste in Shanghai, Journal of hazardous materials, 323, 99-108.
52. Radjenović, J., Petrović, M., Ventura, F., & Barceló, D. (2008). Rejection of pharmaceuticals in nanofiltration and reverse osmosis membrane drinking water treatment. Water Research, 42(14), 3601-3610.
53. Azaïs, A., Mendret, J., Gassara, S., Petit, E., Deratani, A., & Brosillon, S. (2014). Nanofiltration for wastewater reuse: counteractive effects of fouling and matrice on the rejection of pharmaceutically active compounds. Separation and Purification Technology, 133, 313-327.
54. Nielsen, L., & Bandosz, T. J. (2016). Analysis of sulfamethoxazole and trimethoprim adsorption on sewage sludge and fish waste-derived adsorbents. Microporous and Mesoporous Materials, 220, 58-72.
55. Lladó, J., Solé-Sardans, M., Lao-Luque, C., Fuente, E., & Ruiz, B. (2016). Removal of pharmaceutical industry pollutants by coal-based activated carbons. Process Safety and Environmental Protection, 104, 294-303.
56. Herrera-Herrera, A. V., González-Curbelo, M. Á., Hernández-Borges, J., & Rodríguez-Delgado, M. Á. (2012). Carbon nanotubes applications in separation science: a review. Analytica Chimica Acta, 734, 1-30.
57. Pasti, L., Martucci, A., Dondi, F., & Alberto, A. (2010). Adsorption of pharmaceuticals from dilute aqueous solutions on synthetic zeolites. In 16th International Zeolite Conference joint with the 7th International Mesostructured Materials Symposium (pp. 1429-1430).
58. Bhatnagar, A., Hogland, W., Marques, M., & Sillanpää, M. (2013). An overview of the modification methods of activated carbon for its water treatment applications. Chemical Engineering Journal, 219, 499-511.

59. Babel, S., & Kurniawan, T. A. (2003). Low-cost adsorbents for heavy metals uptake from contaminated water: a review. Journal of hazardous materials, 97(1-3), 219-243.
60. Jiang, C., Cui, S., Han, Q., Li, P., Zhang, Q., Song, J., & Li, M. (2019, February). Study on Application of Activated Carbon in Water Treatment. In IOP Conference Series: Earth and Environmental Science (Vol. 237, No. 2, p. 022049). IOP Publishing.
61. Delgado, N., Capparelli, A., Navarro, A., & Marino, D. (2019). Pharmaceutical emerging pollutants removal from water using powdered activated carbon: the study of kinetics and adsorption equilibrium. Journal of environmental management, 236, 301-308.
62. Dutta, M., Dutta, N. N., & Bhattacharya, K. G. (1999). Aqueous phase adsorption of certain beta-lactam antibiotics onto polymeric resins and activated carbon. Separation and Purification Technology, 16(3), 213-224.
63. Latorre, C. H., Méndez, J. Á., García, J. B., Martín, S. G., & Crecente, R. P. (2012). Carbon nanotubes as solid-phase extraction sorbents prior to atomic spectrometric determination of metal species: A review. Analytica chimica acta, 749, 16-35.
64. Tuzen, M., Saygi, K. O., & Soylak, M. (2008). Solid-phase extraction of heavy metal ions in environmental samples on multi-walled carbon nanotubes. Journal of hazardous materials, 152(2), 632-639.
65. Mubarak, N. M., Sahu, J. N., Abdullah, E. C., & Jayakumar, N. S. (2014). Removal of heavy metals from wastewater using carbon nanotubes. Separation & Purification Reviews, 43(4), 311-338.
66. Gong, J. L., Wang, B., Zeng, G. M., Yang, C. P., Niu, C. G., Niu, Q. Y., & Liang, Y. (2009). Removal of cationic dyes from aqueous solution using magnetic multi-wall carbon nanotube nanocomposite as adsorbent. Journal of hazardous materials, 164(2-3), 1517-1522.
67. Yang, K. U. N., Wu, W., Jing, Q., & Zhu, L. (2008). Aqueous adsorption of aniline, phenol, and their substitutes by multi-walled carbon nanotubes. Environmental science & technology, 42(21), 7931-7936.

68. Braschi, I., Blasioli, S., Gigli, L., Gessa, C. E., Alberti, A., & Martucci, A. (2010). Removal of sulfonamide antibiotics from water: evidence of adsorption into an organophilic zeolite Y by its structural modifications. Journal of Hazardous Materials, 178(1-3), 218-225.
69. Rossner, A., Snyder, S. A., & Knappe, D. R. (2009). Removal of emerging contaminants of concern by alternative adsorbents. Water Research, 43(15), 3787-3796.
70. A. Martucci, M.A. Cremonini, S. Blasioli, L. Gigli, G. Gatti, L. Marchese, I. Braschi, Adsorption and reaction ofsulfachloropyridazine sulfonamide antibiotic on a high silica mordenite: a structural and spectroscopic combined study, Micropor. Mesopor. Math., 170 (2013) 274–286.
71. De Ridder, D. J., Verberk, J. Q. J. C., Heijman, S. G., Amy, G. L., & Van Dijk, J. C. (2012). Zeolites for nitrosamine and pharmaceutical removal from demineralized and surface water: mechanisms and efficacy. Separation and purification technology, 89, 71-77.
72. Chauhan, A., Sillu, D., & Agnihotri, S. (2019). Removal of pharmaceutical contaminants in wastewater using nanomaterials: A comprehensive review. Current drug metabolism, 20(6), 483-505.
73. Dasgupta, A. (2012). Advances in antibiotic measurement. Advances in clinical chemistry, 56, 75.
74. Reddy, V. P. (2015). Organofluorine compounds in biology and medicine. Newnes.
75. Anderson, V. R., & Perry, C. M. (2008). Levofloxacin. Drugs, 68(4), 535-565.
76. Grayson, M. L., Cosgrove, S. E., Crowe, S., Hope, W., McCarthy, J. S., Mills, J., ... & Paterson, D. L. (Eds.). (2017). Kucers' The Use of Antibiotics: A Clinical Review of Antibacterial, Antifungal, Antiparasitic, and Antiviral Drugs, -Three Volume Set. CRC Press.
77. Davis, R., & Bryson, H. M. (1994). Levofloxacin. Drugs, 47(4), 677-700.
78. Anderson, V. R., & Perry, C. M. (2008). Levofloxacin. Drugs, 68(4), 535-565.
79. Khan, A. A. P., Khan, A., Asiri, A. M., & Khan, S. A. (2016). Studies on the oxidation of levofloxacin by N-bromosuccinimide in acidic medium and their mechanistic pathway. Journal of Molecular Liquids, 218, 604-610.

80. Kim, J. W., Jang, H. S., Kim, J. G., Ishibashi, H., Hirano, M., Nasu, K., ... & Arizono, K. (2009). Occurrence of pharmaceutical and personal care products (PPCPs) in surface water from Mankyung River, South Korea. Journal of Health Science, 55(2), 249-258.
81. Qin, X., Liu, F., Wang, G., Weng, L., & Li, L. (2014). Adsorption of levofloxacin onto goethite: effects of pH, calcium, and phosphate. Colloids and Surfaces B: Biointerfaces, 116, 591-596.
82. Epold, I., Trapido, M., & Dulova, N. (2015). Degradation of levofloxacin in aqueous solutions by Fenton, ferrous ion-activated persulfate, and combined Fenton/persulfate systems. Chemical Engineering Journal, 279, 452-462.
83. Mihciokur, H., & Oguz, M. (2016). Removal of oxytetracycline and determining its biosorption properties on aerobic granular sludge. Environmental toxicology and pharmacology, 46, 174-182.
84. Liu, H., Ning, W., Cheng, P., Zhang, J., Wang, Y., & Zhang, C. (2013). Evaluation of animal hairs-based activated carbon for sorption of norfloxacin and acetaminophen by comparing with cattail fiber-based activated carbon. Journal of Analytical and Applied Pyrolysis, 101, 156-165.
85. Martucci, A., Pasti, L., Marchetti, N., Cavazzini, A., Dondi, F., & Alberti, A. (2012). Adsorption of pharmaceuticals from aqueous solutions on synthetic zeolites. Microporous and Mesoporous Materials, 148(1), 174-183.
86. Yi, S., Gao, B., Sun, Y., Wu, J., Shi, X., Wu, B., & Hu, X. (2016). Removal of levofloxacin from aqueous solution using rice husk and wood-chip biochars. Chemosphere, 150, 694-701.
87. Yu, Y., Wang, W., Shi, J., Zhu, S., & Yan, Y. (2017). Enhanced levofloxacin removal from water using zirconium (IV) loaded corn bracts. Environmental Science and Pollution Research, 24(11), 10685-10694.
88. Boruah, P. K., Sharma, B., Hussain, N., & Das, M. R. (2017). Magnetically recoverable Fe3O4/graphene nanocomposite towards efficient removal of triazine pesticides from aqueous solution: investigation of the adsorption phenomenon and specific ion effect. Chemosphere, 168, 1058-1067.

89. Narain, R., Gonzales, M., Hoffman, A. S., Stayton, P. S., & Krishnan, K. M. (2007). Synthesis of monodisperse biotinylated p (NIPAAm)-coated iron oxide magnetic nanoparticles and their bioconjugation to streptavidin. Langmuir, 23(11), 6299-6304.
90. Minerals Education Coalition. (Accessed September 20, 2015). Graphite [Online], Available:https://www.mineralseducationcoalition.org/minerals/graphi
91. King,H.M.(Nov.28,2018)"Graphite"[Online].Available:https://geology.com/minerals/graphite.shtmlGraphenea. (Accessed September 20, 2015). Graphene & Graphite [Online], Available: http://www.graphenea.com/pages/graphene-graphite_
92. Viko Minerals.net. (Accessed September 20, 2015). The Mineral Graphite [Online], Available: http://www.minerals.net/mineral/graphite.aspx
93. WikiMedia Commons. (Accessed Nov. 28, 2018). File: Diamond and graphite2.jpg [Online], Availablehttps://en.wikipedia.org/wiki/Allotropes_of_carbon#/media/File:Diamond_and_graphite
94. P. Dutta. (Accessed September 20, 2015). What are the essential properties and uses of graphite? [Online], Available: http://www.preservearticles.com/201012291918/properties-and-uses-of-graphite.html
95. Wikipedia. http://en.wikipedia.org/wiki/Iron (accessed February 12, 2012).
96. Alipour, E., Majidi, M. R., Saadatirad, A., mahdi Golabi, S., & Alizadeh, A. M. (2013). Simultaneous determination of dopamine and uric acid in biological samples on the pretreated pencil graphite electrode. *Electrochimica Acta*, *91*, 36-42.
97. Gong, Z. Q., Sujari, A. N. A., & Ab Ghani, S. (2012). Electrochemical fabrication, characterization, and application of carboxylic multi-walled carbon nanotube modified composite pencil graphite electrodes. Electrochimica Acta, 65, 257-265.
98. Liv, L., & Nakiboğlu, N. (2016). Simple and rapid voltammetric determination of boron in water and steel samples using a pencil graphite electrode. *Turkish Journal of Chemistry*, *40*(3), 412-421.
99. Kariuki, J. K. (2012). Electrochemical and spectroscopic characterization of pencil graphite electrodes. *Journal of the Electrochemical Society*, *159*(9), H747.

100. Tavares, P. H. C. P., & Barbeira, P. J. S. (2008). Influence of pencil lead hardness on the voltammetric response of graphite reinforcement carbon electrodes. *Journal of Applied Electrochemistry*, *38*(6), 827-832.
101. Crane, R. A., & Scott, T. B. (2012). Nanoscale zero-valent iron: prospects for an emerging water treatment technology. Journal of hazardous materials, 211, 112-125.
102. Sayan, B., Indranil, S., Aniruddha, M., Dhrubajyoti, C., Uday, C. G., & Debashis, C. (2013). Role of nanotechnology in water treatment and purification: potential applications and implications. Int J Chem Sci Technol, 3(3), 59.
103. Zhang, H., Liu, G., Shi, L., & Ye, J. (2018). Single-atom catalysts: emerging multifunctional materials in heterogeneous catalysis. Advanced Energy Materials, 8(1), 1701343.
104. Chokshi, N., & Bora, L. (2014). An overview of nanotechnology in wastewater treatment.
105. Qu, X., Brame, J., Li, Q., & Alvarez, P. J. (2013). Nanotechnology for a safe and sustainable water supply: enabling integrated water treatment and reuse. Accounts of chemical research, 46(3), 834-843.
106. Kunduru, K. R., Nazarkovsky, M., Farah, S., Pawar, R. P., Basu, A., & Domb, A. J. (2017). Nanotechnology for water purification: applications of nanotechnology methods in wastewater treatment. Water purification, 33-74.
107. Theron, J., Walker, J. A., & Cloete, T. E. (2008). Nanotechnology and water treatment: applications and emerging opportunities. Critical reviews in microbiology, 34(1), 43-69.
108. Vanek, P. Electrochemical Series. In CRC Handbook of Chemistry and Physics, 89th ed.; Lide, D. R., Ed.; Taylor and Francis Group: Boca Raton,2009; pp 8-20
109. Li, X. Q., & Zhang, W. X. (2006). Iron nanoparticles: The core-shell structure and unique properties for Ni (II) sequestration. Langmuir, 22(10), 4638-4642.
110. Bystrzejewska-Piotrowska, G., Golimowski, J., & Urban, P. L. (2009). Nanoparticles: their potential toxicity, waste, and environmental management. Waste Management, 29(9), 2587-2595.

111. Olvera, R. C., Silva, S. L., Robles-Belmont, E., & Lau, E. Z. (2017). Review of the nanotechnology value chain for water treatment applications in Mexico. Resource-Efficient Technologies, 3(1), 1-11.
112. Zhang, Y., Chen, W., Dai, C., Zhou, C., & Zhou, X. (2015). Structural evolution of nanoscale zero-valent iron (nZVI) in anoxic Co 2+ solution: Interactional performance and mechanism. Scientific reports, 5(1), 1-9.
113. Kanel, S. R., Manning, B., Charlet, L., & Choi, H. (2005). Removal of arsenic (III) from groundwater by nanoscale zero-valent iron. Environmental science & technology, 39(5), 1291-1298.
114. Sun, Y. P., Li, X. Q., Zhang, W. X., & Wang, H. P. (2007). A method for the preparation of stable dispersion of zero-valent iron nanoparticles. Colloids and Surfaces A: Physicochemical and Engineering Aspects, 308(1-3), 60-66.
115. Thiruvenkatachari, R., Vigneswaran, S., & Naidu, R. (2008). The permeable reactive barrier for groundwater remediation. Journal of Industrial and Engineering Chemistry, 14(2), 145-156.
116. Bae, S., & Hanna, K. (2015). Reactivity of nanoscale zero-valent iron in unbuffered systems: effect of pH and Fe (II) dissolution. Environmental science & technology, 49(17), 10536-10543.
117. Kaushik, P., & Malik, A. (2009). Fungal dye decolorization: recent advances and future potential. Environment International, 35(1), 127-141.
118. Metcalf & Eddy, Burton, F. L., Stensel, H. D., & Tchobanoglous, G. (2003). Wastewater engineering: treatment and reuse. McGraw Hill.
119. Brezonik, P. L., & Arnold, W. A. (2012). Water chemistry: Fifty years of change and progress. Environmental science & technology, 46(11), 5650-5657.
120. Grahn, M. (2006). Development of a novel experimental technique for studying zeolites: combining zeolite-coated ATR elements and FTIR spectroscopy (Doctoral dissertation, Luleå tekniska universitet).
121. Shaw, D. J. (1980). Introduction to colloid and surface chemistry. Butterworths.
122. Asmaly, H. A., Ihsanullah, Abussaud, B., Saleh, T. A., Laoui, T., Gupta, V. K., & Atieh, M. A. (2016). Adsorption of phenol on aluminum oxide impregnated fly ash. Desalination and Water Treatment, 57(15), 6801-6808.

123. Levine, I. N., Busch, D. H., & Shull, H. (2009). Quantum chemistry (Vol. 6). Upper Saddle River, NJ: Pearson Prentice Hall.
124. Agarwal, A. K., Kadu, M. S., Pandhurnekar, C. P., & Muthreja, I. L. (2016). Brunauer-Emmett-Teller (BET), Langmuir, and Freundlich isotherm study for the adsorption of nickel ions onto coal fly ash. Asian Journal of Water, Environment and Pollution, 13(2), 49-53.
125. Yadav, O. (2017). Research article removal of phenol red dye from contaminated water using barley (Hordeum vulgare L.) husk-derived activated carbon Kingussie alebachew department of chemistry, Haramaya University, PO Box 138, Dire Dawa, Ethiopia. Sci. Int, 5.
126. Limousin, G., Gaudet, J. P., Charlet, L., Szenknect, S., Barthes, V., & Krimissa, M. (2007). Sorption isotherms: A review on physical bases, modeling, and measurement. Applied Geochemistry, 22(2), 249-275.
127. Hashemian, S., Ardakani, M. K., & Salehifar, H. (2013). Kinetics and thermodynamics of adsorption methylene blue onto tea waste/CuFe2 O4 composite.
128. Allen, S. J., Gan, Q., Matthews, R., & Johnson, P. A. (2003). Comparison of optimized isotherm models for basic dye adsorption by kudzu. Bioresource Technology, 88(2), 143-152.
129. Bulut, Y., & Aydın, H. (2006). A kinetics and thermodynamics study of methylene blue adsorption on wheat shells. Desalination, 194(1-3), 259-267.
130. Badhai, P., Kashyap, S., & Behera, S. K. (2020). Adsorption of phenol red onto GO-Fe3O4 hybrids in aqueous media. Environmental Nanotechnology, Monitoring & Management, 13, 100282.
131. Martins, A. E., Pereira, M. S., Jorgetto, A. O., Martines, M. A., Silva, R. I., Saeki, M. J., & Castro, G. R. (2013). The reactive surface of Castor leaf [Ricinus communis L.] powder as a green adsorbent for the removal of heavy metals from natural river water. Applied Surface Science, 276, 24-30.
132. Yuh-Shan, H. (2004). Citation review of Lagergren kinetic rate equation on adsorption reactions. Scientometrics, 59(1), 171-177.
133. Hashem, A., & El-Khiraigy, K. (2013). Bio-adsorption of Pb (II) onto Anethum graveolens from contaminated wastewater: Equilibrium and Kinetic studies.

134. Rashed, M. N. (2013). Adsorption technique for the removal of organic pollutants from water and wastewater. Organic pollutants-monitoring, risk, and treatment, 7, 167-194.

135. Akinyeye, O. J., Ibigbami, T. B., & Odeja, O. (2016). Effect of chitosan powder prepared from snail shells to remove lead (II) ion and nickel (II) ion from aqueous solution and its adsorption isotherm model. Am. J. Appl. Chem, 4, 146.

136. Rafatullah, M., Sulaiman, O., Hashim, R., & Ahmad, A. (2010). Adsorption of methylene blue on low-cost adsorbents: a review. Journal of hazardous materials, 177(1-3), 70-80.

137. Chen, Z. X., Jin, X. Y., Chen, Z., Megharaj, M., & Naidu, R. (2011). Removal of methyl orange from aqueous solution using bentonite-supported nanoscale zero-valent iron. Journal of colloid and interface science, 363(2), 601-607.

138. Sulaiman, S., & Shahwan, T. (2017). Mefenamic acid stability and removal from wastewater using bentonite-supported nanoscale zero-valent iron and activated charcoal. Desalination and Water Treatment, 97, 175-183.

139. Noubactep, C., Caré, S., & Crane, R. (2012). Nanoscale metallic iron for environmental remediation: prospects and limitations. Water, Air, & Soil Pollution, 223(3), 1363-1382.

140. Ponder, S. M., Darab, J. G., Bucher, J., Caulder, D., Craig, I., Davis, L.,& Mallouk, T. E. (2001). Surface chemistry and electrochemistry of supported zerovalent iron nanoparticles in the remediation of aqueous metal contaminants. Chemistry of Materials, 13(2), 479-486.

141. Wang, C., Baer, D. R., Amonette, J. E., Engelhard, M. H., Antony, J., & Qiang, Y. (2009). Morphology and electronic structure of the oxide shell on the surface of iron nanoparticles. Journal of the American Chemical Society, 131(25), 8824-8832.

142. Carpenter, E. E., Calvin, S., Stroud, R. M., & Harris, V. G. (2003). Passivated iron as core-shell nanoparticles. Chemistry of Materials, 15(17), 3245-3246.

143. Liang, W., Dai, C., Zhou, X., & Zhang, Y. (2014). Application of zero-valent iron nanoparticles for the removal of aqueous zinc ions under various experimental conditions. PloS one, 9(1), e85686.

144. Balko, B. A., & Tratnyek, P. G. (1998). Photo effects on the reduction of carbon tetrachloride by zero-valent iron. The Journal of Physical Chemistry B, 102(8), 1459-1465.

145. Sun, Y. P., Li, X. Q., Cao, J., Zhang, W. X., & Wang, H. P. (2006). Characterization of zero-valent iron nanoparticles. Advances in colloid and interface science, 120(1-3), 47-56.

146. Beltrán, F. J., Pocostales, P., Alvarez, P., & Oropesa, A. (2009). Diclofenac removal from water with ozone and activated carbon. Journal of Hazardous Materials, 163(2-3), 768-776.

147. Yuan, P., Annabi-Bergaya, F., Tao, Q., Fan, M., Liu, Z., Zhu, J., ... & Chen, T. (2008). A combined study by XRD, FTIR, TG, and HRTEM on the structure of delaminated Fe-intercalated/pillared clay. Journal of Colloid and Interface Science, 324(1-2), 142-149.

148. Khalkhali, M., Sadighian, S., Rostamizadeh, K., Khoeini, F., Naghibi, M., Bayat, N., ... & Hamidi, M. (2015). Synthesis and characterization of dextran-coated magnetite nanoparticles for diagnostics and therapy. BioImpacts: BI, 5(3), 141.

149. Qassim, A. W. (2015). Determination of levofloxacin in pharmaceutical formulation galvanic by Visible spectrophotometry of its chelating complex with aluminum ion (iii). Int. J. Dev. Res, 5(6), 4702-4706.

150. Asmaly, H. A., Ihsanullah, Abussaud, B., Saleh, T. A., Laoui, T., Gupta, V. K., & Atieh, M. A. (2016). Adsorption of phenol on aluminum oxide impregnated fly ash. Desalination and Water Treatment, 57(15), 6801-6808.

151. Thilagan, J., Gopalakrishnan, S., & Kannadasan, T. (2013). A comparative study on adsorption of copper (ii) ions in aqueous solution by;(a) chitosan blended with cellulose and cross-linked by formaldehyde, (b) chitosan immobilized on red soil, (c) chitosan reinforced by banana stem fiber. Int. J. Appl. Eng. Technol., 3(1), 35-60.

152. Monteiro Jr, O. A., & Airoldi, C. (1999). Some thermodynamic data on copper–chitin, and copper–chitosan biopolymer interactions. Journal of Colloid and Interface Science, 212(2), 212-219.

153. Ira N. Levine. PHYSICAL CHEMISTRY (2009); Brooklyn, New York, PP1-967.

154. Liu, L., Lin, Y., Liu, Y., Zhu, H., & He, Q. (2013). Removal of methylene blue from aqueous solutions by sewage sludge-based granular activated carbon: adsorption equilibrium, kinetics, and thermodynamics. Journal of Chemical & Engineering Data, 58(8), 2248-2253.

155. Shahwan, T. (2015). Lagergren equation: Can maximum loading of sorption replace equilibrium loading?. Chemical Engineering Research and Design, 96, 172-176.

156. Wu, W., He, Q., & Jiang, C. (2008). Magnetic iron oxide nanoparticles: synthesis and surface functionalization strategies. Nanoscale research letters, 3(11), 397-415.

157. Vijayakumar, G., Tamilarasan, R., & Dharmendirakumar, M. (2012). Adsorption, Kinetic, Equilibrium, and Thermodynamic Studies on the removal of basic dye Rhodamine-B from aqueous solution by the use of natural adsorbent perlite. J. Mater. Environ. Sci, 3(1), 157-170.

158. Oboh, I. O., Aluyor, E. O., & Audu, T. O. K. (2013). Second-order kinetic model for the adsorption of divalent metal ions on Sida acuta leaves. International Journal of Physical Sciences, 8(34), 1722-1728.

159. Azizian, S. (2004). Kinetic models of sorption: a theoretical analysis. *Journal of Colloid and Interface Science*, *276*(1), 47-52.

160. Ho, Y. S. (2014). Using of "pseudo-second-order model" in adsorption. Environmental Science and Pollution Research, 21(11), 7234-7235.

161. Hisham, J., Elsousy, K. M., & Hartany, K. A. (2016). Kinetics, equilibrium, and isotherm of the adsorption of cyanide by MDFSD. Arabian Journal of Chemistry, 9, S198-S203.

162. Shahwan, T. (2014). Sorption kinetics: obtaining a pseudo-second-order rate equation based on a mass balance approach. Journal of Environmental Chemical Engineering, 2(2), 1001-1006.

163. Weber Jr, W. J., & Morris, J. C. (1963). Kinetics of adsorption on carbon from solution. *Journal of the sanitary engineering division*, *89*(2), 31-59.

164- Aksu, Z., & Kabasakal, E. (2004). Batch adsorption of 2, 4-dichlorophenoxy-acetic acid (2, 4-D) from aqueous solution by granular activated carbon. *Separation and purification technology*, *35*(3), 223-240.

165- Sheha, R. R., & Someda, H. H. (2005). Removal of some chelators from aqueous solutions using polymeric ingredients. *Chemical engineering journal*, *114*(1-3), 105-113.

166- Mckay, G., Blair, H. S., & Gardner, J. (1983). The adsorption of dyes in chitin. III. Intraparticle diffusion processes. *Journal of Applied Polymer Science*, *28*(5), 1767-1778.

167- Özcan, A., Öncü, E. M., & Özcan, A. S. (2006). Adsorption of Acid Blue 193 from aqueous solutions onto DEDMA-sepiolite. *Journal of Hazardous materials*, *129*(1-3), 244-252

168-Zhao, G., Li, J., Ren, X., Chen, C., & Wang, X. (2011). Few-layered graphene oxide nanosheets as superior sorbents for heavy metal ion pollution management. Environmental science & technology, 45(24), 10454-10462.

169-Hall, K. R., Eagleton, L. C., Acrivos, A., & Vermeulen, T. (1966). Pore-and solid-diffusion kinetics in fixed-bed adsorption under constant pattern conditions. Industrial & Engineering Chemistry Fundamentals, 5(2), 212-223. p212–223.

170-Hameed, B. H., Mahmoud, D. K., & Ahmad, A. L. (2008). Equilibrium modeling and kinetic studies on the adsorption of basic dye by a low-cost adsorbent: Coconut (Cocos nucifera) bunch waste. Journal of hazardous materials, 158(1), 65-72.

171-Umoren, S. A., Etim, U. J., & Israel, A. U. (2013). Adsorption of methylene blue from industrial effluent using poly (vinyl alcohol). J. Mater. Environ. Sci, 4(1), 75-86.

172-Shahryari, Z., Goharrizi, A. S., & Azadi, M. (2010). Experimental study of methylene blue adsorption from aqueous solutions onto carbon nanotubes. International Journal of Water Resources and Environmental Engineering, 2147483647(2), 016-028.

173-Patil, S., Renukdas, S., & Patel, N. (2011). Removal of methylene blue, a basic dye from aqueous solutions by adsorption using teak tree (Tectona grandis) bark powder. International Journal of Environmental Sciences, 1(5), 711.

174-Abd El-Latif, M. M., Ibrahim, A. M., & El-Kady, M. F. (2010). Adsorption equilibrium, kinetics, and thermodynamics of methylene blue from aqueous solutions using biopolymer oak sawdust composite. Journal of American Science, 6(6), 267-283.

175-Li, M. F., Liu, Y. G., Zeng, G. M., Liu, S. B., Hu, X. J., Shu, D., ... & Yan, Z. L. (2017). Tetracycline absorbed onto nitrilotriacetic acid-functionalized magnetic graphene oxide: influencing factors and uptake mechanism. Journal of colloid and interface science, 485, 269-279.

176-Wallis, S. C., Gahan, L. R., Charles, B. G., Hambley, T. W., & Duckworth, P. A. (1996). Copper (II) complexes of the fluoroquinolone antimicrobial ciprofloxacin. Synthesis, X-ray structural characterization, and potentiometric study. Journal of inorganic biochemistry, 62(1), 1-16.

177-Wu, Q., Li, Z., Hong, H., Yin, K., & Tie, L. (2010). Adsorption and intercalation of ciprofloxacin on montmorillonite. Applied Clay Science, 50(2), 204-211.

178-Cottet, L., Almeida, C. A. P., Naidek, N., Viante, M. F., Lopes, M. C., & Debacher, N. A. (2014). Adsorption characteristics of montmorillonite clay modified with iron oxide for methylene blue in aqueous media. Applied Clay Science, 95, 25-31.

179- Jia, M., Wang, F., Bian, Y., Jin, X., Song, Y., Kengara, F. O., ... & Jiang, X. (2013). Effects of pH and metal ions on oxytetracycline sorption to maize-straw-derived biochar. *Bioresource Technology*, *136*, 87-93.

180- Tanis, E., Hanna, K., & Emmanuel, E. (2008). Experimental and modeling studies of sorption of tetracycline onto iron oxides-coated quartz. *Colloids and Surfaces A: Physicochemical and Engineering Aspects*, *327*(1-3), 57-63.

181-Boruah, P. K., Sharma, B., Hussain, N., & Das, M. R. (2017). Magnetically recoverable Fe3O4/graphene nanocomposite towards efficient removal of triazine pesticides from aqueous solution: investigation of the adsorption phenomenon and specific ion effect. Chemosphere, 168, 1058-1067.

182-Mahmoud, M. A. (2015). Kinetics and thermodynamics of aluminum oxide nanopowder as adsorbent for Fe (III) from aqueous solution. Beni-Suef University Journal of Basic and Applied Sciences, 4(2), 142-149.

183-Anirudhan, T. S., & Suchithra, P. S. (2010). Humic acid-immobilized polymer/bentonite composite as an adsorbent for the removal of copper (II) ions from aqueous solutions and electroplating industry wastewater. Journal of Industrial and Engineering Chemistry, 16(1), 130-139.

184-Yu, Y., Zhuang, Y. Y., & Wang, Z. H. (2001). Adsorption of water-soluble dye onto the functionalized resin. Journal of colloid and interface science, 242(2), 288-293.

185-Neyens, E., & Baeyens, J. (2003). A review of classic Fenton's peroxidation as an advanced oxidation technique. Journal of Hazardous materials, 98(1-3), 33-50.

Appendix

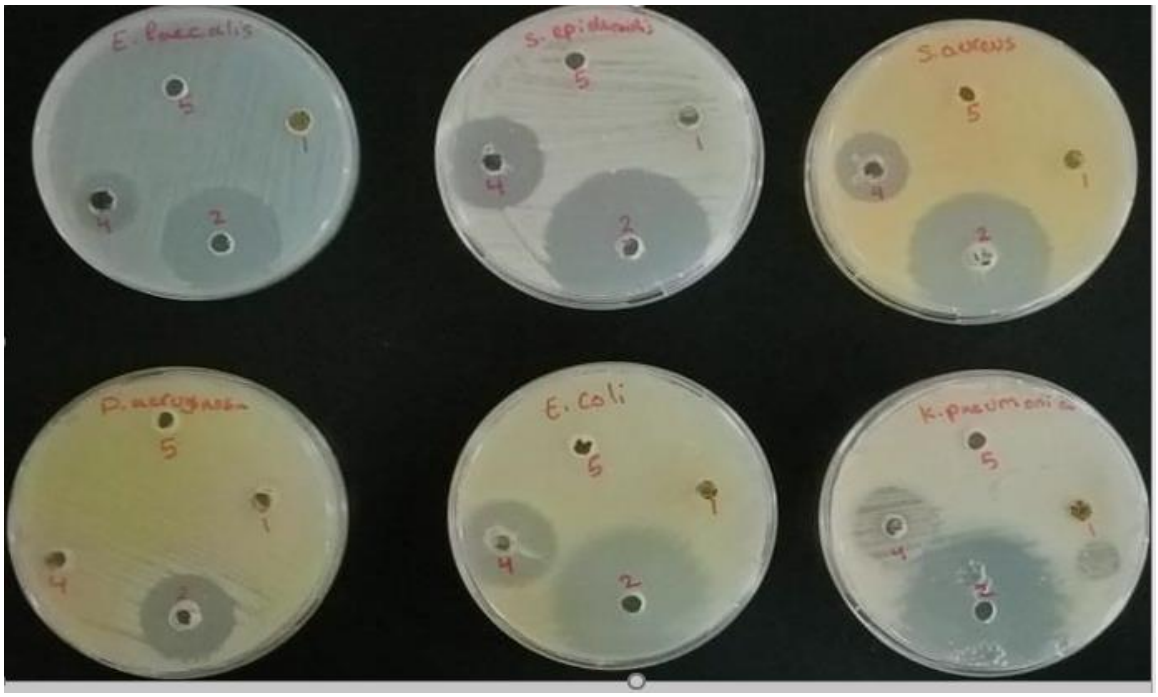

Figure S1 Photographs of petri plates utilized in agar-well diffusion method; (1) PG-Fe^0composite, (2) LEV (1.6 mg), (3) PG-Fe0-LEV, and (4) negative control (water).

Table S1. Antibacterial activity of PG-Fe^0 composite, LEV, PG-Fe^0-LEV, and negative control (water) in terms of zone inhibition via agar-well diffusion method. (LEV=1.6mg)

Type of bacteria	Diameter of inhibition zone (mm)			
	PG-Fe^0 Composite	Levofloxacin (LEV) (1.6 mg)	PG-Fe^0@LEV	Negative control (Water)
E.Coli	6	43.7	27.18	6
K.pneumoniae	6	35.86	23.595	6
P.aeruginosa	6	25.17	6	6
S.epidemidis	6	42.255	20.695	6
S.aureus	6	39.94	18.86	6
E.faecalis	6	31.625	14.65	6

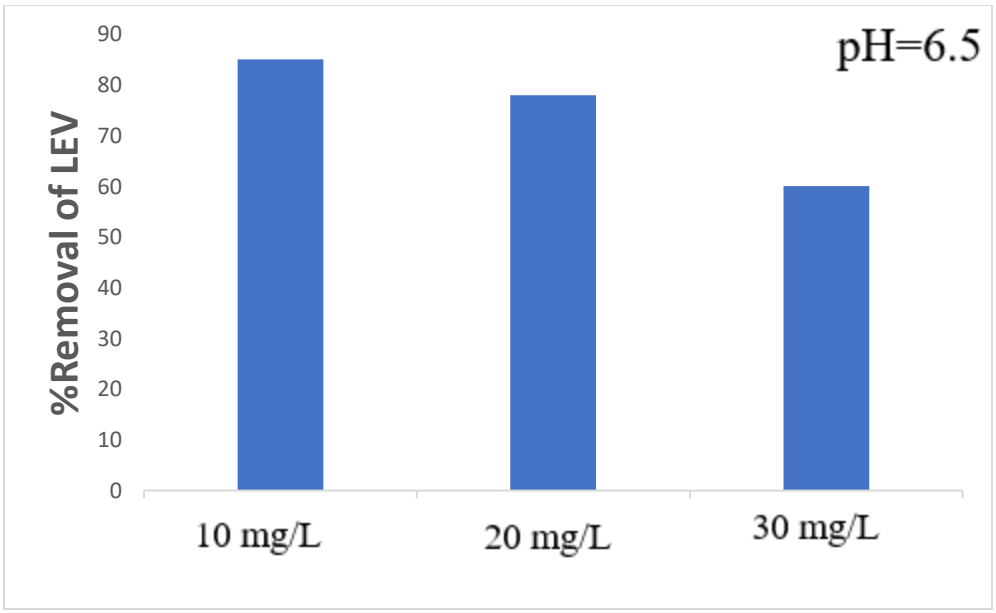

Figure S2: Effect of LEV concentration on % removal by using PG-Fe^0 composite at pH=6.5.

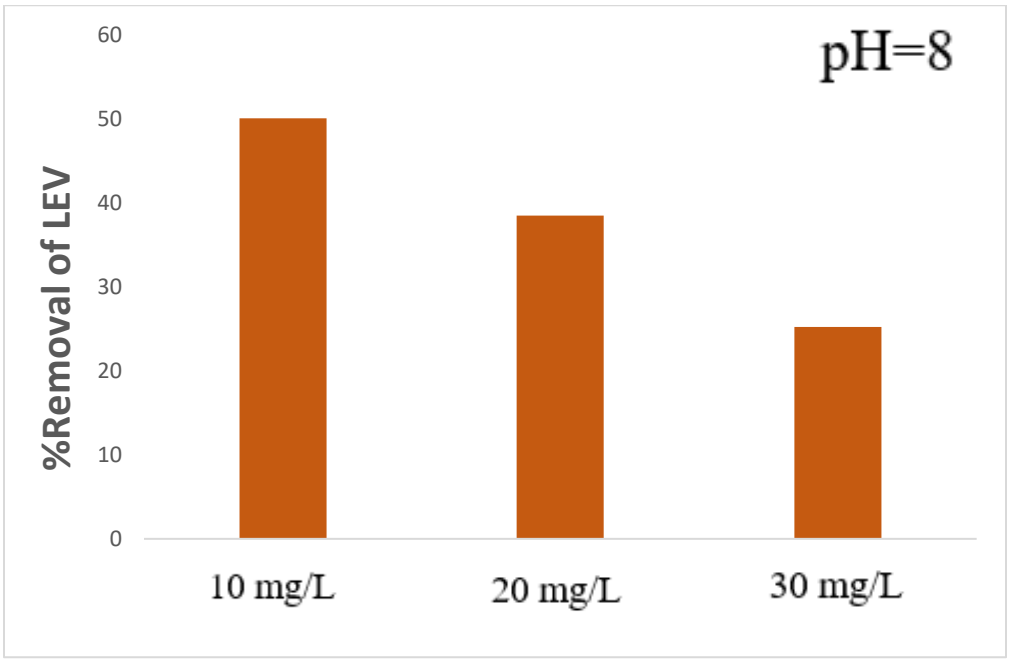

Figure S3: Effect of LEV concentration on % removal by using PG-Fe^0 composite at pH=8.0.